UNIVERSITÀ DEGLI STUDI DI PADOVA

**Dipartimento di Ingegneria Industriale DII**

Corso di Laurea Magistrale in Ingegneria dei Materiali

# Flow synthesis of anisotropic Au nanoparticles

Relatore: Prof. Alessandro Martucci

Correlatore: Prof. Luis M. Liz-Marzán

Laureando: Gregorio Carolo

Matricola: 1129104

Anno Accademico 2017/2018

# Abstract

The present thesis reports the experimental work done from March to August 2017, as part of the Erasmus+ Traineeship program, in the laboratories of BioNanoPlasmonics Group, inside the research centre CIC biomaGUNE – Centro de Investigación Cooperativa en Biomateriales, directed by Professor Luis M. Liz-Marzán, in Donostia San Sebastián (Basque Country, Spain). The activities concerned the use of a millifluidic reactor for the flow synthesis of anisotropic gold nanoparticles and the characterization of the samples through UV-vis-NIR spectroscopy and transmission electron microscopy.

# Index

# Introduction

What underlies the vision system of a moth, a black-eyed insect, in low light conditions, and the brightness of edelweiss bracts, an alpine flower living at high altitudes? What allows homing pigeons to find the flight direction and marine algae such as diatoms to be so efficient in the use of solar energy? What is common to geckos, able to climb everywhere, and to magnetotactic bacteria, known to navigate according to the Earth's geomagnetic field?

The explanation of the special features exhibited by the living species mentioned above, to which many other examples could be added, resides beyond the level of observation permitted to the human eye, neither can be investigated recurring to optical microscopy, classically utilized for observing micro-organisms. The answer is found only with the use of higher resolution microscopes, since it involves the organization of matter in a lesser scale, i.e., the nanometric order.

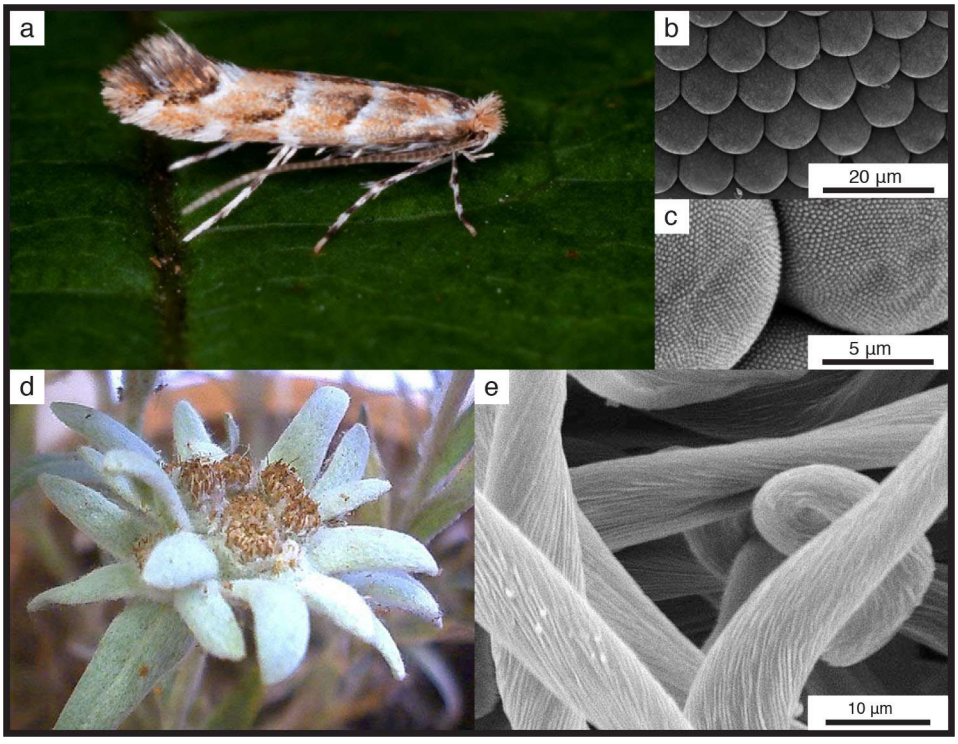


**Figure 1:** Macroscopic image of the moth *Cameraria ohridella*, in (**a**), and SEM micrographs of the corneal protuberance arrays, in (**b**) and (**c**); adapted from [1]. Macroscopic image of the Edelweiss flower, in (**d**), and SEM micrograph of the entangled fibrous structure, in (**e**). Adapted from [2].

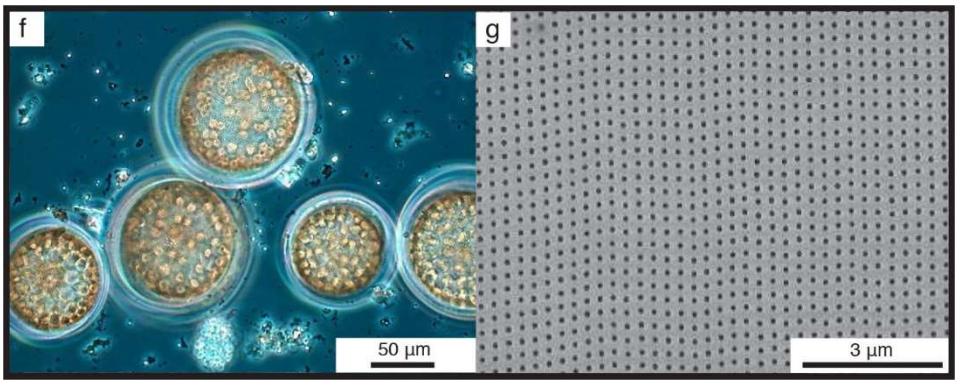


**Figure 2:** Macroscopic image of the diatom *Coscinodiscus granii*, in (**f**), and SEM micrograph of the side wall, in (**g**). Adapted from [4].

The presence of nanostructures constitutes the explanation for the case studies previously listed, with effects that can evidently be discussed in terms of photonics, mechanics and electromagnetics. Thanks to scansion and transmission electron microscopy (indicated respectively as SEM and TEM, from now on), images of the nanosized structures are available and permit to understand the phenomena. As reported in Figures 1 – 3, scanned and transmitted electrons reveal the nanostructures inside the moth cornea, edelweiss bracts, diatom side wall and magnetotactic bacteria.

In the case of the moth, for instance, protuberances arranged in a hexagonal array of periodicity around 240 nm in the cornea, reducing thus the reflectivity and maximizing instead the coupling of light in the eye.[1] Differently, the edelweiss – that lives at altitudes subjected to strong UV radiation – is covered and protected by thin hollow filaments, whose dimensions are comparable with the wavelength of the high energy radiation, that is therefore absorbed, while all the visible light is reflected, resulting in the characteristic white color.[2,3] To conclude this section on photonics, in the diatoms it is the regular pattern of nanopores in the silica-based walls that diffracts the visible light, allowing it to reach all the chloroplasts of the photosynthetic organism.[4]

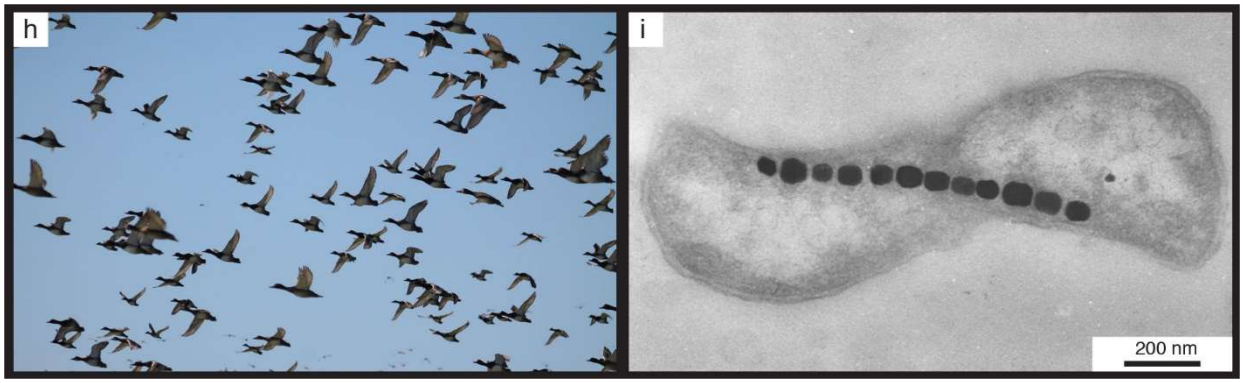


**Figure 3:** Macroscopic image of migrating birds, in (**h**), and TEM micrograph of a magnetotactic bacterium with magnetite nanoparticles arranged along the long axis of the cell, in (**i**). Adapted from [7].

Dealing with the climbing ability of the gecko, its adhesive toes are found to be constituted of setae, branched to form nanoarrays of spatula structures, the true responsible of attachment and

detachment in milliseconds to every surface by van der Waals forces.[5] Finally, focusing on the orientation skills performed by homing pigeons, migrating birds and magnetotactic bacteria, a biological compass is inside them and leads their movements according to Earth's geomagnetic field lines: magnetite nanoparticles nucleated and grown by proteins named magnetosomes.[6-8]

All these insights prove the existence in nature of nanostructures in life forms belonging to different dominions and kingdoms, as well as the evolutive advantages resulting from it and concerning multiple experiences and interactions of the reality, e.g., with light, gravity and magnets. Nowadays, many scientists and technologists study the nanostructures existing known in nature exactly with the purpose of mimic it, in order to develop products and devices able to work so efficiently responding to the same operative principles.

The awareness of the scale on which matter is organized for having the effects mentioned, and the consequent aim to replicate it, has been reached only since the appropriate tools can be used for observing the world at such depth. Notwithstanding the lack of scientific knowledge, artisan masters were able to leave us over the centuries several notable objects with properties determined on the nanoscale: empiricism evidently succeeded to chart territories then unknown to science.

**Figure 4:** Lycurgus cup exhibiting dichroic effect, reflecting (on the left) and transmitting light (on the right).

The first and most ancient example arrived at our days is represented by the Lycurgus cup, a Roman glass-cut vessel dated to the IV century that appears green if illuminated from the outside, i.e., reflecting light, and red from the inside, in transmission, as shown in Figure 4. TEM analyses on fragments revealed that the dichroic effect is to be attributed to the presence of Au-Ag alloyed nanoparticles, dispersed in the glassy matrix.

In the Middle Ages and the subsequent centuries, the secret on how to obtain warm colors in the glasses was kept by Venetians, a technique named colloidal coloration – on the meaning of such adjective we will return later, explaining what colloids are. The technique consists in the

solubilization of metals and semiconductors in the glass at high temperature and the successive precipitation in the form of nanosized particles during the cooling, or after a specific heat treatment.

In the seventeenth century, the so-called Purple of Cassius became a popular dye for clothes, obtained through a procedure consisting in the preparation of a gold sol, then stabilized with tin hydroxide. Two centuries later, the optical properties of these solutions containing gold attracted the attention of Michael Faraday, who investigated on its instability, the change of color with time, due to variations of the particles dimension, and finally discovered the first protocol for the synthesis and stabilization of gold nanoparticles in water.

Faraday can rightfully be considered the founder of modern colloid science and just some decades after his work, in the beginning of the 1900, other scientists such as Mie dealt with the properties of nanosized metal particles, but it's only in the late 1970s that the word *nanotechnology* was firstly coined by Norio Taniguchi, referred to the electronic industry, as the "materials processing with an atomic or molecular size working unit".[9]

A promising trend had been observed in the progressive reducing of gate length in transistors, that could then be integrated in a higher number in circuits, giving better performances, lower costs and higher reliability. All this was and is still obtained thanks to the power of miniaturization, the techniques currently employed by industry for nanofabrication, the top-down approach, for example recurring to lithography or milling, with nanosized structures physically cut out from bigger ones.

The approach pursued in this thesis work is instead a chemical one, the bottom-up approach, where the building blocks are atoms or molecules assembled into nanostructures working in three dimensions and obtaining less defects, more homogeneous composition and order, without waste or unused materials. Kinetic factors may exert some forms of control on the synthesis, but it's generally the achievement of thermodynamic equilibrium to prevail, with the reduction of Gibbs free energy.

Energy is indeed a point to consider – alongside with size, polydispersity, morphology and composition, growth or agglomeration, because of the presence of high surface energy. The ratio of surface atoms number over that of interior ones hugely increases switching from macroscopic objects to nanostructures, leading to the impact of the latter in manifold and distinct research fields, those already mentioned that attempt to mimic nature, but many others too, as we will see in next Chapter.

Engineering the optical properties of nanoparticles moves exactly towards the development of functional nanomaterials, or nanodevices. As depicted in Figure 5, to the formulation or the refining of a hypothesis follows the fabrication and the assembly of different components into a desired structure, that is then to characterize and analyze in the experimental data within the

framework given by an existing or a new theory.[10] The improvement loop here presented refers to a specific class of nanomaterials, the plasmonic ones based on noble metals, subject of the next pages.

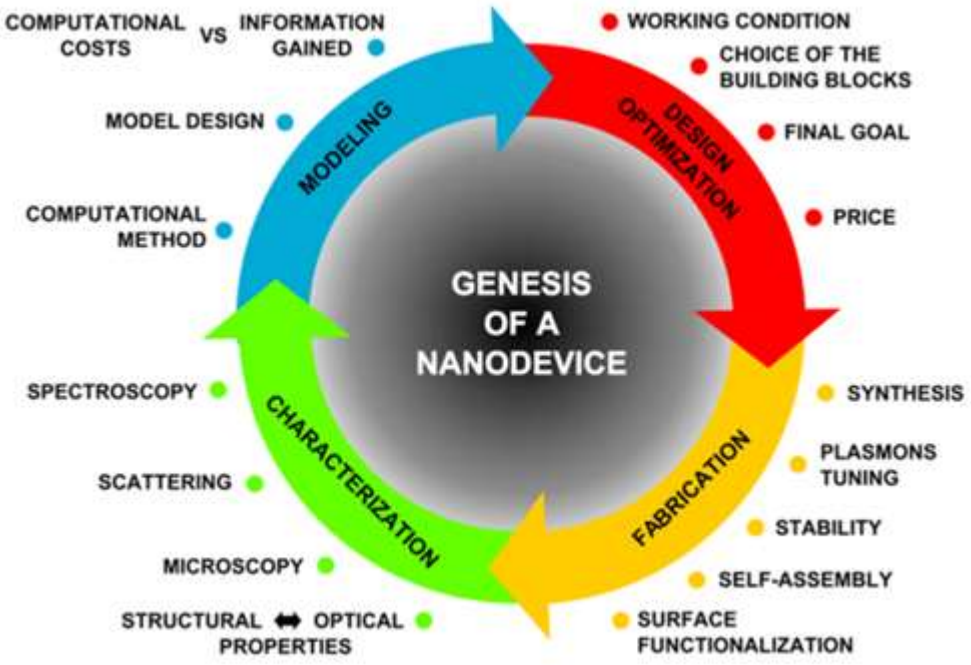


**Figure 5:** Improvement loop leading to the development of a new functional nanomaterial; adapted from [10].

Innovating nanodevices are likely to be developed from each of the stages just listed, the starting point that proves to be more appropriate derives indeed from the definition of a scientific problem, with related issues. The complexity met with the implementation of nanosystems, that may need for instance improved instrumentation, connects it unequivocally with the introduction of new characterization techniques such as electron tomography, electron energy loss spectroscopy, or cathodoluminescence to name a few.

After the overview presented on the main concepts driving research in nanoscience and nanotechnology, we now turn the focus on the pathway followed experimentally in the present work, firstly defining two terms that we already used without clarifying the specificities: colloids and sols. Nanoparticles are synthesizable through wet-chemistry methods, with the formation of colloids, solutions in which the dispersed phase has dimensions in the range of 1 – 1000 nm, unaffected by gravitational forces but instead influenced by van der Waals and electrostatic interactions. Specifically, the class of colloids constituted by solid particles in a liquid phase take the name of sols.

Compared to other nanofabrication techniques, sols require low-cost chemical synthesis processes, that are on the other hand usually difficult to control and therefore hardly scalable.[11] In this work we are going to deal with the batch synthesis of anisotropic gold nanoparticles and then to adapt it into flow conditions for having a scale-up in the production, with a constant evaluation of the

products quality and reproducibility. The objective of these studies is to determine whether the use of a millifluidic reactor allows to reach results unseen until now, representing a promising choice for the implementation to an upper level of this synthesis, so far only realized in laboratory small-scale.

**Chapter 1 – Plasmonic Nanoparticles** sums up the features of optical response given by metals, focusing on the localized resonance found in nanosized particles of various shapes and the practical consequences of it as applications to implement in different research disciplines.

**Chapter 2 – Batch Synthesis of Au NRs** presents the seed-mediated method for the growth of gold nanorods in batches, providing some insights known from literature and direct experience.

**Chapter 3 – Flow Synthesis of Au NRs** reports the work done in adapting the batch synthesis of gold nanorods into flow conditions with the use of a millifluidic reactor.

**Conclusions** close this thesis underlying the results obtained in the flow synthesis of gold nanorods with a millifluidic reactor, foreseeing its future use for other anisotropic noble metal NPs.

# REFERENCES


[1] Dewan, R.; Fischer, S.; Meyer-Rochow**,** V. B.; Ozdemir, Y.; Hamraz, S.; Knipp**,** D. Studying Nanostructured Nipple Arrays of Moth Eye Facets Helps to Design Better Thin Film Solar Cells. *Bioinspiration & Biomimetics*, **2012**, *7***,** 016003.

[2] Kertész, K.; Bálint, Z.; Vértesy, Z.; Márk, G.I.; Lousse, V.; Vigneron, J.-P.; Biró, L.P. Photonic Crystal Type Structures of Biological Origin: Structural and Spectral Characterization. *Current Applied Physics*, **2006**, *6*, 252–258.

[3] Eadie, L.; Ghosh, T. K. Biomimicry in Textiles: Past, Present and Potential. An Overview. *Journal of the Royal Society Interface*, **2011**, *8*, 761–775.

[4] Parker, A.; Townley, H. E. Biomimetics of Photonic Nanostructures. *Nature Nanotechnology*, **2007**, *2*, 347-353.

[5] Autumn, K.; Gravish, N. Gecko Adhesion: Evolutionary Nanotechnology. *Philosophical Transactions of the Royal Society A* **2008**, *366*, 1575–1590.

[6] Fleissner, G.; Holtkanprotzeler, E.; Hanzlik, M.; Winklhofer, M.; Fleissner, G.; Petersen, N.; Wiltschko, W. Ultrastructural Analysis of a Putative Magnetoreceptor in the Beak of Homing Pigeons. *The Journal of Comparative Neurology*, **2003**, *458*, 350–360.

[7] Chen, L.; Bazylinski, D. A.; Lower, B. H. Bacteria that Synthesize Nano-Sized Compasses to Navigate Using Earth's Geomagnetic Field. *Nature Education Knowledge*, **2010**, *3*, 30.

[8] Stanley, S. Biological Nanoparticles and Their Influence on Organisms. *Current Opinion in Biotechnology*, **2014**, *28*, 69–74.

[9] Taniguchi, N. Nanotechnology. Materials Processing with an Atomic or Molecular Size Working Unit. *Kinzoku Hyomen Gijutsu*, **1978**, *29* (5), 220-31.

[10] Scarabelli, L.; Hamon, C.; Liz-Marzań, L. M. Design and Fabrication of Plasmonic Nanomaterials Based on Gold Nanorod Supercrystals. *Chemistry of Materials*, **2017**, *29*, 15-25.

[11] Biswas, A.; Bayer, I. S.; Biris, A. S.; Wang, T.; Dervishi, E.; Faupel, F. Advances in Top–Down and Bottom–Up Surface Nanofabrication: Techniques, Applications & Future Prospects. *Advances in Colloid and Interface Science*, **2012**, *170*, 2–27.

# Chapter 1

# Plasmonic nanoparticles

Optical properties, such as color effect, due to the dispersion of metal nanoparticles in a medium, are found in a glassy matrix or liquid solutions because a phenomenon takes place there, the localized surface plasmon resonance. Firstly, we are going to recall some elements of metals electromagnetism, for understanding what are the plasmons; secondly, we will tackle the consequences of size reduction to nanostructure for such phenomena; finally, we will cover some of the multiple applications and opportunities spread from the wide world of research on plasmonic nanoparticles in the future society.

## 1.1 Electromagnetics of metals: bulk and surface plasmons

Metals are known to behave in very different ways with electromagnetic waves, according to the frequency of the latter: high reflectivity is exhibited in the microwave and far infrared region; an increase of penetration is found in the near-infrared and visible region; in the ultraviolet, propagation is permitted and the dielectric character comes to depend on the electronic structure indeed, transparency in the case of the alkali metals (that have a free electron) or strong absorption due to band transitions for Au and Ag.

These properties can be properly described in the terms of dielectric function, also named relative permittivity, expressed in (1.1.1), whose imaginary part quantifies the absorbance in the medium, as well as in those of conductivity, since a fundamental relation relates the two functions.

$$\varepsilon(\omega) = \varepsilon_1(\omega) + i\varepsilon_2(\omega) \qquad (1.1.1)$$

where $\omega$: angular frequency

The dielectric function is determinable via reflectivity measurements and refractive index, a complex function of angular frequency too, expressed in (1.1.4), quantifying in its real part the decrease in the phase velocity of propagating waves due to the polarization of the medium. The coefficient of the imaginary part is proportional to the absorptivity coefficient of Lambert-Beer's law,

respectively given in (1.1.5) and (1.1.6), that describes the exponential attenuation in intensity of a beam propagating through a medium.

$$\tilde{n}(\omega) = n(\omega) + ik(\omega) \tag{1.1.4}$$

$$a(\omega) = \frac{2k(\omega)\omega}{c} \tag{1.1.5}$$

$$I(x) = I_0 e^{-a(\omega)x} \tag{1.1.6}$$

where $n(\omega)$: phase velocity

$k(\omega)$: extinction coefficient

$a(\omega)$: absorptivity coefficient

$c$: light velocity

$x$: distance from beam source

$I(x)$: beam intensity at $x$

$I_0$: incident beam intensity

According to the plasma model, metals contain a gas of conduction electrons free to move with respect to fixed positive ions and oscillating coherently with the electromagnetic field applied, with a motion damped by collisions. Plasma frequency is determined by the density number and the effective mass of the electrons; the dielectric function can be rewritten in terms of plasma and collision frequencies, in its real and imaginary parts, and metals are supposed to radiate only for frequencies above the plasma one.

A famous representation of this model was given by Drude, with the image of the metallic slab: changes in surface charge density are verified at the borders, with consequent polarizability and the instauration of a homogenous electromagnetic field into the slab, while the electrons experience a restoring force. The electrons move in phase and have $\omega_P$ as frequency of the oscillations, whose quanta are called volume plasmons. This model does not account electronic interband transitions, that for noble metals take place already in the near infrared and the visible regions, the trends of the dielectric constant predicted by it do not fit with the experimental values.[1]

The plasma oscillations of a conductor coupled with electromagnetic fields originate surface waves, a situation verified classically in presence of a flat interface between a conductor and a dielectric. Solving the Maxwell equations for it, it is found that electromagnetic excitations are propagating and dispersing along the interface, confined with evanishing decay in the perpendicular direction, named surface plasmon polaritons or excitations.

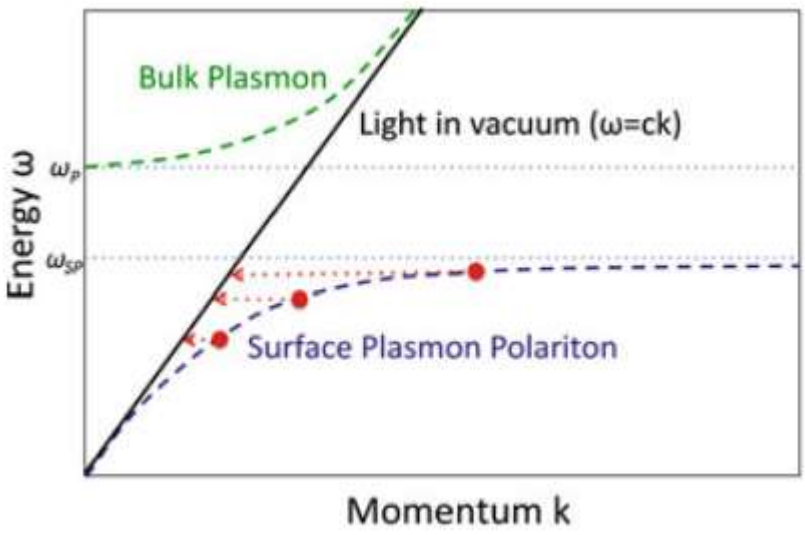


**Figure 1.1:** Dispersion curves of the bulk plasmon (green-dashed line) and surface plasmon polariton (blue-dashed line), with curve of light in vacuum displayed as solid black line, red dots and red-dashed lines denoting the momentum provision for effective coupling to light. Adapted from [2].

While volume plasmons are linked with radiative modes and are verified in the transparency regime for metals, at frequencies above $\omega_P$, the bound nature of surface plasmons prevents the direct excitation using a tridimensional beam, special phase-matching techniques such as prism-coupling are needed, as evidenced in Figure 1.1 by the dispersion curves lying to the right of the light line in different media.[2] We are now going to analyze how these phenomena arise on nanostructured metals.

## 1.2 Localized surface plasmon resonance

Surface plasmons have been so far defined as surface waves involving collective electron motion and propagating on metal surfaces, a definition to enrich with their presence as localized in metal nanostructures, where they couple efficiently to light, producing strong confinement of the electromagnetic field (since the size is largely inferior to the wavelength) and generating huge enhancement of the optical electric-field intensity.[3] We see in Figure 1.2 the both surface plasmons.

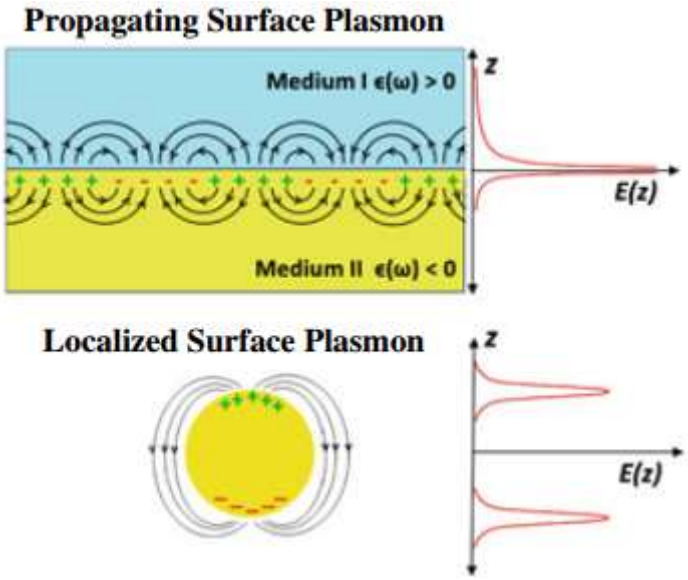


**Figure 1.2:** Schematics of the surface charge density of a propagating surface plasmon polariton (on the top) and of a localized surface plasmon (on the bottom), the latter with stationary oscillation. Adapted from [2].

In the case of a metallic nanosphere, after excitation by direct illumination the curved surface exerts a restoring force on the conduction electrons and a resonance is generated, amplifying the field inside the particle and near-outside, a condition verified in the visible region for noble metals, originating the so-known color effects. Such nanoparticle is considerable in all respects as the simplest optical antenna, analogously to other regions of the electromagnetic spectrum, with properties implementable as applications in different research disciplines, as we will deal with.[2]

The case can be treated at first making the quasi-static approximation, since the diameter of the particle is largely inferior to the wavelength and the phase of the electric camp can therefore be considered constant over the particle volume. Following an electrostatic approach for a homogeneous and isotropic sphere in a uniform and unidirectional field, a solution of the Laplace equation is found for the potential and the time dependence is then introduced into the results. From the potential it is obtained the dipole moment oscillating, depicted schematically in Figure 1.3 and properly expressed in (1.2.1), from which can be isolated the part referred to polarizability, as in (1.2.2).

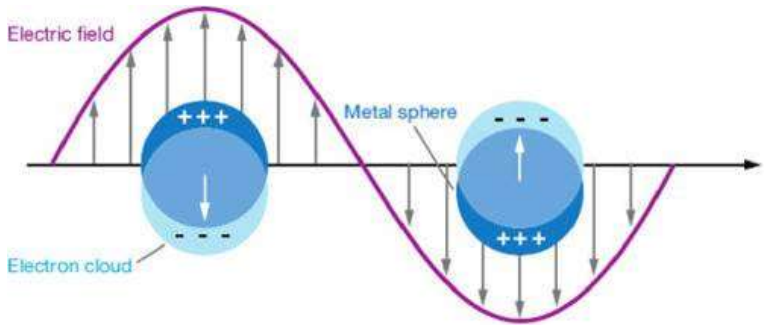


**Figure 1.3:** Schematics of the effect caused by an incoming electromagnetic wave on the electron cloud of a spherical nanoparticle. Adapted from [4].

$$\mathbf{p}(t) = 4\pi\varepsilon_0\varepsilon_m r^3 \frac{\varepsilon(\omega) - \varepsilon_m}{\varepsilon(\omega) + 2\varepsilon_m}\mathbf{E}_0 e^{-i\omega t} \tag{1.2.1}$$

$$\alpha = 4\pi r^3 \frac{\varepsilon(\omega) - \varepsilon_m}{\varepsilon(\omega) + 2\varepsilon_m} \tag{1.2.2}$$

where $t$: time

$r$: radius of the sphere

$\mathbf{E}_0$: uniform electrostatic field

$\varepsilon_m$: dielectric constant of the surrounding medium

$\varepsilon(\omega)$: dielectric function of the sphere

Observing the terms constituting the polarizability, it is deducible the condition for having a resonance enhancement, i.e., when $|\varepsilon(\omega) + 2\varepsilon_m|$ assumes a minimum value, the Fröhlich condition.

$$\mathrm{Re}[\varepsilon(\omega)] = -2\varepsilon_m \tag{1.2.3}$$

For metal nanoparticles, in resonance condition the extinction of light takes place, and its components of scattering and absorption are calculated with Mie theory, as expressed respectively in (1.2.5) and (1.2.6), in terms of the corresponding cross section, i.e., the effective area of a screen with which the incoming light interacts in a straight-ray picture. When the polarizability is resonantly enhanced, it is verified an increase in both scattering, the energy sent to the far-field, and absorption, the energy dissipated as lattice vibrations.

$$C_{ext} = C_{sca} + C_{abs} \tag{1.2.4}$$

$$C_{sca} = \frac{k^4}{6\pi}|\alpha|^2 = \frac{8\pi}{3}k^4 r^6 \left|\frac{\varepsilon - \varepsilon_m}{\varepsilon + 2\varepsilon_m}\right|^2 \tag{1.2.5}$$

$$C_{abs} = k\mathrm{Im}[\alpha] = 4\pi k r^3 \mathrm{Im}\left[\frac{\varepsilon - \varepsilon_m}{\varepsilon + 2\varepsilon_m}\right] \tag{1.2.6}$$

In the case of a colloidal solution containing $N$ particles per unit volume, Lambert-Beer's law is then formulable accounting the distinct phenomena involved in the attenuation of light, as in (1.2.7), expressing the previous absorptivity coefficient as the product of extinction cross section and NPs

concentration. In real experiments, the spectrophotometer measures the rate of loss of photons over a pathlength, the ratio of transmitted light over incident light, quantified as absorbance.

$$I = I_0 e^{[-(C_{sca}+C_{abs})NL]} \tag{1.2.7}$$

where $N$: number of particles per unit volume

$L$: pathlength inside the dispersion

As consequence of the quasi-static approximation, the electric field constant over the volume of the particle is coupled with a dipolar charge distribution and LSPR position is not dependent by the sphere size. Increasing the dimensions of the latter, indeed, retardation effects are found, the spatial variation of the exciting electric field is no longer negligible and higher multipole modes emerge, red-shifted and generally less intense, with a broader bandwidth.

The shift towards lower energies derives from the rise of the distance found between the charges increasing size, leading to a smaller restoring force and a lower resonance frequency, while the retardation effects are two competing processes, a radiative decay into photons and a non-radiative decay due to the creation of electron-hole pair via intraband or interband transitions, as in Figure 1.4.

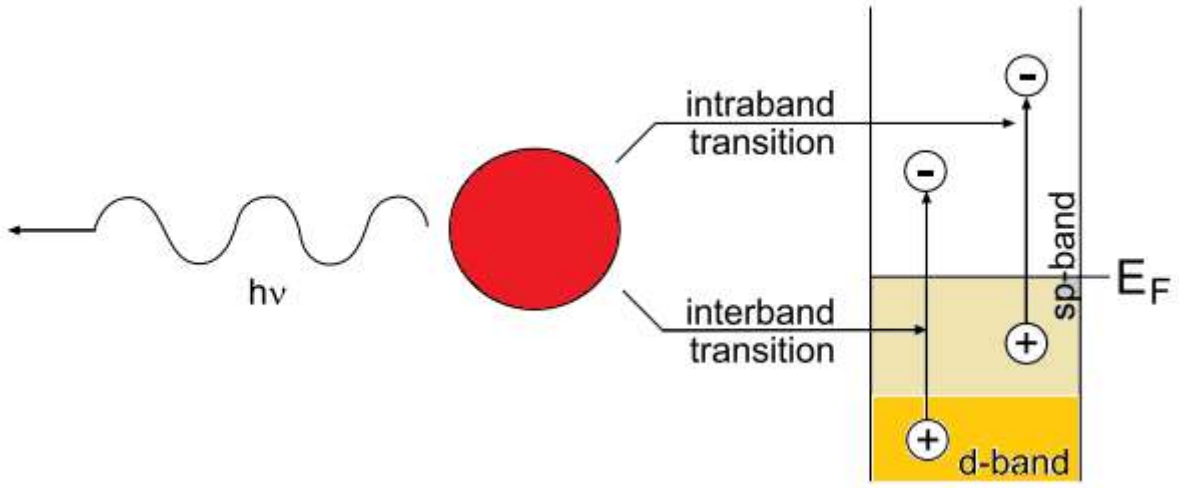


**Figure 1.4:** Schematics of radiative (on the left) and non-radiative (on the right) decay of particle plasmons. Adapted from [1].

In the case of particles with radius shorter than 10 nm, oppositely, the size is smaller than the mean free path of the conduction electrons, that are scattered at the surface with both elastic and inelastic collisions, losing the phase coherence, with a red-shift of the mode and a broader bandwidth. All this is explainable within the framework given by classical physics, while moving to sizes below 1 nm the situation abruptly changes, because quantum effects take the lead.

As we previously stated, Fröhlich condition is met when the real part of the metal dielectric function equals to the dielectric constant of the medium; it means that a spectral shift of the plasmon

band may correspond to variations in the medium properties, and the monitoring of LSPR position proves to be a useful tool for sensing. Another possibility for the tuning of plasmon resonance, in terms of spectral position as in those of modes number, is given instead by nanoparticle shapes.

Gans theory extended the work of Mie to ellipsoids, rod-like nanoparticles (from now on NRs, nanorods), considering the optical anisotropy and predicting the splitting of the plasmon mode in two distinct ones, as long as the dipole approximation holds. The NRs that are experimentally fabricated look more like sphere-capped cylinders than ellipsoids, but Gans theory calculations are valid in most of the cases for the optical properties, whereas instead the exact shape of the particles is modelled recurring to numerical methods recently developed, such as the Boundary Elements Method (BEM).

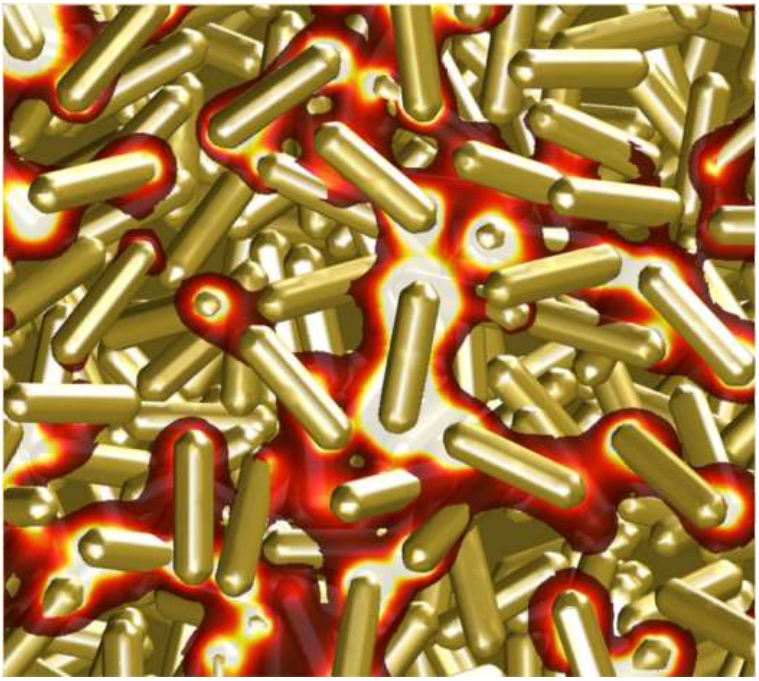

**Figure 1.5:** Representation of LSPR for Au NRs. Adapted from [5].

Oscillations of electrons excited along the short axis originate a plasmon band at almost the same wavelength of nanospheres, the transverse band, while oscillations along the long axis give rise to a much stronger plasmon band, in the region of longer wavelength, the longitudinal band. In a steady-state extinction spectrum of NRs dispersed in a solvent the two bands of transverse and longitudinal plasmons are contemporaneously observable, because of the particles random orientation given by the continuous Brownian motion.

Retardation effects with increase in size are found also for NRs, a red-shift of the longitudinal band is found for higher aspect ratios (AR, the ratio of length over width), produced by shape-dependent depolarization.[6] Mathematical considerations on the terms composing the extinction cross

section lead to find that absorption lowers with the red-shift of the mode, narrowing the band, while scattering increases significantly in longer particles, broadening the plasmon resonance.

Nowadays, colloidal chemistry offers multiple ways for synthesizing nanoparticles with very different shapes, on which several effects depend and have their role in tuning the LSPR and determining the field enhancement, such as: elongation, yielding strong anisotropy in optical response and therefore valuable for localizing the field at the ends and tuning it; curvature, providing more intense field with decreasing radius; asymmetry, giving Fano-like shapes in the optical spectrum and manipulating the incoming light polarization; intracoupling, tuning effectively the optical response thanks to the presence of inner and outer walls, arms or edges.[7]

| NANOPARTICLE | PROPERTIES |
|---|---|
| Sphere | Isotropic scattering, moderate enhancement. |
| Spheroid | Anisotropic scattering and enhancement. Two modes. |
| Rod | Transverse and longitudinal modes. Linear behavior with rod length. Modification of plasmon decaying length. |
| Disk | Substrates for biosensing. Useful as constituents for patch antennas. |
| Shell | Tunability due to shell thickness. |
| Ring | Tunability due to ring thickness. |
| Rice | Intense resonances, large field enhancements. Rod and shell properties. |
| Star | Intense hot spots at the tips. |
| Egg | Tunability, asymmetric system, Fano spectral profiles. |
| Cup | Capability to bend light. |
| Spiral | Complex response. |
| Crescent | Tunable narrow resonances in the mid-infrared with good figures of merit for sensing. |
| Prism | Presence of sharp edges. Breaking of symmetry. |
| Hole | Inverse symmetry. Babinet's principle. Similar trends for complementary electric and magnetic fields. |
| L-shaped | No center of inversion symmetry. Strong dependence on polarization. Presence of bulk-like plasmons. |

**Table 1:** Selected nanostructures of Au and deriving optical properties. Adapted from [7].

## 1.3 Applications of Plasmonic Nanoparticles

As we previously stated, the localized surface modes are often referred to as optical antenna resonances, since the nanostructure is effectively able to convert the electromagnetic radiation from the far-field into the near-field and vice versa; these optical properties are expected to have a tremendous impact in the future over several aspects of our lives, from the development of green energy sources to the more advanced biomedical treatments.[8] We'll focus particularly on the promising implications in the use of Au NRs, that are the object of studies in the present thesis work.

Among the several plasmonic materials recognized, such as aluminum, heavily doped semiconductors and metal oxides, chalcogenides and graphene, special attention has been so far focused on noble metals, Ag and Au, because of their LSPR peaks positioned in the visible and near-infrared region of the electromagnetic spectrum, properties making them more valuable, compared to non-plasmonic nanosized materials working as carriers in the biomedical field. Although the higher enhancement given by Ag NPs, the superior chemical inertness and synthetic accessibility proven by Au NPs decreed their supremacy as objects of research interest.

In the field of solar technology, the incorporation of plasmonic nanoparticles into solar cell devices has proven to be a success, as the objectives are enhanced absorption and efficiency by trapping sunlight at specific wavelengths. Thin-film silicon solar cells, obtainable from abundant raw materials at low cost and highly stable, presenting instead weaknesses as poor light absorption and high recombination, are improvable in terms of power-conversion efficiency by the incorporation of Au NPs, whose size determines the degree and wavelength range of the enhancement.

The overall optical response results to be improvable by plasmonics in the various existing kinds of solar cells. Advantages are found also by the integration of metallic nanoparticles into organic photovoltaic, dye-sensitized and inorganic solar cells, contributing therefore actively to the current efforts of the scientific community to value renewable and clean energy resources instead of fossil fuels. In the cases mentioned, the plasmonic enhancement concerned solar energy harvesting, we are now going to see how it affects heat generation, again from the nanoscale.

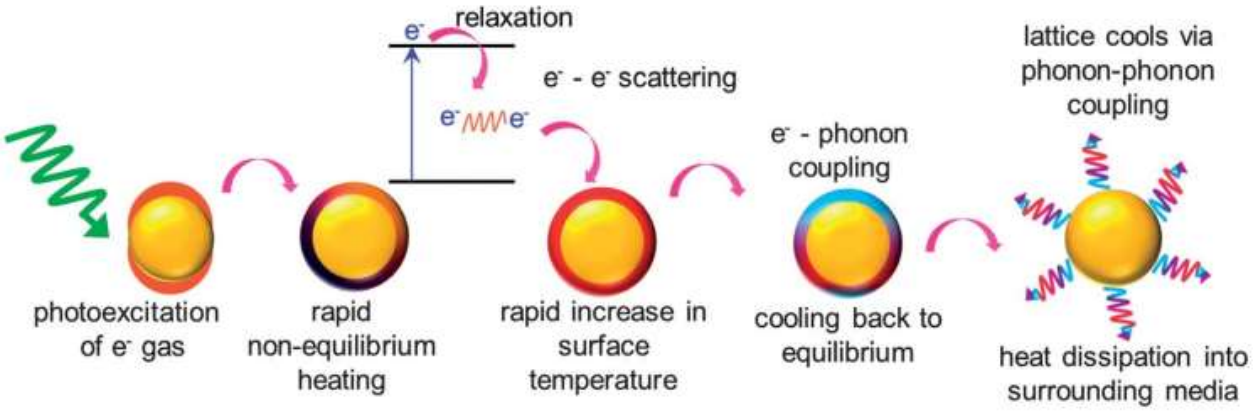


**Figure 1.6:** Schematics of light-to-heat conversion process by plasmonic nanostructures. Adapted from [9].

The photothermal characteristics of plasmonic NPs, with so many potential implications in distinct fields, are understandable looking at the process operated to convert light into heat, schematized in Figure 1.6. Photoexcitation of the electron gas implies a non-equilibrium heating, at subpicosecond timescales relaxation takes place by electron-electron scattering and an increase in the surface temperature of the metal is verified, followed within picoseconds by cooling to equilibrium by energy exchange between electrons and phonons, while finally the phonon-phonon coupling is accounted for the lattice cooling and the heat dissipation into the surrounding medium.[9]

For their photothermal effect, Au NPs are usable as heat sources for thermoelectric devices: the broadband light-absorbing particles in aqueous solutions, subjected to solar radiation, are found to rise the temperature over 100°C, generating steam bubbles with a very high energy yield. Such nanoheaters prove to be employable for multiple purposes, such as water purification or sterilization, and extendable as system to the geographical areas with sunlight as the only available energy source.

The same principle underlies the use of Au NRs in the biomedical field, which combines multiple functionalities within the same plasmonic nanostructures, acting as both diagnostic agents and therapeutic actuators, for theranostics.[10] The extensive light absorption and scattering in the visible and the infra-red regions makes the NRs useful to chemical sensing – via color change upon aggregation, de-aggregation or change in local refractive index, and to biological imaging, as contrast agents for live tissues; moreover, NRs enhance the inelastic light scattering of molecular vibrations near the metal surface, enabling identification with a signal stronger than that of spherical particles.

A plasmonic nanostructure in the body can serve as heat source or drug deliver upon illumination, with the arrive of light to the proper place made feasible thanks to advances in fiber optics, solid-state lasers and endoscopes. Near-infrared light is required for penetration in tissues, since blood has high absorption coefficients in the visible region and water at higher wavelengths,

two biological transparency windows are found to exist at 650-950 nm and 1000-1350 nm. The tunability of optical absorption and scattering in the vis-NIR for Au NRs provides them therefore an inherent advantage over their spherical counterparts, absorbing only in the visible region.

Compared to molecules, Au NRs absorb large amounts of energy, as resulting from the high extinction coefficient exhibited, and by photothermal effect lead to increase in temperature from 10°C to 1000°C, depending on laser power, irradiation time, spot size and their concentration. With the photothermal treatment, irreversible damages to pathogens, cultured cancer cells and tumor tissue are indeed caused even by modest temperature changes, as proved using both *in vitro* and *in vivo* models.

Au NRs are good candidates also as drug delivery vehicles. The high ratio of surface area to volume, common to all the NPs, offers enough space for loading drug and recognition molecules, the latter for the active targeting of the damaged tissue; differently from the other nanocarriers, in the case of Au NRs, the energy absorbed with light and then dissipated releases actively the drugs. Anyway, despite the evident advantages in the use of Au NRs for drug delivery and cancer therapy, more specific studies are necessary before the implementation, because interactions with biological media, with cells and with the same organism are still to be accounted in detail.

# REFERENCES


[1] Maier, S. *Plasmonics. Fundamentals and Applications*; Springer: New York, 2004; Vol. 677.

[2] Aizpurua, J.; Hillenbrand, R. Localized Surface Plasmons: Basics and Applications in Field-Enhanced Spectroscopy. In *Plasmonics. From Basics to Advanced Topics*; Enoch, S.; Bonod, N., Eds.; Springer Series in Optical Sciences; Vol. 167, pp. 151–176.

[3] García de Abajo, F. J. Simple Analytical Theory Methods in Nanophotonics. Seminary given at CIC biomaGUNE in July 2017.

[4] https://nanocomposix.com/pages/plasmonics

[5] Solís, D. M.; Taboada, J. M.; Obelleiro, F.; Liz-Marzán L. M.; García de Abajo F. J. Toward Ultimate Nanoplasmonics Modeling. *ACS nano*, **2014**, *8* (8), 7559-7570.

[6] Myroshnychenko, V.; Rodríguez-Fernández, J.; Pastoriza-Santos, I.; Funston, A. M.; Novo, C.; Mulvaney, P.; Liz-Marzán, L. M.; García de Abajo, F. J. Modelling the optical response of gold nanoparticles. *Chemical Society Reviews*, **2008**, *37*, 1792–1805.

[7] Jing, H.; Zhang, L.; Wang, H. Geometrically Tunable Optical Properties of Metal Nanoparticles. In *UV-VIS and Photoluminescence Spectroscopy for Nanomaterials Characterization*; Kumar, Challa S.S.R., Ed.; Springer Series in Nanoscience and Nanotechnology; Springer Berlin Heidelberg: Berlin, Heidelberg, 2013; Vol. 2, pp 1-74.

[8] Jimenez de Aberasturi, D.; Serrano-Montes, A. B.; Liz-Marzán, L. M. Modern Applications of Plasmonic Nanoparticles: From Energy to Health. *Advanced Optical Materials*, **2015**, *3*, 602–617.

[9] Webb, J. A.; Bardhan, R. Emerging Advances in Nanomedicine with Engineered Gold Nanostructures. *Nanoscale*, **2014**, *6*, 2502-2530.

[10] Alkilany, A. M.; Thompson, L. B.; Boulos, S. P.; Sisco, P. N.; Murphy, C. J. Gold Nanorods: Their Potential for Photothermal Therapeutics and Drug Delivery, Tempered by the Complexity of Their Biological Interactions. *Advanced Drug Delivery Reviews*, **2012**, *64*, 190–199.

# Chapter 2

# Batch synthesis of Au NRs

Shape and size control are keys to the engineering of metallic nanostructures as functional materials, giving access to the tunability in the position of localized surface plasmon resonance. Empirically developed synthetic methods, such as the seed-mediated one, are nowadays used for the growth of anisotropic nanocrystals, among which Au NRs are undoubtedly the most intensively studied. We are going to present the silver-assisted route, accounting all the variables and agents involved, providing insights on the growth mechanism and reporting some experimental results obtained in our laboratory.

## 2.1 Questing for shape control

Metallic and semiconductor wires of nanoscale dimensions, also known as whiskers, were synthesized by the vapor-liquid-solid approach since the 1960s, but only in the mid-1990s it was demonstrated that Au NRs could be obtained recurring to wet chemistry methods. As in the steps reported in Figure 2.1.1, chronological progresses implied improvement in material quality and decrease in the synthesis difficulty.[1]

The initial pioneering studies were made by Martin and co-workers using the hard template method, based on the electrochemical deposition of Au on metallic films previously sputtered within the nanopores of polycarbonate, silica or alumina membranes, and the selective

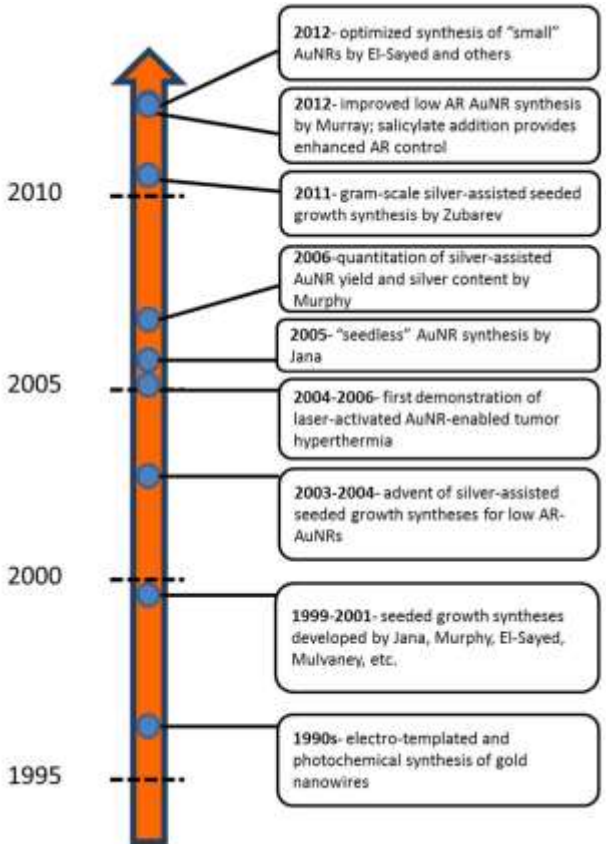


**Figure 2.1.1**: timeline of significant developments in the synthesis of Au NRs. Adapted from [1].

dissolution of both membrane and film. The so-performed syntheses were limited by a low yield and gave arrays of wires with micrometer scale dimensions, confirming basic optical effects but not displaying plasmonic properties.[1],[2]

High yields and plasmonic absorbances were observed instead with the soft template method, a synthesis conducted within an electrochemical cell. A gold metal plate was used as sacrificial anode, a platinum plate worked as cathode and behind it a silver plate was gradually immersed. Alkyl bromide salts, such as CTAB and TCAB, were chosen as cationic surfactants, because known to be effective electrolytes and to form cylindrical micelles that might influence the growth direction, with CTAB serving also as stabilizer, preventing the nanoparticles aggregation. Earliest studies were thus enabled on the optics of these Au NRs, that were single crystalline and with dimensions of approximately 60 × 12 nm.[1],[2]

Major defects – common to the soft template electrochemical method and to the photoreduction approaches concurrently developed, were the intensive requirement of energy, the difficulty to scale and the shape distribution of the synthesis, leading always to a mixture of spheres, rods, cubes, plates and prisms. A new and still valid approach to Au NRs synthesis was introduced at the dawn of XXI century, the seeded growth method, in which preformed small gold NPs (the seeds) are added to solutions containing Au(I) and CTAB and grow into NRs. Guaranteeing strict control over shape and size distributions, the convenient and versatile method gave to the scientists unprecedented access to Au NRs and extended to other anisotropic NPs.[1]-[3]

Specifically, shape control is given by the main characteristics of the method, the temporal and physical separation between nucleation and growth, that depend on opposite conditions. High supersaturation leads to fast nucleation rate of uniform and isotropic Au nanocrystals, with sizes in the 1-5 nm range. Such conditions would ensure also rapid growth of all facets and are therefore altered; milder reducing conditions are met, implying that growth proceeds at a slower rate than the previous stage, with the addition of more Au ions, a weaker reductant and a kind of shape templating surfactant or agent. A symmetry-breaking event occurs, and thus selective growth of facets takes place: isotropic seeds grow into anisotropic NPs.

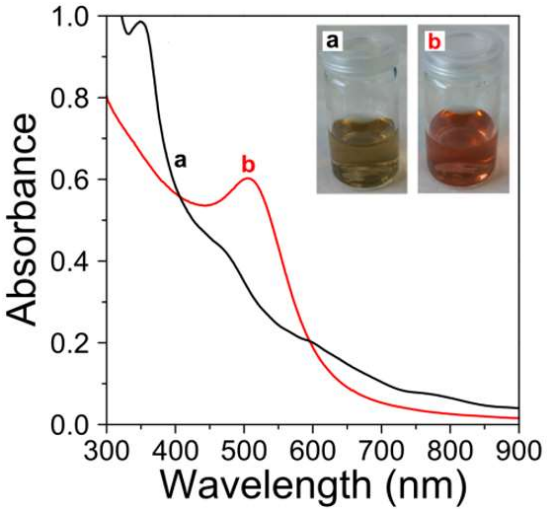


**Figure 2.1.2:** UV-vis-NIR absorbance spectra of CTAB-coated (a) and citrate-coated (b) Au seeds to grow into single crystal and penta-twinned NRs.

The earliest formulation of the synthesis involved citrate-stabilized seeds, with a size of 3.5 nm, that grow into penta-twinned crystals characterized by aspect ratios varying from 6 to 20, in low overall yield. It was soon found that seeds are stabilizable with CTAB, resulting smaller, with a size of 1.5 nm. The difference in size is denotable in Figure 2.1.2, as we see that citrate-stabilized seeds present a plasmonic band, while CTAB-stabilized do not, since quantum effects prevail over classical electromagnetism at such range. Other features differentiate them, it is to say that CTAB-stabilized seeds grow into single crystal rods with ARs from 1,5 to 5, a rod yield of 95% relative to other shapes and a 15% yield as referred to total [Au]. [4]

Differences are observable even between the crystalline structures of the seeds, as evidenced in Figure 2.1.3d&e, since high resolution TEM analysis revealed that citrate-stabilized seeds are intrinsic multiply-twinned particles (MTPs), while the CTAB-stabilized are single crystalline (SC). MTP seeds present the wine-red color so typical of gold colloids and the larger dimensions enhance the stability up to some days if stored in fridge. It is nevertheless to remark that in any synthesis a mixture of seeds presenting different crystallographic habits is obtained: single crystalline, mono-twinned and penta-twinned populations, then dramatically impacting the shape yield in rods growth.

Experiments run in the years demonstrated that rods grown from MTP seeds in absence of silver ion exhibit a pentagonal cross section and a perfect five-fold twinning, as in Figure 2.1.3g, while the addition of $Ag^+$ leads to an increase in rod yield and a stricter control over aspect ratio but results also in the formation of needle-like particles, as that in Figure 2.1.3c, recognized to be bipyramids. Conversely, for SC seeds the absence of $Ag^+$ causes the growth of nanoparticles showing a wide variety of shapes, mainly spheres, triangles and rods, as in Figure 2.1.3f, while we are going to see that its presence assures a high shape yield, allowing to tune the rods AR, as in Figure 2.1.3a&b.

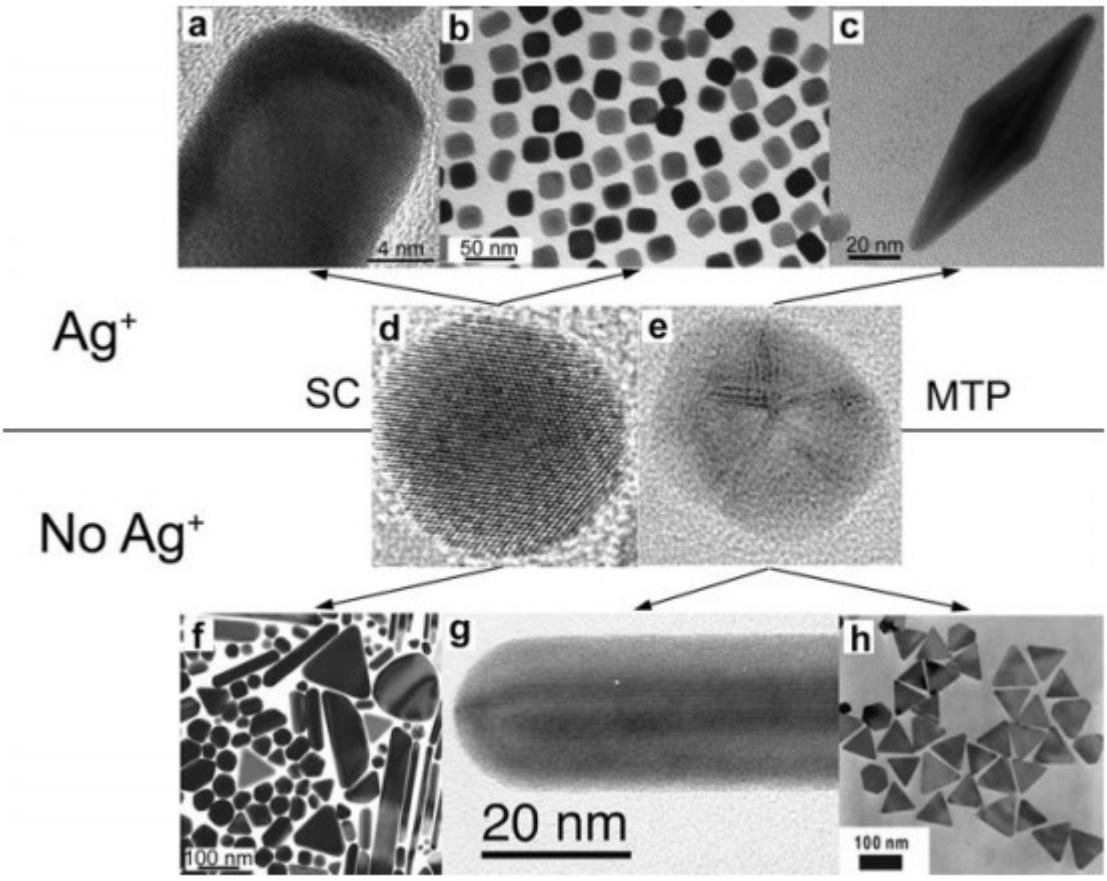


**Figure 2.1.3**: Morphology dependence of Au NPs grown from either single crystal (d) or multiply twinned (e) seeds, in the presence (a-c) and absence (f-h) of silver nitrate. Adapted from [4].

The present work concerns specifically single crystal NRs, we are therefore going to detail all the variables and agents involved in the silver-assisted synthesis – but, before that, we deal with its crystalline structure. They possess an octagonal cross section as those synthesized electrochemically but, differently from the latter, present the same higher-index lateral facets characterized by equal surface areas. It was demonstrated only in 2010, when all different orientations and crystallographic directions could be studied, on NRs standing perpendicular to the TEM grid, and many interpretations regarding growth, reactivity and adsorption properties had consequently to be revisited.[5]

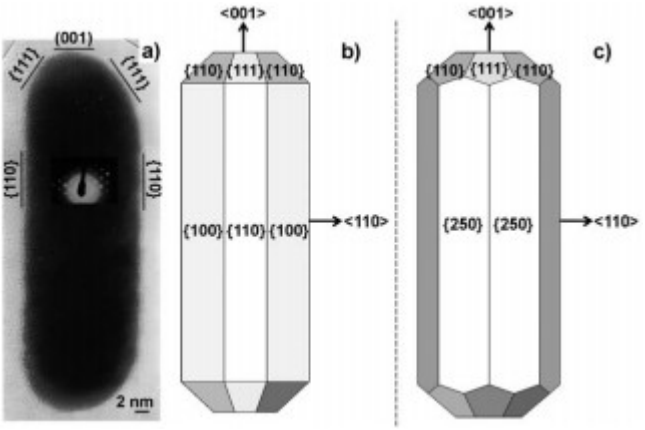


**Figure 2.1.4:** Comparison of analysis (a) and model (b) based on electrochemically synthesized NRs with the model (c) for NRs obtained by seeded chemical growth. Adapted from [5].

The {250} facets display a more open and accessible structure for silver, uniformly decreasing the growth rate compared to the other ones of Au face-centered-cubic lattice and favoring thus the one-dimensional growth. The reason for the system to expose such high-index facets may relate to its single-crystalline structure: indeed, the tendency of Au NPs to develop stacking faults and twin plans derives from the need to release the inner stress of each twin, seen as a single crystal. The absence of twin planes in single crystal NRs could be energetically compensated by exhibiting such indexes, which allow greater structural flexibility, and by the rounding of the facets. The presence of {250} facets explain also the low thermal stability of Au NRs, with consequent reshaping into more spherical shapes, even at mild temperatures.

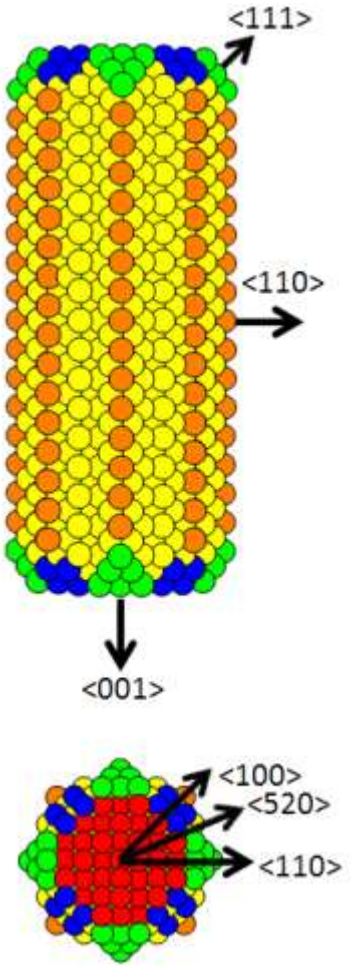


**Figure 2.1.5:** Model in the [110] and in the [001] zone axes, in top and in bottom panels. Color code refers with yellow to inner atoms, with red to {100} facets, with blue to the {110}, with green to the {111} and with orange to the {250}. Adapted from [5].

The model proposed for crystalline structure, based on rods both lying flat and standing perpendicular during the observations, is reported in Figure 2.1.5, respectively in the [110] zone axis for the lateral view and in the [001] zone axis for the view from the top or

from the bottom. The directions <100> and <110> point to the edges between the {250} facets, that converge at the tips in the form of {110} and {111} facets.

## 2.2 The silver-assisted route

The main features of the path leading to the growth of single crystal NRs have already been mentioned; firstly, in an aqueous CTAB-solution, supersaturate Au(III) ions are reduced to Au(0) by a very strong reductant, sodium borohydride, and nucleate into isotropic particles; secondly, these seeds are injected into a growth solution, with the same [CTAB], in presence of $Ag^+$ and of Au(I) ions, the latter previously reduced by a moderate reductant, ascorbic acid. In this section we are going to analyze in detail the roles of each chemical specie involved.

### 2.2.1 The surfactant

Hexadecyl trimethylammonium bromide, abbreviated as CTAB, has been chosen as surfactant from the very beginning, since a wide range of literature on its rheology and phase behavior was available; it was thought to act as face-specific capping agent alone for penta-twinned rods, and in the form of a $CTA^+$–$Br^-$–$Ag^+$ complex for single crystals, favoring the one-dimensional growth. Particularly for the silver-assisted procedure, recent works proved the higher importance of $Br^-$ counterion than that of $CTA^+$ in directing the NRs growth, equally verified in the presence of CTAB or KBr.

The requirements to NRs growth satisfied by the choice of CTAB are identified with the presence of, respectively, a quaternary ammonium head group (forming a complex with gold precursor, whose redox potential is then modified), bromide as counterion, a carbon tail of the proper length (stabilizing the rods and achieving solubility at room temperature).

NRs are produced with a CTAB bilayer, with one leaflet associated with the gold surface and the other facing the aqueous media, both via the quaternary ammonium head groups and guaranteeing hydrophilic interactions, while surfactant tails interact hydrophobically in the bilayer core. Surfactant is bound to gold surface through electrostatic interactions between the cationic head group and anionic sites, but the nature of the latter remains still objects of studies and discussions, maybe bromide ions, bromide and silver related species, or other ones too.[6]

Another aspect to remark here is that most syntheses are conducted in 0.1 M CTAB solutions, and then finally the surfactant is found to coexist bound to the NRs and free, even after purification. Temperature decrease and time passing lead to free surfactant crystallization and precipitation in form of white flocs, that is the reason for centrifuging at least once the samples at growth completed and removing the supernatant. From the applicative point of view, moreover, free CTAB is demonstrated to cause cell death, NRs must therefore be subjected to several cleaning controls before being used in biomedical field.

### 2.2.2 The gold precursor

The most employed salt for Au NPs synthesis is undoubtedly tetra chloroauric acid, $HAuCl_4$, usually prepared as stock solution, with a yield and other characteristics that may variate in each laboratory. Au(III) is the oxidation state of gold in $HAuCl_4$, a $d^8$ metal center presenting the tendency to form square planar complexes, in the case of halides with a complexation strength in the order $I^->Br^->Cl^-$. In presence of CTAB, the chlorides ligands in $[AuCl_4]^-$ are replaced by bromide ions, as in (2.2.2).

$$[AuCl_4]^- \rightleftharpoons [AuCl_3Br]^- \rightleftharpoons [AuCl_2Br_2]^- \rightleftharpoons [AuClBr_3]^- \rightleftharpoons [AuBr_4]^- \quad (2.2.2)$$

As the exchange occurs, a color change is observable in the solution, from pale to dark-orange yellow; $[AuBr_4]^-$ ions form an ion-pair with the cationic head groups, while both ligand exchange and $[AuBr_4]^- – CTA^+$ formation shift in cathodic sense the respective reduction potentials, influencing the growth kinetics. It is understandable then the importance to ensure, for instance stirring the solution, the complete dissolution of gold salt and the completion of ligand exchange.[7]

### 2.2.3 The seeds

An aqueous solution of excess $NaBH_4$, a hygroscopic specie reactive with the water in the air, is added as fast as possible to that containing CTAB, supersaturate in Au(III), under vigorous stirring. The rapid reduction produces metallic gold nuclei, or nanoclusters, i.e., molecular-like species, that coalesce to form larger nanocrystals, that are generally 1.5 nm in diameter. Seeds formation results in the almost instantaneous turn in solution color from dark-orange yellow to light brown, honey-like.

Such seeds are highly reactive but also storable for 2 hours between 27 and 29°C, allowing the complete decomposition of the borohydride ions. There is no plasmonic band for so small particles, as already stated, and monitoring the solution color may provide valuable information: a red-pink shade unequivocally means the presence of bigger and spherical NPs, likely unable to grow into anisotropic particles. Aging is also known to affect the seeds quality, as we see in Figure 2.2.3, with absorbance spectra subjected to changes over time, from monotonously-decaying profiles to the emergence of maximum peaks, attributable to localized surface plasmon resonance of nanospheres.[8]

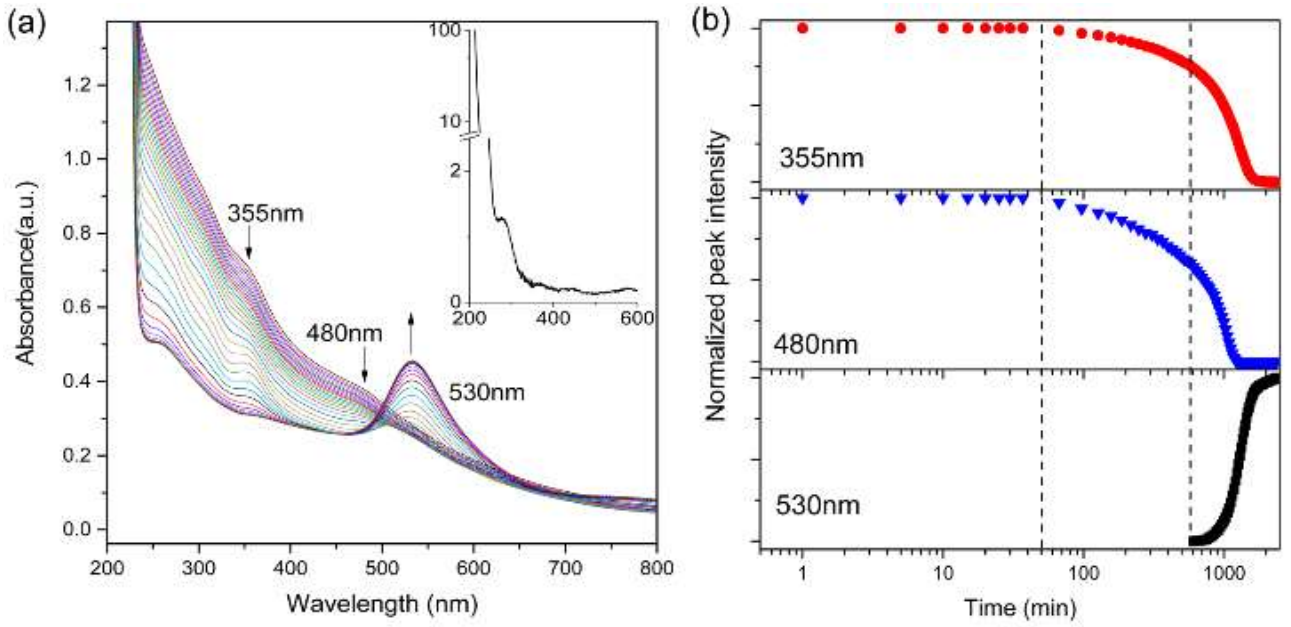


**Figure 2.2.3:** UV-vis-NIR absorbance spectra of seed solution during seed aging at 25°C taken at 30 min intervals, with absorbance of CTAB 0.1 M solution shown as inset, in (**a**); normalized absorbance peak intensity as function of time, respectively at 355, 480 and 530 nm, in (**b**). Adapted from [8].

Analyzing the temporal evolution of spectra, the strong absorbance measured initially for seed solution at wavelengths lower than 225 nm derives from that shown by CTAB, while flexes are observable at 355 and 480 nm, progressively less pronounced as 40 min passed from the $NaBH_4$ injection, and then, after 10 h, a peak is found at 530 nm. As known from literature, the flexes may be related to electronic transitions between quantized levels of energy in nanoclusters composed by different amounts of Au atoms, that determine the size and consequently the optical energy gap.[8]-[10]

According to the framework presented, the decrease over time in the intensity measured at 355 and 480 nm is readable as the disappearance of nanoclusters, and the increase at 530 nm as the appearance of particles with diameter higher than 2 nm, hence supporting plasmon resonance. Aging evidently affects the seeds, with agglomeration and formation of nanospheres. These specific data on seeds absorbance and stability are included here because in the experimental section we will examine the aging effect on NRs growth, presenting instead our findings.

## 2.2.4 The weak reductant

Once seeds are formed, they must be injected into a growth solution, containing CTAB and Au(I); the equilibrium among the gold oxidation states is reported in (2.2.4), movable towards comproportionation or disproportionation reactions according to the relative stability of each specie.

$$Au^{3+} + 2Au^{0} \rightleftharpoons 3Au^{+} \qquad (2.2.4)$$

The most popular choice for reducing Au(III) into Au(I) ions is L-ascorbic acid, defined as weak because is not so strong to give reduction into Au(0) but guarantees a high yield, avoiding therefore secondary nucleation during the growth and the oxidation of seeds injected by the comproportionation reaction. When ascorbic acid is added, the solution containing CTAB and $HAuCl_4$ turns colorless since there is no ligand-to-metal charge transfer band for a $d^{10}$ metal center as Au(I). Seeds then act as catalysts for the final reduction step on their surface, from Au(I) to Au(0) contained in NRs. The net reaction is depicted in Figure 2.2.4, with the two mechanisms hypothesized for the final reduction.

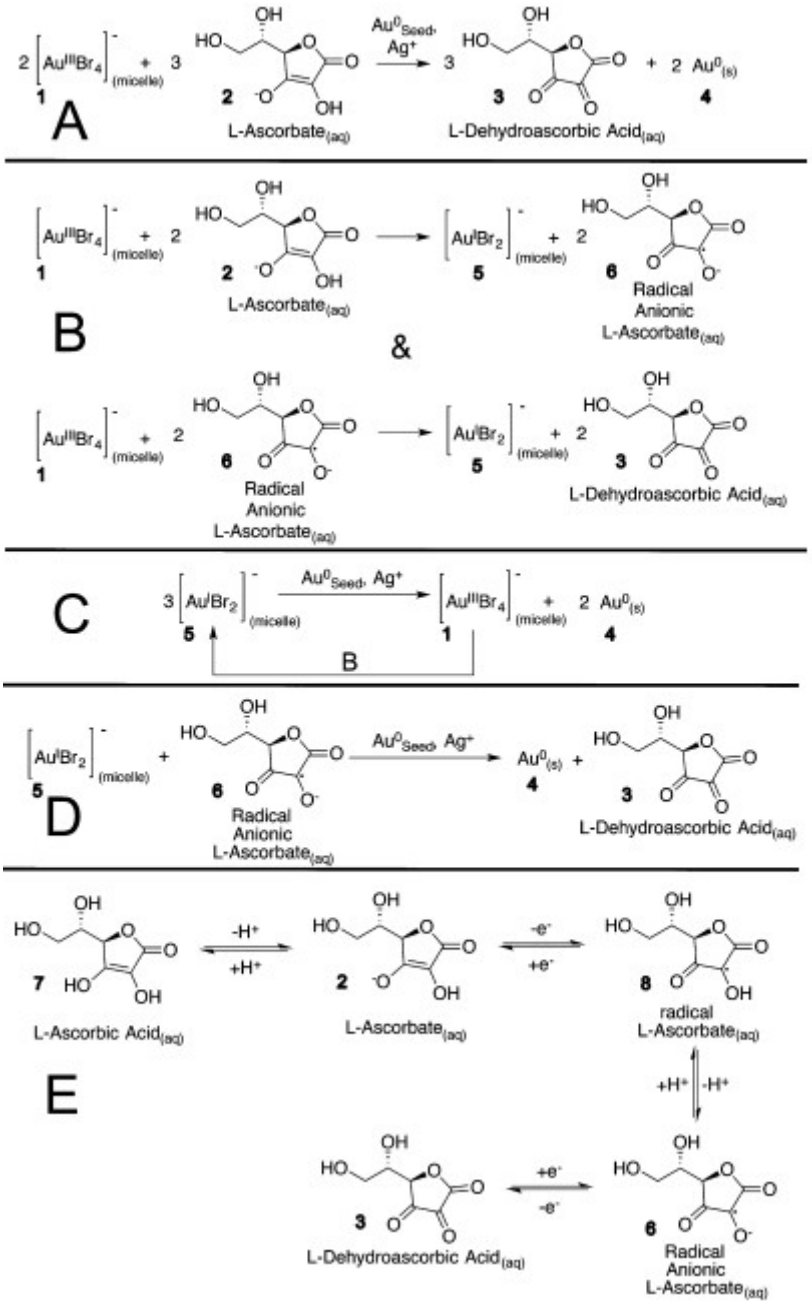


**Figure 2.2.4:** Net reaction, in (A); primary reduction of Au(III) to Au(I), in (B); disproportionation reaction of Au(I) to Au(III) and Au(0), in (C); direct reduction of Au(I) to Au(0), in (D); oxidation of L-ascorbic acid to L-dehydroascorbic acid, in (E). Differently from bromide ions, only Au is shown balanced. Adapted from [11].

Under the acidic conditions of the synthesis, L-ascorbic acid is present in the form of L-ascorbate, whose radical anion act as secondary reductant for Au(III) ions in micelles, as in Figure 2.2.4B. The two mechanisms generally proposed for the final reduction are instead the disproportionation and the direct reduction, reported respectively in Figure 2.2.4C&D, both catalyzed by metallic gold and producing it too, and thereby classifiable as autocatalytic.[11]

It is also to report that ascorbic acid has a pH-dependent reduction potential, lower at acidic conditions and higher at lower ones, inevitably influencing the growth of Au NRs. Decomposition of ascorbic acid is indeed catalyzed by the presence of metallic surface as that of the Au seeds and of the growing NPs, and the radical anionic L-ascorbate is identified as active reductant in the system; in this context, the lowering of solution pH results in slower reaction rate and high fraction of single crystalline NRs.[12]

A lost point to remark here is that the reduction-yield is easily estimable, just recurring to spectrophotometry. The absorbance measured at 400 nm determines the amount of gold precursor reduced to the metallic state, with a value of 1.2 corresponding to a 0.5 mM Au concentration, as demonstrated by numerical calculations and then elemental analyses. Regardless of particles shape and size, at the wavelength of 400 nm the main contribution to absorbance stems from absorption due to interband transitions in metallic gold.

## 2.2.5 The silver ions

The specific role of silver ions in Au NRs synthesis still constitutes matter of debate, it remains unclear whether they are involved in just the symmetry breaking step or influence also the subsequent growth step. Elemental analysis showed that about 9% of a NR is Ag, present as surface atoms, X-ray photoelectron spectroscopy confirmed Br adsorption and both Au–Br, Ag–Br interactions, while surface-assisted laser desorption/ionization time-of-flight mass spectroscopy identified adsorbed $[Br–Ag–Br]^-$ ions on the gold surface.

It is well-established the ability to control the NRs aspect ratio by varying the silver nitrate concentration in the synthesis, but the way it happens is still to clarify definitely – as reported in Figure 2.2.5, three mechanisms

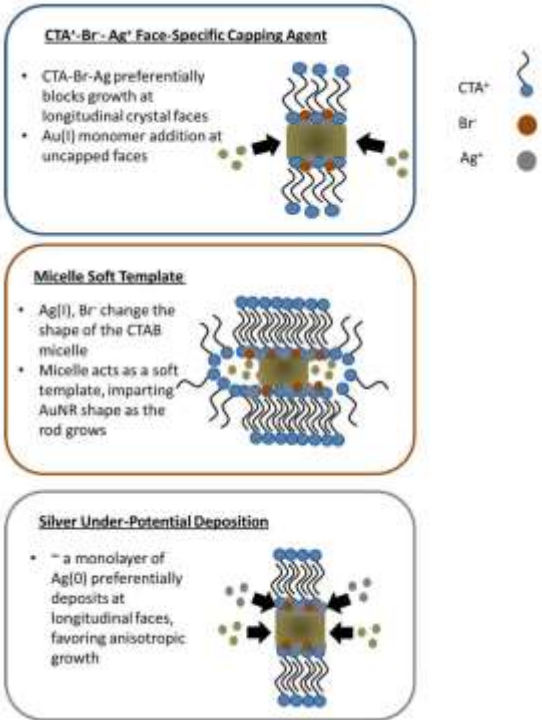


**Figure 2.2.5:** Main proposed mechanisms explaining the role of Ag in the seeded growth of single crystal Au NRs. Adapted from [1].

have been advanced to account for it: the action of a CTA–Br–$Ag^+$ complex as face-specific capping agent; the synergy of Ag and Br in altering the shape of CTAB micelles from spherical to cylindrical, as soft template agents; the deposition of a sub-monolayer quantity of metallic Ag on the longitudinal facets of Au NRs. Experimental data have been so far supporting each mechanism, and it is also possible that all them are verified in the same pot to some extent.[13]-[15]

## 2.3 From isotropic seeds to anisotropic NPs

The growth of Au NRs is characterized by slow kinetics, requiring indeed several hours to be complete. Two separate stages are identifiable, observing the temporal evolution of optical spectra and the TEM micrographs taken after samples stabilization. As reported in Figure 2.3.1, a fast redshift of the longitudinal band is verified during the first minutes, evidently due to the anisotropy institution during Au reduction to metallic state, then followed by a slow blueshift, that continues even at reduction completed, attributable to the reshaping from a dumbbell-like morphology to proper rods, at the tips.

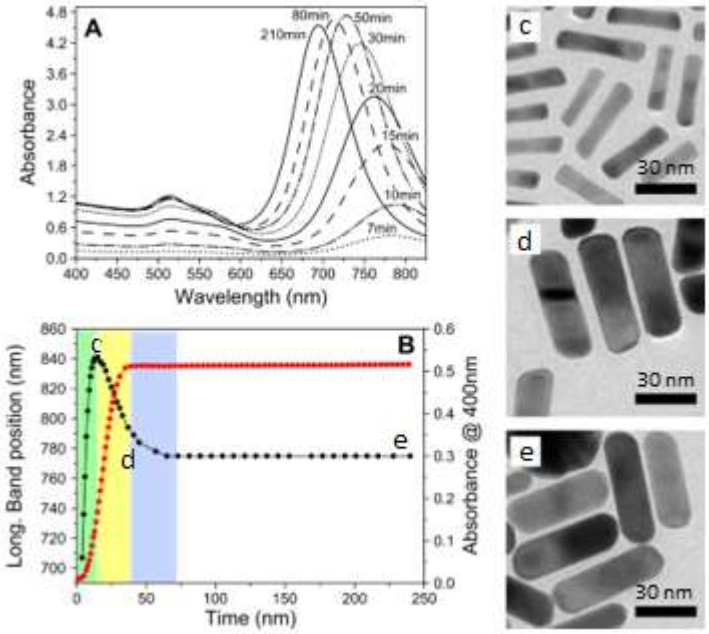


**Figure 2.3.1:** UV-vis-NIR spectra of a growing Au NRs solution, in (A); position of the longitudinal plasmon band (black line) and absorbance value at 400 nm (red line) as functions of time, in (B); TEM micrographs of growing NRs at the maximum red-shift of the longitudinal plasmon band, in (c), at reduction completed, in (d), and at growth concluded, in (e).

Mystery still pervades on what happens in the earliest stage, the symmetry-breaking event, on how and why an isotropic seed particle with a face-centered cubic lattice grows into two of six symmetry-equivalent directions. Many interpretations have been proposed in the years, here we limit to expose the latest discoveries on that useful to understand more deeply the influence of the agents already described.

TEM analyses reveal that more than half of the seeds synthesized in CTAB are single-crystals, specifically recognized as cuboctahedra. Wulff theory predicts indeed the cuboctahedron to be the minimum energy structure for face-centered cubic metals, but on that size range, below 10 nm, the free energy in gold is minimized by multiple twins, with the inclusion of {111} facets leading to strained structures such icosahedra and decahedra. CTAB adsorbs to the particle surface and evidently modifies the energetics of {100} facets relative to the {111}, resulting in a minimum energy morphology different from that expected, given by conventional thermodynamics considerations.[13]

Decahedra is, as a matter of fact, the crystalline structure of citrate-stabilized seeds, that grow into penta-twinned NRs. Focusing again on our cuboctahedra, presenting 8 {111} facets and 6 {100} arranged symmetrically, the reason for asymmetric growth remains unknown. With {111} and {100} facets respectively allowing and inhibiting growth, the resulting particle is supposable to be a cube bound by {100}, a common byproduct of NRs synthesis. Instead, a symmetry-breaking event occurs.

Investigations conducted with atomic resolution TEM on seeds overgrown, 4-6 nm in diameter, permitted to observe higher-index truncations: a plane face parallel to the <110> direction is present where the two {111} should meet, as reported in Figure 2.3.2. Such incorporation of higher-index truncating surface may be read in terms of edge effects removal, as energetically favorable. Since for seeds overgrown in absence of $Ag^+$ ions the truncations are instead sub-nanometer in size, it is possible that the truncations are stabilized by a silver layer, given the more open atomic structure compared to close-packed {111} and {100} surfaces, a stabilization that prevents further Au atoms deposition on them, becoming instead side facets in the growing embryonic NR structure.[14]

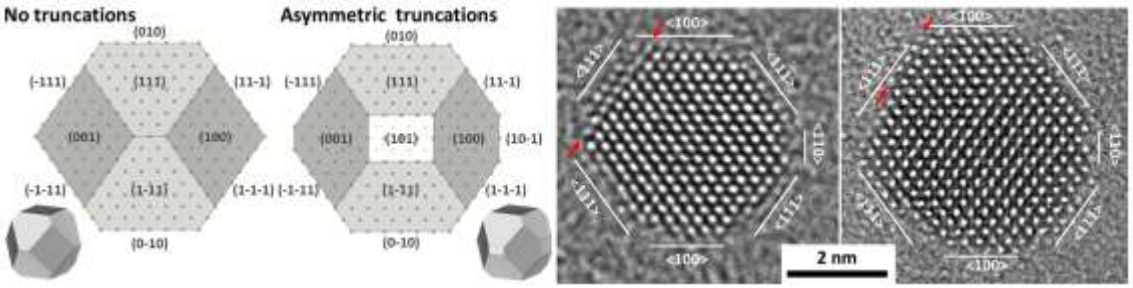


**Figure 2.3.2:** particle models of a perfect cuboctahedron and a cuboctahedron incorporating asymmetric {110} truncations, on the left; TEM micrographs of Au seeds overgrown in presence of $AgNO_3$, matching the asymmetrically truncated cuboctahedron model, with arrows indicating the additional atoms, on the right. Adapted from [14].

Atomic level characterization, this time on particles grown for 6 and 20 minutes after the seed injection, revealed surprisingly the presence of twin planes in the growing NRs, as in Figure 2.3.3, while the final products were found again to be single-crystal structures. Twins are along the {111} plane, lying few atomic layers from the surface and terminating where tip and side facets meet. With the further Au atoms deposition, the layers become complete and are shifted via a simple glide mechanism, that gives coherent interfaces at the edges of the meeting facets, forming a single crystal.[14]

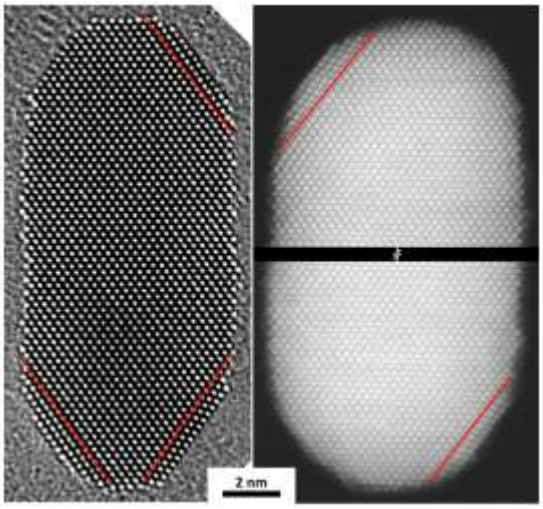


**Figure 2.3.3:** TEM micrograph of Au NR after 6 min of growth, on the left, and ADF STEM micrograph of NR tips after 20 min of growth, on the right, both displaying twin planes parallel to tips facets, with boundaries delineated by red lines. Adapted from [14].

Twins and partial surface layers parallel to the {111} plane suggest such facets as the preferred sites for Au deposition, explaining thereby the dumbbell-like morphologies observed at intermediate stages. Bipyramids presenting a high proportion of {111} facets are also found as typical byproducts, grown up to five times the size of the NRs from the same growth solution. To sum up what found, some

clues on the process of asymmetric growth are evidently provided by the observation of twin planes and truncations, with the latter appearing for seeds size of 4-6 nm and likely stabilized by $Ag^+$ ions.

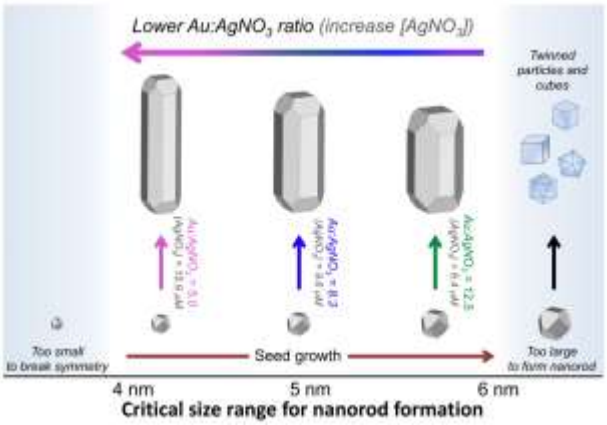


**Figure 2.3.4:** Summary of the effect of $[AgNO_3]$ on the symmetry-breaking size and asymmetric growth start, with corresponding width and aspect ratio control. Adapted from [15].

Other experiments under a wide range of solution conditions, with exhaustive statistical studies based on TEM micrographs, confirmed that the symmetry breaking occurs within the 4-6 nm range for cuboctahedral seeds, and found that the absolute size is determined by the ratio of $[HAuCl_4]$ over $[AgNO_3]$, increasing proportionally with it, at constant concentrations of ascorbic acid and CTAB. The symmetry-breaking size is naturally considerable as the one at which asymmetric growth properly starts; as summarized in Figure 2.3.4, it was verified that symmetry-breaking size arrives to define the final width of the NR, whose length depends instead upon the available [Au], both concurring in the aspect ratio control.[15]

These latest findings exposed furtherly reaffirmed the importance of $Ag^+$ ions and emphasize how crucial is the symmetry-breaking moment for the particles to form. The sections on the state-of-the-art knowledge on Au NRs batch synthesis are now concluded: the main features have so far been described, giving space to all the agents and variables involved, with some insights on the growth mechanism and the models proposed for understanding it – we are now going to present our work.

## 2.4 Experimental section

MATERIALS Hexadecyltrimethylammonium bromide (CTAB, ≥ 96%), hydrogen tetrachloroaurate trihydrate ($HAuCl_4 \cdot H_2O$, ≥ 99.9%), silver nitrate ($AgNO_3$, ≥ 99%), L-ascorbic acid (≥ 99%), and sodium borohydride ($NaBH_4$, ≥ 99%) were purchased from Aldrich. All the chemicals were used as received. Milli-Q water (with resistivity 18 MΩ·cm at 25°C) was used in all the experiments. All glassware was washed with aqua regia, rinsed with water, sonicated three-fold for 3 min with Milli-Q water and dried before use.

CHARACTERIZATION Optical extinction spectra were recorded using an Agilent 8453 UV-vis-NIR diode-array spectrophotometer and were multiplied by the respective dilution factors to facilitate comparison of the data. TEM micrographs were collected with a JEOL JEM-1400PLUS instrument operating at 120 kV, using carbon-coated 400 square mesh copper grids; all samples were centrifuged three times before dropping it on the TEM grids.

UV-vis-NIR spectroscopy and transmission electron microscopy are complementary to each other for Au NRs characterization. We will recur systematically to TEM analyses only in the next chapter, characterizing the peculiar and unique work done on NRs, while here the mostly already-known aspects are studied from optical extinction spectra. As we see in Figure 2.4, the absorbance measured at 400 nm is a parameter to monitor, indicative of reduction-yield to metallic Au, since the Au(0) concentration is derivable from it.

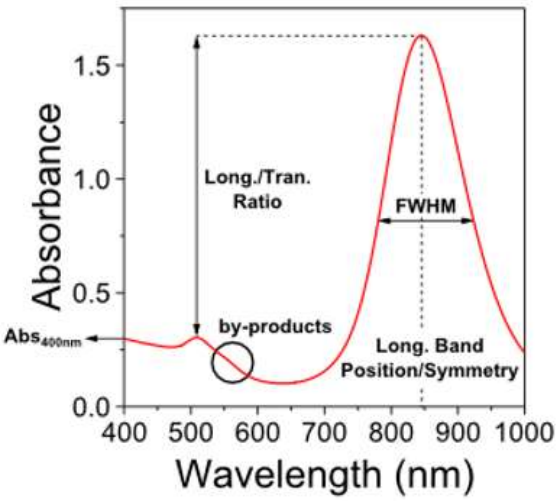


**Figure 2.4**: Typical UV-vis-NIR spectrum of a single-crystal Au NR colloid, with parameters indicative of product quality.

Shape purity (i.e., the fraction of NPs presenting the desired shape) is semi-quantitatively measured by determining the ratio of the longitudinal over the transverse LSPR peaks, due to the overlap of the latter of rods with that of spheres; it will be calculated and indicated in each case as quality ratio, whereas instead a more quantitative measure of purity is the fraction of particles with rod-like morphology as counted in TEM micrographs.

Furthermore, in optical spectra, the presence of a shoulder on the transverse band indicates the formation of by-products with different shapes. Other precious information is readable specifically from the longitudinal band: the peak position allows an estimation of the average aspect ratio, and the symmetry (valued in terms of full width at half maximum, FWHM) is a measure of size dispersion.

METHODS In a water bath at 30°C, 25 µL of 50 mM $HAuCl_4$ are added to 5 mL of 0.1 M CTAB solution, then stirred until the disappearing of any turbidity sign. 300 µL of freshly prepared 10 mM $NaBH_4$ are rapidly injected under vigorous stirring, with solution turning brown as seeds nucleate. Meanwhile, growth solution is prepared: 10 mL of 0,1 M CTAB, to which 100 µL of 50 mM $HAuCl_4$, 120 µL of 10 mM $AgNO_3$ and 200 µL of 1 M HCl are added; 80 µL of 0,1 M ascorbic acid are added, and then, after the solution turns colorless, 16 µL of seeds solution are poured into it. At least 2 h are to be waited before considering the growth completed and analyzing the so-formed Au NRs.

Such procedure is the standard protocol followed in our laboratory for the growth of Au NRs with longitudinal LSPR in the range of 800 – 900 nm, i.e., with AR close to 3, we are now going to prove its validity with some experiences, modifying the quantities and parameters involved, for observing then the results obtained. As already stated several times, the effectiveness of the seed-mediated method is founded on the separation between seeds nucleation and anisotropic growth, the experiments are thus classified as affecting, distinctively, seeds quality or growth.

## 2.4.1 Experiences with seeds quality

As reported in previous sections, the initial step is the very fast nucleation of seeds, octahedral Au NPs smaller than 2 nm in size, by adding a strong reductant in Au supersaturated solution under vigorous stirring. Seeds with such size are found to form only in presence of CTAB, that stabilizes certain facets, and to aggregate with time into plasmonic nanospheres, thereby unable to grow into anisotropic NPs when moved to the growth solution. Our first experience, as reported in Figure & Table 2.4.1.1, concerned the set-on of different stirring conditions and the aging effect on seeds.

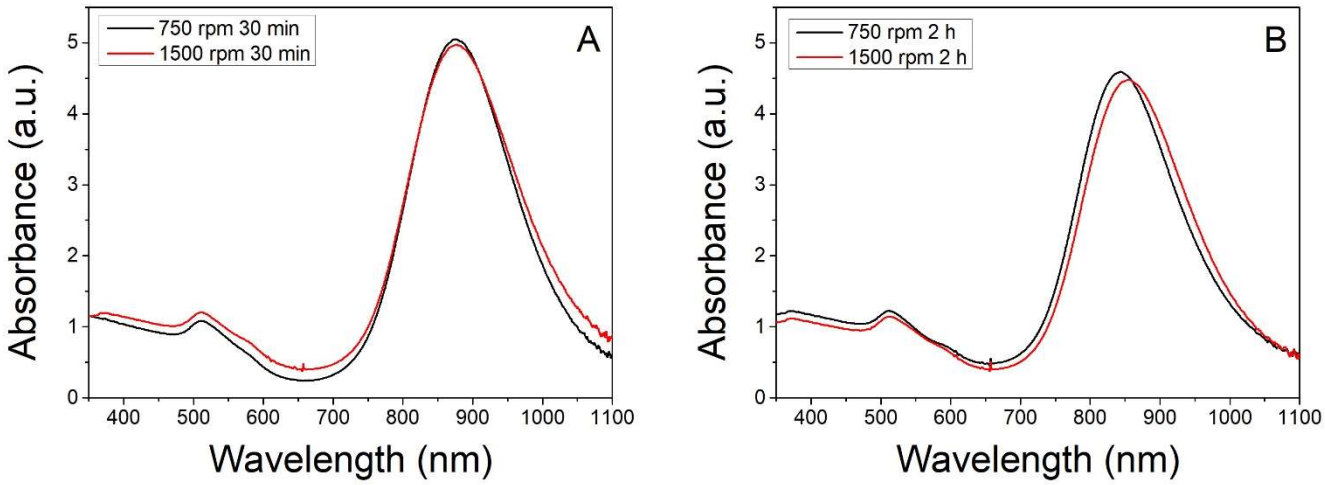


**Figure 2.4.1.1:** UV-vis-NIR absorbance spectra of Au NRs grown from seeds synthesized at 750 rpm (black line) and 1500 rpm (red line), respectively 30 min (in **A**) and 2 h old (in **B**).

| **Stirring conditions at $NaBH_4$ addition** | **Seeds age** | **Longitudinal LSPR position [nm]** | **Quality ratio [adim]** | **FWHM [nm]** |
|---|---|---|---|---|
| **750 rpm** | 30 min | 874 | 4,6 | 178 |
| | 2 h | 844 | 3,7 | 178 |
| **1500 rpm** | 30 min | 878 | 4,1 | 190 |
| | 2 h | 856 | 3,9 | 184 |

**Table 2.4.1.1:** data from the absorbance spectra of Au NRs grown from seeds synthesized at 750 rpm and 1500 rpm, 30 min and 2 h old.

Observing the data on NRs grown from fresher seeds, the change in stirring conditions from 750 to 1500 rpm, the double, results in different shape and size dispersions, better in the case of lower rotational speed; the position found for longitudinal LSPR differs just by 4 nm, indicating that such change in stirring does not influence the AR. Comparing also the spectra of NRs grown from 2 h old seeds, a blue-shift is measured instead for both rotational speeds, readable as lower AR, exhibited by

NRs grown from older and consequently bigger seeds; distinctively, aging is here found to affect shape purity for seeds synthesized at 750 rpm and size dispersion for those at 1500 rpm.

From the absorbance values recorded at 400 nm, in each case a good reduction yield is found, always above 1. Keeping the rotational speed at 750 rpm, in the successive experience the conditions of seeds synthesis were changed by the rapid injection of the same reductant in different concentrations. As presented in Figure & Table 2.4.1.2, the seeds nucleated from such additions – 300 µL solutions respectively 5, 10, 25 and 50 mM in $NaBH_4$, successively put under the same growth conditions, grew into very different populations of NPs, in shape and size.

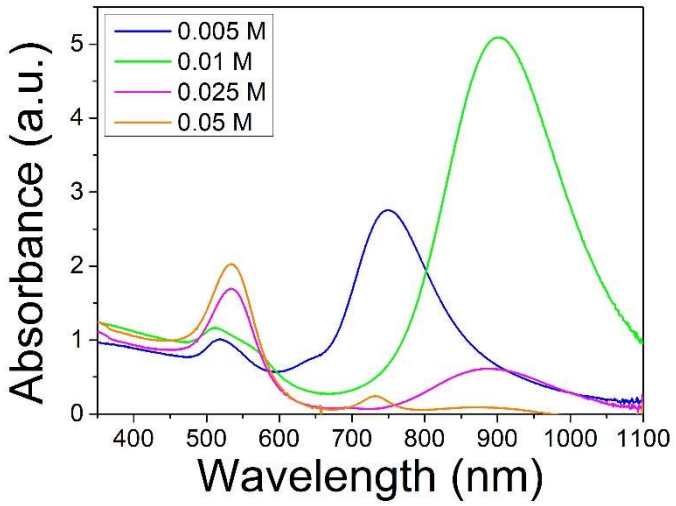


**Figure 2.4.1.2:** UV-vis-NIR absorbance spectra of Au NRs grown from seeds synthesized by the addition of 5-50 mM $NaBH_4$ solution.

| **$NaBH_4$ concentration [mM]** | **Longitudinal LSPR position [nm]** | **Quality ratio [adim]** | **FWHM [nm]** |
|---|---|---|---|
| **5** | 750 | 2.7 | 140 |
| **10** | 901 | 4.4 | 192 |
| **25** | 887 | 0.4 | 190 |
| **50** | 733 | 0.1 | 54 |

**Table 2.4.1.2:** data from the absorbance spectra of Au NRs grown from seeds synthesized by the addition of 5-50 mM $NaBH_4$ solution.

Looking at the position of longitudinal LSPR, it is included in the predicted range just for 10 mM and 25 mM $NaBH_4$ solutions, with the same size dispersion but a dramatical increase of shape polydispersity in the case of the latter. A red-shifted peak is found for the NRs grown from seeds nucleated by adding 5 mM $NaBH_4$, a concentration lower than the protocolized one, resulting in the formation of more NPs that contribute to the transversal band, however in a lesser extent compared

to those found by adding higher $NaBH_4$ concentrations, 25 mM and 50 mM, both giving a quality ratio below 0,5; in the latest case, so few NRs grow that are also monodisperse in size, as evident from the 54 nm of FWHM, the lowest value ever found.

The choice of 10 mM $NaBH_4$ solution results so justified, since different concentrations of reductant evidently cause the growth of seeds into larger spheres, not into NRs, for the availability of respectively too few or too many seeds formed by the reduction of less or more Au(III) ions to Au(0) metallic atoms. Established the reductant concentration and the stirring conditions to apply, whether the rapidity of 0,1 M $NaBH_4$ injection exerts influence was investigated, as in Figure & Table 2.4.1.3.

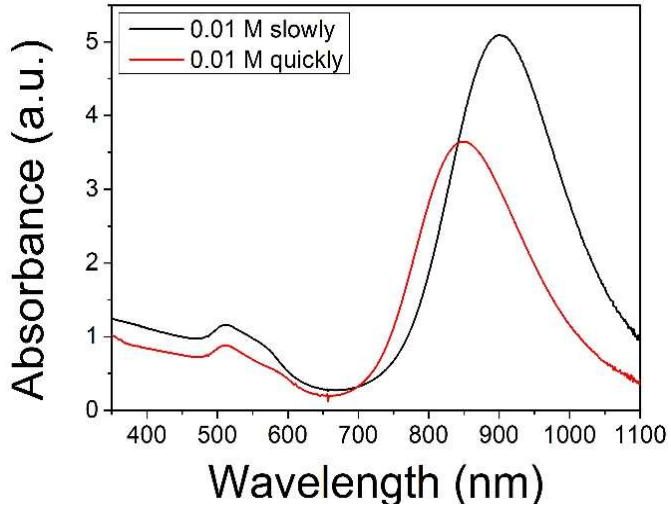


**Figure 2.4.1.3:** UV-vis-NIR absorbance spectra of Au NRs grown from seeds synthesized by slow and fast injection of 0,1 M $NaBH_4$ solution.

| Au NRs from seeds synthesized | Longitudinal LSPR position [nm] | Quality ratio [adim] | FWHM [nm] |
|---|---|---|---|
| **By slow $NaBH_4$ injection** | 901 | 4,4 | 192 |
| **By quick $NaBH_4$ injection** | 850 | 4,1 | 186 |

**Table 2.4.1.3:** data from absorbance spectra of Au NRs grown from seeds synthesized by slow and fast injection of 0,1 M $NaBH_4$ solution.

Seeds nucleated by the slow and quick 0,01 M $NaBH_4$ injection were not found to grow into very different Au NRs, in both cases with the longitudinal LSPR position included in the range of 800 – 900 nm and the presence of byproducts verified by the shoulder on the transverse band. The first sample presents less dispersion in terms of shape and the latter in those of size, but general

conclusions cannot be drawn only from this experience, while the wide existing literature on NRs seed-mediated growth testifies the importance of fastness during injection.

In this case, the result may depend on the ability and sensibility of the operator in handling pipettes, since only experience provides some sense of measure for slowness or quickness when executing such operations. As evident from Figure & Table 2.4.1.4, some of the TEM micrographs of the samples are reported here and provide information on geometrical characteristics and dispersion; since it is known that the drying process leads to shape segregation of byproducts in zones of the grid, the images were taken at different magnifications in several parts, to assure a globally representative picture of the situation, leading to statistically significative data.

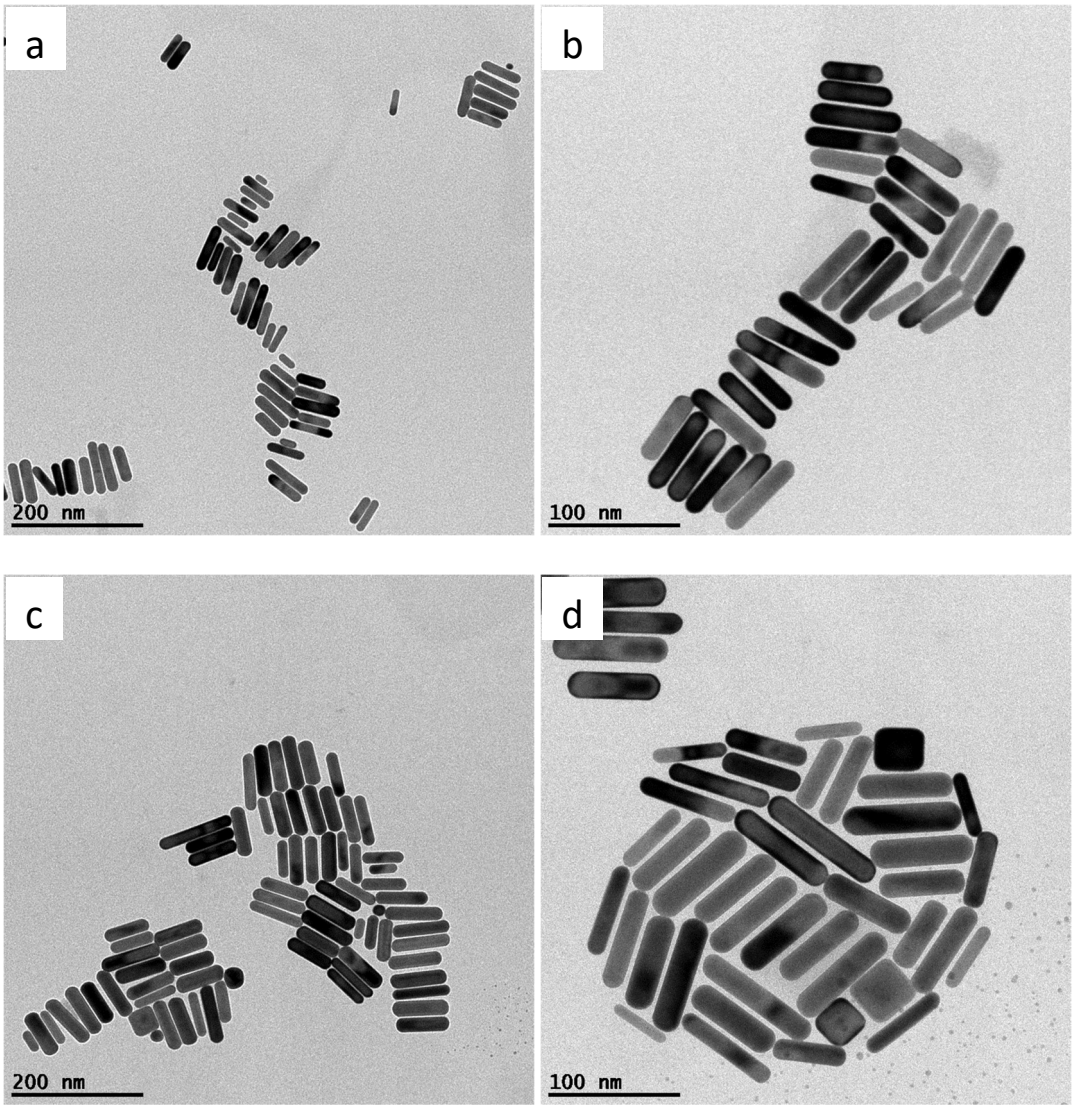


**Figure 2.4.1.4:** TEM micrographs of Au NRs grown from seeds synthesized by slow (on the top) and by quick addition (on the bottom) of $NaBH_4$, with scale bars of 200 nm (in **a** and **c**) and 100 nm (in **b** and **d**).

| Au NRs from seeds synthesized | Length [nm] | Width [nm] | Aspect ratio [adim] | NRs fraction [adim] |
|---|---|---|---|---|
| **By slow $NaBH_4$ addition** | 60 ± 12 (20%) | 16 ± 3 (19%) | 3,7 ± 0,6 (16%) | 97% |
| **By quick $NaBH_4$ addition** | 74 ± 13 (18%) | 21 ± 4 (19%) | 3,6 ± 0,6 (17%) | 95% |

**Table 2.4.1.4:** data from statistics on TEM images of Au NRs grown from seeds synthesized by slow and quick additions of $NaBH_4$.

Comparing the data of the two samples, obtained from statistics on the information readable in the TEM micrographs, it results that the NRs grown from seeds synthesized by quick addition of $NaBH_4$ are more monodisperse in size than those from seeds by slow addition, while for those latter a higher fraction of NRs over the total amount of NPs is found; almost the same AR is recorded. These findings totally agree with the outcomes of the analysis previously carried on the absorbance spectra, confirming a lower size dispersion in one case and a higher shape purity in the other.

It is to reaffirm at this point that no general conclusions are drawable from the data emerged just in our experiments on the effects of slowness or quickness; in the next chapter, we will judge the effects of addition speed relying on a measure system more trustable and univocal than the operator experience. The last experiment in this section on seeds quality investigates instead the aging effect, as exposed in Figure & Table 2.4.1.5, with seeds synthesized 24 h before grown into the same conditions used for previous experiences.

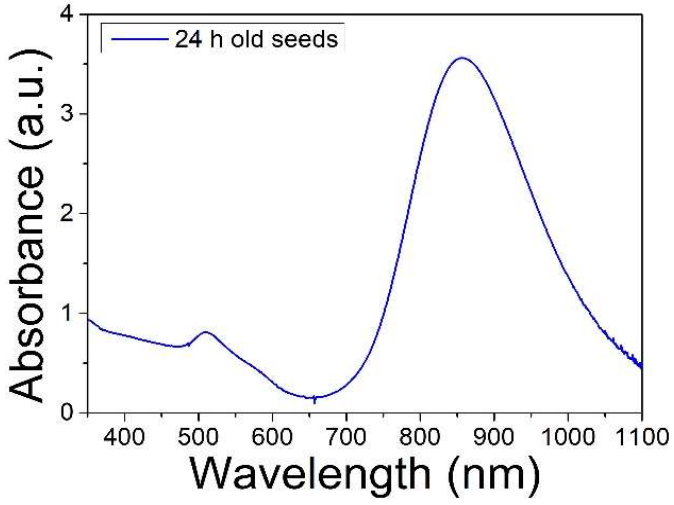


**Figure 2.4.1.5:** UV-vis-NIR spectrum of Au NRs grown from 24 h old seeds.

| | Longitudinal LSPR position [nm] | Quality ratio [adim] | FWHM [nm] |
|---|---|---|---|
| **NRs grown from 24 h old seeds** | 857 | 4,4 | 196 |

**Table 2.4.1.5:** data from absorbance spectrum of Au NRs grown from 24 h old seeds.

Contrarily to many predictions on the full growth into plasmonic spheres within 24 h, these seeds effectively grew into anisotropic NPs, displaying the longitudinal LSPR in the desired range, with a good ratio over the transversal one. Such finding, that contradicts the supposed short-time stability of seeds, will be investigated under different light in next chapter, alongside with the influence of rapidity in $NaBH_4$ injection.

## 2.4.2 Experiences with growth

As already described, seeds are injected into a growth solution, characterized by milder reduction conditions than the seeds synthesis, and growth proceeds at slower speed. Au(III) ions reduced to Au(I) by ascorbic acid are furtherly promoted to Au(0) metallic state on the surface of seeds, that grow into anisotropic shape with the silver-assisted deposition of Au atoms specifically on the tips; we are now going to deal with the agents involved in the growth, influencing yield and ARs.

As evident from Figure & Table 2.4.2.1, the volume of 0,1 M ascorbic acid added to the growth solution before seeds injection determines the final product quality. With the addition of only 45 µL a flat profile of absorbance is recorded, solution remains colorless; with 55 µL the value measured at 400 nm is approximately half of that found with bigger volume additions, indicating a lower concentration of metallic Au in the final solution, attributable to a less extended reduction; in the remaining cases, a value around 1,2 is almost found, as expectable from the quantities involved.

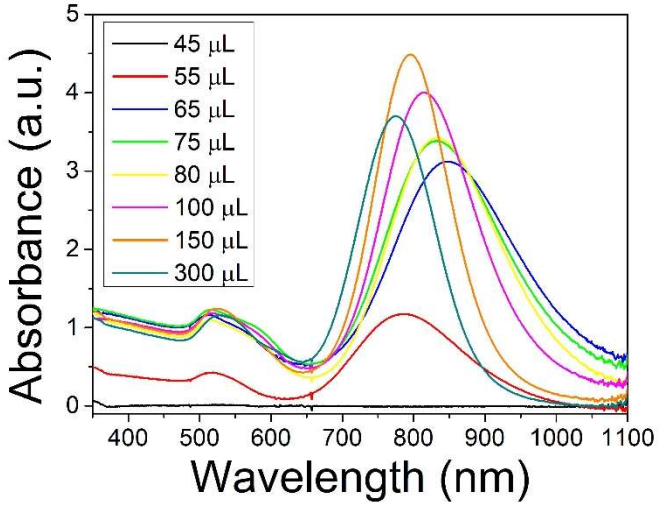


**Figure 2.4.2.1:** UV-vis-NIR absorbance spectra of Au NRs grown after adding 45 – 300 µL of 0,1 M ascorbic acid.

| NRs grown after adding 0.1 M ascorbic acid in | Longitudinal LSPR position [nm] | Quality ratio [adim] | FWHM [nm] |
|---|---|---|---|
| **45 µL** | / | / | / |
| **55 µL** | 784 | 2,7 | 174 |
| **65 µL** | 847 | 2,7 | 220 |
| **75 µL** | 832 | 2,7 | 205 |
| **80 µL** | 836 | 3,1 | 191 |
| **100 µL** | 813 | 3,4 | 162 |
| **150 µL** | 796 | 3,6 | 128 |
| **300 µL** | 774 | 3,2 | 131 |

**Table 2.4.2.1:** data from absorbance spectra of Au NRs grown after adding 45 – 300 µL of 0,1 M ascorbic acid.

Analyzing the data, it emerges that NRs presenting the longitudinal band in the desired range are grown only when adding 65 – 150 µL, and among these samples the best results in terms of dispersion are found with 80 – 150 µL of 0,1 M ascorbic acid. With such little differences of volume, success may highly depend on the skills of the operator in preparing the reductant solution and pouring it, in the right quantities. Repeating the experience likely lead to still distinct outcomes, since the synthesis of Au NRs is indeed well-known for its lack of reproducibility; that is the reason for keeping 80 µL as optimum volume, as obtained from previous experiences, despite in our case the most monodisperse NRs were not found for that addition.

Besides the considerations on shape and size dispersion, a progressive blue-shift of longitudinal LSPR is instead observable when adding more than 80 µL of ascorbic acid. Since the dependence of growth rate on reductant concentration is demonstrated, the blue-shift is ascribable to the excess of ascorbic acid, that results in high growth rates preventing the continuous deposition of Au atoms at the tips and favoring instead the formation of rods with lower ARs. When adding in the solution 75 – 80 µL of ascorbic acid, conditions for proper growth rate are met and NRs form. The results obtained with addition of 65 – 80 µL were also studied recurring to TEM analyses, as reported in Figure & Table 2.4.2.2.

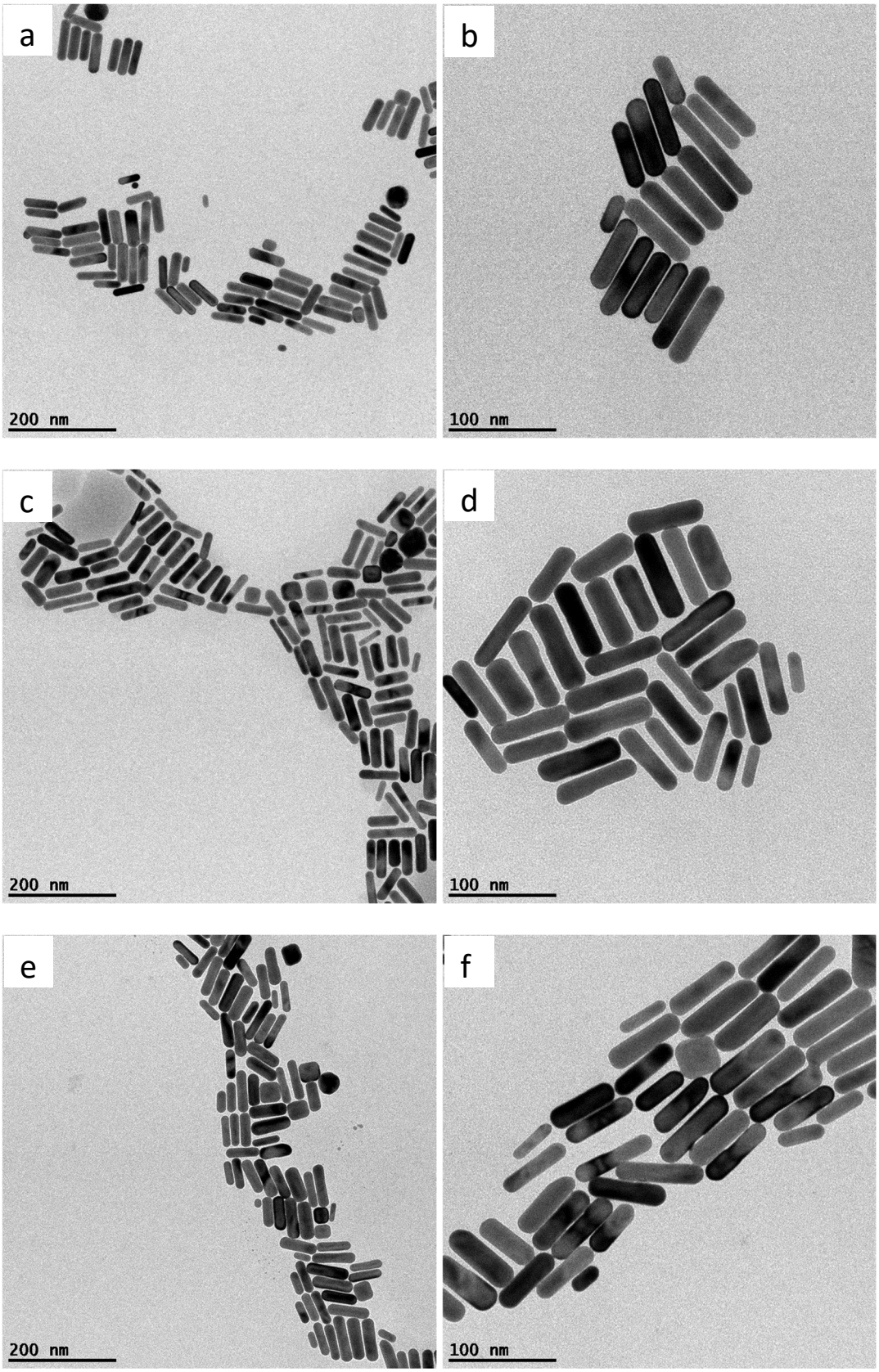


**Figure 2.4.2.2:** TEM micrographs of Au NRs grown after adding 65 µL (on the top), 75 µL (on the center) and 80 µL (on the bottom) of 0,1 M ascorbic acid, with scale bars of 200 nm (in **a**, **c** and **e**) and 100 nm (in **b**, **d** and **f**).

| NRs grown after adding 0.1 M ascorbic acid in | Length [nm] | Width [nm] | Aspect ratio [adim] | NRs fraction [adim] |
|---|---|---|---|---|
| **65 µL** | 65 ± 15 (23%) | 19 ± 3 (16%) | 3,4 ± 0,7 (21%) | 96% |
| **75 µL** | 64 ± 14 (22%) | 20 ± 5 (25%) | 3,3 ± 0,7 (21%) | 94% |
| **80 µL** | 67 ± 14 (21%) | 21 ± 4 (19%) | 3,1 ± 0,6 (19%) | 94% |

**Table 2.4.2.2:** data from statistics on TEM images of Au NRs grown after adding 65-80 µL of 0,1 M ascorbic acid.

The distinct NRs present ARs in the 3,1 – 3,4 range, accordingly with the position of the longitudinal LSPRs, shifting from 836 to 847 nm. The best sample in terms of size dispersion is obtained with the addition of 80 µL of ascorbic acid, presenting the same shape purity found with 75 µL, in both cases lower than that with 65 µL; while the outcomes on size dispersion are found to agree with the analysis of absorbance spectra, discrepancies are verified when looking at shape dispersion: the spectra of the samples with 65 and 75 µL exhibited the same quality ratio, lower than that with 80 µL, suggesting a different situation. The reason for such contradiction may originate from the take of micrographs in zones of TEM grid with shape segregation of byproducts.

Another agent influencing the anisotropic growth, that passivates the lateral facets, is silver, added as 0,01 M solution of $AgNO_3$. As represented in Figure & Table 2.4.2.2, the addition of different volumes into the growth solution results in the formation of NRs displaying longitudinal LSPR bands in distinct positions, i.e., with various ARs. No evidence of NRs formation emerges in absence of $AgNO_3$, since there is no longitudinal LSPR, and the shoulder on the transverse band suggests the presence of byproducts, besides nanospheres; the best sample in terms of shape dispersion is undoubtedly that obtained by adding 120 µL, as prescribed by our laboratory protocol.

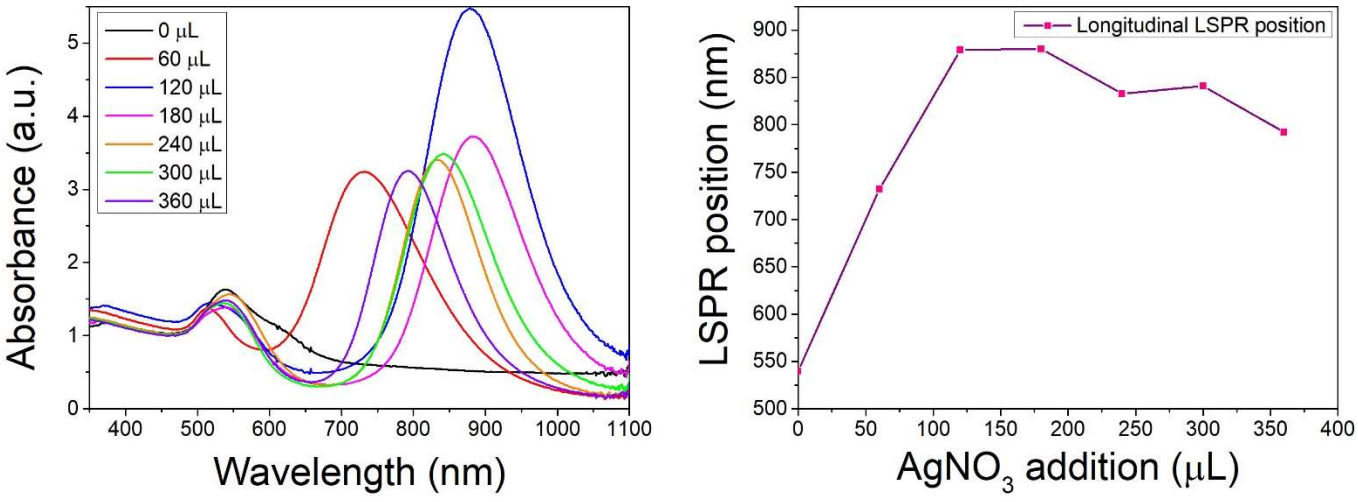


**Figure 2.4.2.3:** UV-vis-NIR absorbance spectra of Au NRs grown after adding 0 – 360 µL of 0,01 M $AgNO_3$.

| NRs grown after adding 0.01 M $AgNO_3$ in | Longitudinal LSPR position [nm] | Quality ratio [adim] | FWHM [nm] |
|---|---|---|---|
| **0 µL** | 540 | 1 | / |
| **60 µL** | 732 | 2,3 | 178 |
| **120 µL** | 879 | 3,8 | 165 |
| **180 µL** | 880 | 2,7 | 158 |
| **240 µL** | 833 | 2,2 | 131 |
| **300 µL** | 841 | 2,4 | 148 |
| **360 µL** | 792 | 2,2 | 133 |

**Table 2.4.2.3:** data from absorbance spectra of Au NRs grown after adding 0 – 360 µL of 0,01 M $AgNO_3$.

Examining the data, the samples presenting the most red-shifted LSPR peaks are those obtained by adding 120 – 180 µL, with similar polydispersity in size but quite different shape purity, whereas instead a blue-shift occurs by adding smaller or bigger volumes of 0,01 M $AgNO_3$. The influence of silver in anisotropic growth is evidently limited to a certain extent, since no linear relationship emerges between the amount of $AgNO_3$ added and the position found for longitudinal LSPR. As evident from Figure & Table 2.4.2.4, the samples obtained with the addition of 60 and 120 µL of $AgNO_3$ were studied recurring to TEM analyses.

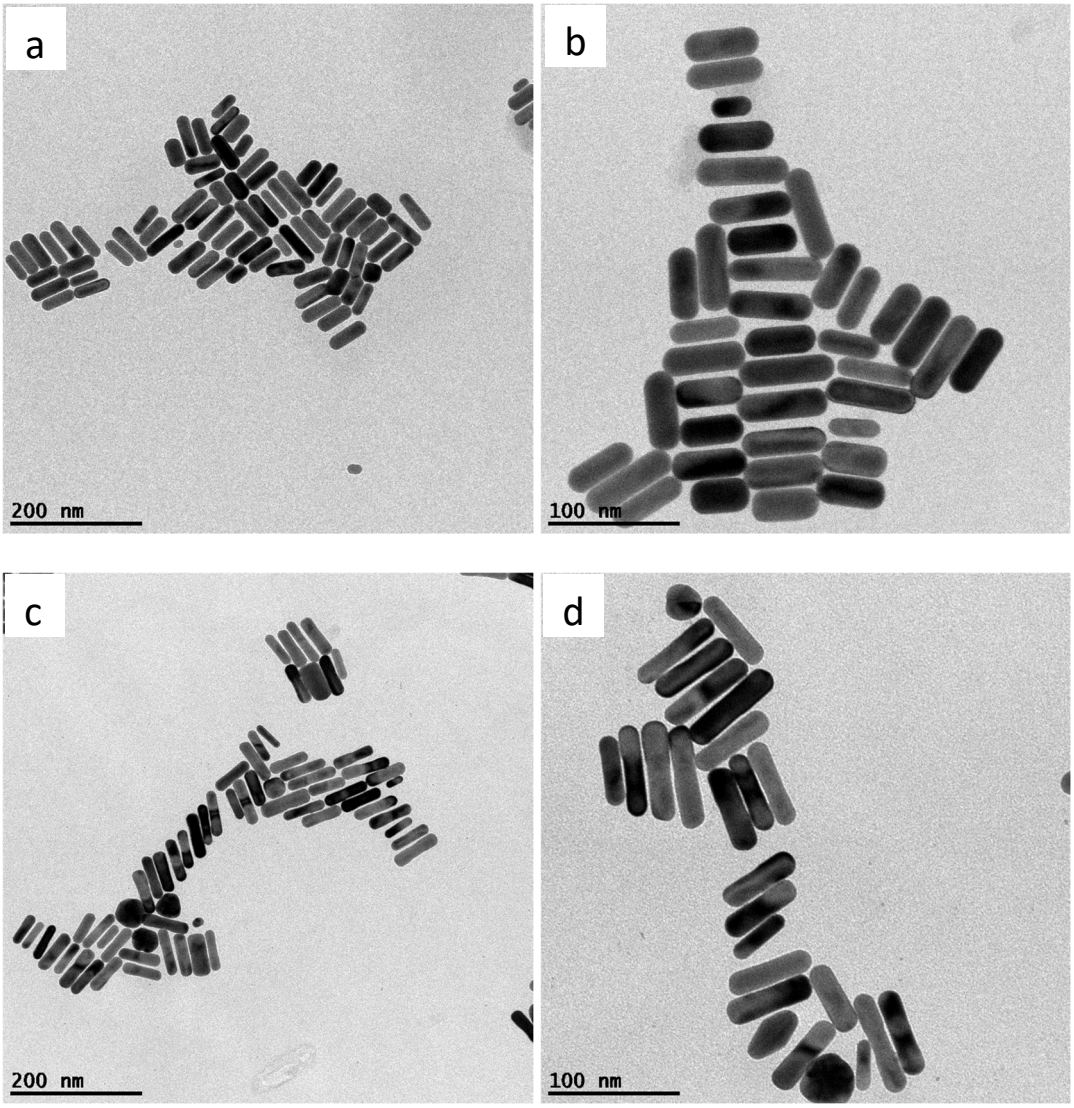


**Figure 2.4.2.4:** TEM micrographs of Au NRs grown after adding 60 µL (on the top) and 120 µL (on the bottom) of 0.01 M $AgNO_3$, with scale bars of 200 nm (in **a** and **c**) and 100 nm (in **b** and **d**).

| NRs grown after adding 0.01 M $AgNO_3$ in | Length [nm] | Width [nm] | Aspect ratio [adim] | NRs fraction [adim] |
|---|---|---|---|---|
| **60 µL** | 57 ± 10 (18%) | 22 ± 4 (18%) | 2,6 ± 0,5 (19%) | 97% |
| **120 µL** | 64 ± 11 (17%) | 19 ± 4 (21%) | 3,4 ± 0,5 (15%) | 95% |

**Table 2.4.2.4:** data from statistics on TEM images of Au NRs grown after adding 60 and 120 µL of 0.01 M $AgNO_3$.

NRs that presented a longitudinal LSPR peak at 732 nm are found to have a 2,6 AR, those with LSPR peak at 879 nm instead a 3,4 AR, as expectable from the well-known influence of $AgNO_3$ over AR. Looking at the size dispersion calculated from analyses of TEM images, NRs grown with 120 µL of $AgNO_3$ are more monodisperse than those grown with 60 µL, as emerged from the FWHM

of absorbance spectra. A discrepancy concerning shape purity is found also in this case, again probably attributable to the scarcity of micrographs taken.

Seeds amount is finally another factor affecting the growth of Au NRs. As anticipated in the previous section, when presenting the results obtained by adding more or less sodium borohydride for seeds synthesis, the same amount of Au(I) ions in a growth solution will reduce to Au(0) and deposit at the tips of NRs with higher ARs in presence of more seeds, while if only few seeds are available, each of those receive at the surface many more atoms and likely grow also in the lateral directions, presenting low ARs once grown. Our final experience regarded seeds amount injected into growth solution, as reported in Figure & Table 2.4.2.3.

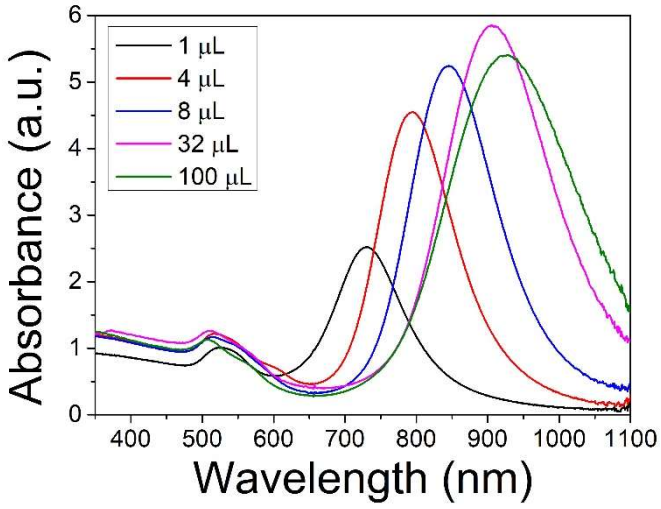


**Figure 2.4.2.3:** UV-vis-NIR absorbance spectra.

| Volume of seeds solution injected [µL] | Longitudinal LSPR position [nm] | Quality ratio [adim] | FWHM [nm] |
|---|---|---|---|
| 1 | 731 | 2,5 | 124 |
| 4 | 795 | 3,7 | 129 |
| 8 | 845 | 4,5 | 146 |
| 32 | 906 | 4,6 | 181 |
| 100 | 927 | 4,8 | 222 |

**Table 2.4.2.3:** data from absorbance spectra.

The addition of 16 µL of seeds solution, the one usually followed, is not performed here; the objective of the experiment was to show the clear tunability of longitudinal LSPR position by adding different amounts of seeds, obtaining also a notable shape purity. The most blue-shifted NRs solution is found by adding only 1 µL of seeds, also the most polydisperse in shape, a progressive red-shift is

then verified increasing the quantities injected, but a final blue-shift is predictable by further addictions, since in the presence of the same amount of available Au(I) ions but too many seeds, the latter cannot grow all in a very pronounced way.

# REFERENCES


[1] Lohse, S. E.; Murphy, C. M. The Quest for Shape Control: a History of Gold Nanorod Synthesis. *Chemistry of Materials*, **2013**, *25*, 1250-1261.

[2] Pérez-Juste, J.; Pastoriza-Santos, I.; Liz-Marzán, L. M.; Mulvaney, P. Gold Nanorods: Synthesis, Characterization and Applications. *Coordination Chemistry Reviews*, **2005**, *249*, 1870-1901.

[3] Nikoobakht, B.; El-Sayed, M. A. Preparation and Growth Mechanism of Gold Nanorods Using Seed-Mediated Growth Method. *Chemical Materials*, **2003**, *15* (10), 1957-1962.

[4] Grzelczak, M.; Pérez-Juste, J.; Mulvaney, P.; Liz-Marzán, L. M. Shape Control in Gold Nanoparticle Synthesis. *Chemical Society Reviews*, **2008**, *37*, 1783-1791.

[5] Carbó-Argibay, E.; Rodríguez-González, B.; Gómez-Graña, S.; Guerrero-Martínez, A.; Pastoriza-Santos, I.; Pérez-Juste, J.; Liz-Marzán, L. M. The Crystalline Structure of Gold Nanorods Revisited: Evidence for Higher-Index Lateral Facets. *Angewandte Chemie International Edition*, **2010**, *49*, 9397-9400.

[6] Murphy, C. J.; Thompson, L. B.; Alkilany, A. M.; Sisco, P. N.; Boulos, S. P.; Sivapalan, S. T.; An Yang, J.; Chernak, D. J.; Huang, J. The Many Faces of Gold Nanorods. *The Journal of Physical Chemistry Letters*, **2010**, *1*, 2867-2875.

[7] Rodríguez-Fernández, J.; Pérez-Juste, J.; Mulvaney, P.; Liz-Marzán, L. M. Spatially-Directed Oxidation of Gold Nanoparticles by Au(III) – CTAB Complexes. *The Journal of Physical Chemistry B*, **2005**, *109*, 14257-14261.

[8] Park, K.; Hsiao, M. S.; Koerner, H.; Jawaid, A.; Che, J.; Vaia, R. A. Optimizing Seed Aging for Single Crystal Gold Nanorod Growth: the Critical Role of Gold Nanocluster Crystal Structure. *Journal of Physical Chemistry C*, **2016**, *120*, 28235-28245.

[9] Reji, P.; Panit, C.; Huifeng, Q.; Rongchao, J.; Jayan, T. Evolution of Nonlinear Optical Properties: from Gold Atomic Clusters to Plasmonic Nanocrystals. *Nano Letters* **2012**, *12*, 4661-4667.

[10] Rongchao, J. Atomically Precise Metal Nanoclusters: Stable Sizes and Optical Properties. *Nanoscale*, **2015**, *7*, 1549-1565.

[11] Burrows, N. D.; Harvey, S.; Idesis, F. A.; Murphy, C. J. Understanding the Seed-Mediated Growth of Gold Nanorods through a Fractional Factorial Design of Experiments. *Langmuir* **2017**, *33*, 1891-1907.

[12] Bullen, C.; Zijlstra, P.; Bakker, E.; Gu, M.; Raston, C. Chemical Kinetics of Gold Nanorod Growth in Aqueous CTAB solutions. *Crystal Growth & Design*, **2011**, *11*, 3375-3380.

[13] Almora-Barrios, N.; Novell-Leruth, G.; Whiting, P.; Liz-Marzán, L. M.; López, N. Theoretical Description of the Role of Halides, Silver and Surfactants on the Structure of Gold Nanorods. *Nano Letters*, **2014**, *14*, 871-875.

[14] Walsh, M. J.; Barrow, S. J.; Wenming, T.; Funston, A. M.; Etheridge, J. Symmetry Breaking and Silver in Gold Nanorod Growth. *Acs Nano*, **2015**, *9* (1), 715-724.

[15] Wenming, T.; Walsh, M. J.; Mulvaney, P.; Etheridge, J.; Funston, A. M. Control of Symmetry Breaking Size and Aspect Ratio in Gold Nanorods: Underlying Role of Silver Nitrate. *The Journal of Physical Chemistry C*, **2017**, *121*, 3549-3559.

# Chapter 3

# Flow synthesis of Au NRs

The core of our thesis work is reported in the present chapter, focusing on the use of a millifluidic reactor, an innovative system that allowed us to obtain unprecedented results in the seed-mediated growth of Au NRs, adapted into flow conditions. NRs were grown from seeds synthesized by hand and by the reactor too, into distinct experiments aimed to evaluate the effects of the flow rates and time on products quality and characteristics, as those of varying the $AgNO_3$ and the seeds amounts.

## 3.1 From batch to automated flow reactors

As known, noble metal nanocrystals are reported to be obtainable in a wide variety of shapes and sizes, recurring to the multiple ways explored by colloidal chemistry, with the bottom-up approach; without mentioning the issue of reproducibility, such syntheses are typically conducted in a batch format, in a flask or a glass vial under magnetic stirring, and thereby generate nanocrystals in a rather limited quantity, with the milligram scale of products still remaining a challenge.

At the current stage of nanotechnology – definitely entering a more application-oriented phase, the solid samples produced per batch are far away from what needed in the industry! Since some applications of Au NPs in biomedicine were previously presented, a proper example draws the attention to that field, here reported. According to a recent study, every person on the Earth could be supplied with the standardized dose for theranostic anticancer treatment, which is a 10 nm thick and 2.25 $cm^2$ extensive monolayer of Au NPs, only with the latter reliably produced on the 100 kg scale.[1]

Difficulties in the scale up are exemplified by the synthesis of Au NRs, which guarantees exceptional control over the shape but converts only approximately 15% of the initial gold to NRs, i.e., providing 7 mg of solid sample per 100 mL of reaction solution.[2] Altering the synthesis conditions, such as in the protocols developed by Jana and Zubarev, gram-scale with low dispersion is achievable at costs of a dimensional control, favoring respectively the formation of NRs with very

small or very large transverse diameters; scale up to gram-scale is indeed challenging in the case of Au NRs.[3]

The first conceivable way to solve the problem, that most people would like to pursue, is to increase the volume of reaction solution by switching to larger reactors. Such increase in the volume, analogously to the case of increasing the reagents concentration, significantly alters the reagents diffusion rates and thermal transport, resulting unequivocally in a loss of control over the product, since nucleation and growth of colloidal nanocrystals are highly sensitive to experimental details.[4] The alternative for the synthesis scale up, a problem appearing conceptually simple, is to transfer from batch to automated reactors, based on continuous flow into microfluidic or millifluidic devices.

Gram-scale synthesis becomes achievable by continuous operation of the reactor, or running multiple reactors in parallel, as theorized but not yet demonstrated. The geometry of the reactor, given by the channels narrowness and the mixing zones, guarantees the factors affecting the product monodispersity, exerting strict control over the timing of reagents addition and improving the thermal transport properties. Moreover, automated reactors potentially provide the opportunity to monitor the product quality with the synthesis on-going, independently of reaction scale, improving control.

Microfluidic devices provide exquisite vantages in terms of reaction control, high throughput and operational environment, features mainly attributable to the large ratio of surface area over volume in the miniaturized components. On the disadvantages side, it is to report that such devices have until now proven to be susceptible to irreversible fouling while operating, and usually require sophisticated and expensive fabrication techniques, such as lithography and etching.[5]

Millifluidic devices, which have a scale length larger than 1 mm, provide approximately the same advantages given by the microfluidic ones, typically flow rate and reagents control, while offering instead many others. Millifluidic reactors are indeed easy to fabricate and nearly inexpensive, to be assembled and operate in any chemistry laboratory; they do not present the fouling issue and work on fluid volume many times larger than that of microfluidic ones, in virtue of the channel size, that allow better opportunities for the in situ characterization with spectroscopy probes.

Millifluidic reactors are the suitable candidates to serve the needs of research laboratories, that very often require practicable systems to scale up the synthesis of monodisperse NPs for carrying on the investigation activities. Despite the clear advantages offered, such systems have so far received little attention, without being investigated for general utility and for NPs synthesis. Only the Murphy group published in 2013 a work reporting evidences of monodisperse Au NPs synthesis – with the

possibility of various sizes and shapes, by the use of a millifluidic reactor, a system just composed of polyvinyl tubing, a peristaltic pump and a polyethylene Y-mixer.[1]

In our work a different, more complex system was tested for the synthesis of Au NRs; the millifluidic reactor was assembled in CAN Centrum für Angewandte Nanotechnologie GmbH, the Center for Applied Nanotechnology, in Hamburg, after years of investigation, and then moved to CIC bioMAGUNE, in Donostia San Sebastián, where the experiences with it were made. The combination of flow rates for the syntheses had been previously optimized by Guillermo Gonzalez-Rubio, using different pumps, in the CAN researches context of adapting Au NRs synthesis into flow conditions.

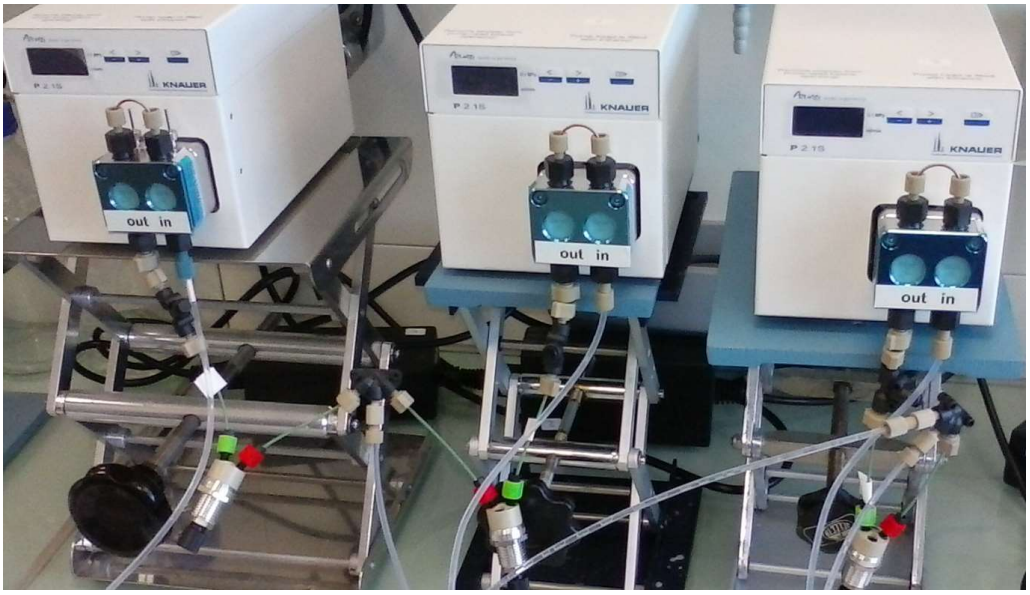


**Figure 3.1:** our millifluidic reactor.

The present chapter represents indeed the core of this thesis work, the newness value, since it reports the results obtained using an innovative device, reported in Figure 3.1, rightfully definable as a pilot plant in its kind. The difficulties in Au NRs synthesis, e.g., the lack of reproducibility and the scale up issue, have been elucidated, the objective is now to assess whether the millifluidic reactor constitutes a valid system for solving such problems that have proved to be so challenging until now.

## 3.2 Flow synthesis of NRs from seeds obtained by hand

During the first experiences, the reactor was used to grow into flow conditions the seeds already synthesized by hand, with the rapid injection of $NaBH_4$. Seeds are grown into NRs after being added in a growth solution containing Au(III) yet reduced to Au(I) by ascorbic acid, as known from the practice of the batch synthesis; in the millifluidic system the method does not change, but it is applied in another way: pumps are connected to solutions of reagents, that are mixed in the mixing chambers and then react along the channels. We are going to see whether such operations, when carried by an automated reactor instead than a human operator, lead to different results.

As depicted in Figure 3.2, the first pump moves the solution containing the Au salt, whose flow is soon joined by that of ascorbic acid solution, moved by the second pump, while instead the seeds colloid, put in motion by the third pump, is the last to be added into the flow. The length between the pump and the mixing chamber is 40 cm in each case, while the distance between the two mixing points – respectively, the one at which the Au(III) solution is mixed with ascorbic acid and that where the seeds join the flow, is 3 m long; as described in the previous section, the 40 cm of each outline channel include a T-connector and a back-pressure regulator, before meeting the w-mixer.

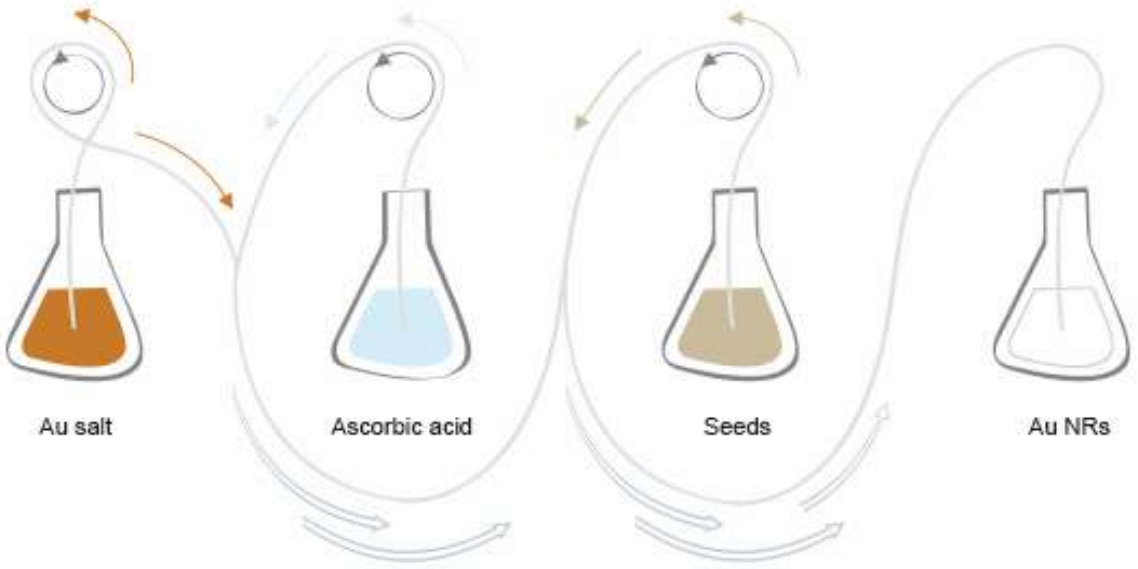


**Figure 3.2:** schematics of the millifluidic reactor as used for the growth of seeds into Au NRs.

The practice of using the reactor means to dispose the three beakers with 0.1 M CTAB solution and the necessary reagents, freshly and daily prepared, and another one empty, to be filled by the others as the system is working. The solution collected in the final beaker is initially colorless and takes time to assume the typical color of Au NRs colloids, as observable in the typical batch synthesis.

As exposed in Table 3.2, the growth solutions contain the usual chemicals of the silver-assisted route prescribed by our protocol.

| Growth Solution 1 | Growth Solution 2 | Growth Solution 3 |
|---|---|---|
| 0,1 M in CTAB | 0,1 M in CTAB | 0,1 M in CTAB |
| $HAuCl_4$ 0,05 M<br>20 µL/mL | Ascorbic acid 0,1 M<br>32 µL/mL | Seeds<br>32 µL/mL |
| $AgNO_3$ 0,01 M<br>24 µL/mL | | |
| HCl 1 M<br>40 µL/mL | | |

**Table 3.2:** composition of the Growth Solutions in the beakers connected to the reactor.

It may be noted that the concentrations of the chemicals diverge from those used in the batch synthesis, a choice motivated by the ratio among the flow rates set for the pumps, that is 2:1:1 for the growth of Au NRs, as optimized in earlier works. Considering thereby that half of the final volume is determined by the first solution, whereas instead the second and the third one contribute each one to a fourth of it, the true concentrations are calculable and correspond to those of the standard protocol, except for that of the seeds, here increased, within a range tested as providing good results.

Respecting always the ratio mentioned, the flow rates were varied from the lowest to the highest limits permitted, that is the interval of 0.5 – 40 mL/min per pump (as recommended by the producers); the sum of the flow rates set in the pumps, i.e., the flux exiting the final mixing point and then collecting, will be indicated to identify the flow rate of each experience. In this section, with the reactor used to grow seeds synthesized by hand, we are going to investigate whether the system is affected in the products quality by factors such as time and the flow rates set.

### 3.2.1 Effect of time

The performance exhibited by the reactor as time passes was investigated, to check whether any changes in the quality or in the same products occur. After setting the flow rate of 10 mL/min (in agreement with the ratio mentioned, 5 mL/min in the first pump and 2,5 mL/min for each of the other two), ten consecutive 10 mL aliquots of the final solution were collected in several vials and then 100 mL in a single beaker. While observing that the color typically expected for grown NRs solution was assumed in less than an hour, we waited the usual 2 hours required in batch synthesis to consider the growth completed and only then the UV-vis-NIR absorbance spectra of the samples were taken.

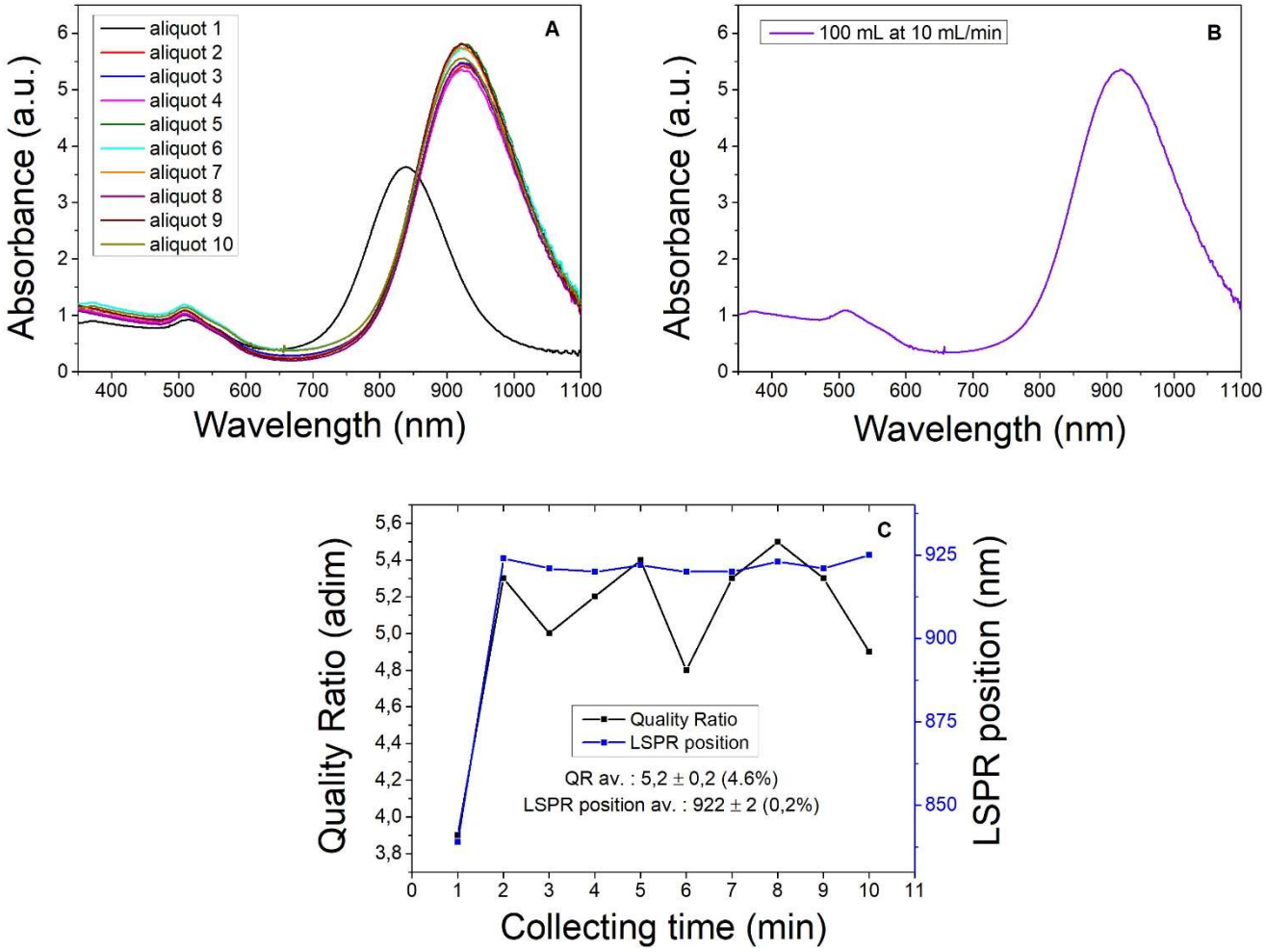


**Figure 3.2.1.1:** UV-vis-NIR absorbance spectra of the 10 mL ten aliquots (in **A**) and the 100 mL sample (in **B**) of Au NRs grown at 10 mL/min from seeds synthesized by hand; trends of QR and longitudinal LSPR position exhibited by the ten aliquots (in **C**).

| | Longitudinal LSPR position [nm] | Quality Ratio [adim] | FWHM [nm] |
|---|---|---|---|
| **Aliquot 1** | 839 | 3,9 | 148 |
| **Aliquot 2** | 924 | 5,2 | 190 |
| **Aliquot 3** | 921 | 5,0 | 190 |
| **Aliquot 4** | 920 | 5,2 | 187 |
| **Aliquot 5** | 922 | 5,4 | 186 |
| **Aliquot 6** | 920 | 4,8 | 190 |
| **Aliquot 7** | 920 | 5,3 | 186 |
| **Aliquot 8** | 923 | 5,5 | 184 |
| **Aliquot 9** | 921 | 5,4 | 185 |
| **Aliquot 10** | 925 | 4,9 | 190 |
| **100 mL sample** | 920 | 4,9 | 188 |

**Table 3.2.1.1:** data from the absorbance spectra of the 10 mL ten aliquots and the 100 mL sample of Au NRs grown at 10 mL/min from seeds synthesized by hand.

As evidenced in Figure & Table 3.2.1.1, except the first aliquot (not considered in the average calculations), LSPR peak position is found to vary in a very narrow range, from 920 to 925 nm, and dispersion in shape and size too, correspondingly with an average quality ratio of 5,2 ± 0,2 and a FWHM in the 184 – 190 nm interval. According to the absorbance spectra, the reactor proves to perform stably with time, from the second to the ninth aliquot, regularly providing the desired products and maintaining the same quality; some significant samples were studied also recurring to TEM, for measuring directly the NRs length and width, the ARs, and valuing the shape purity.

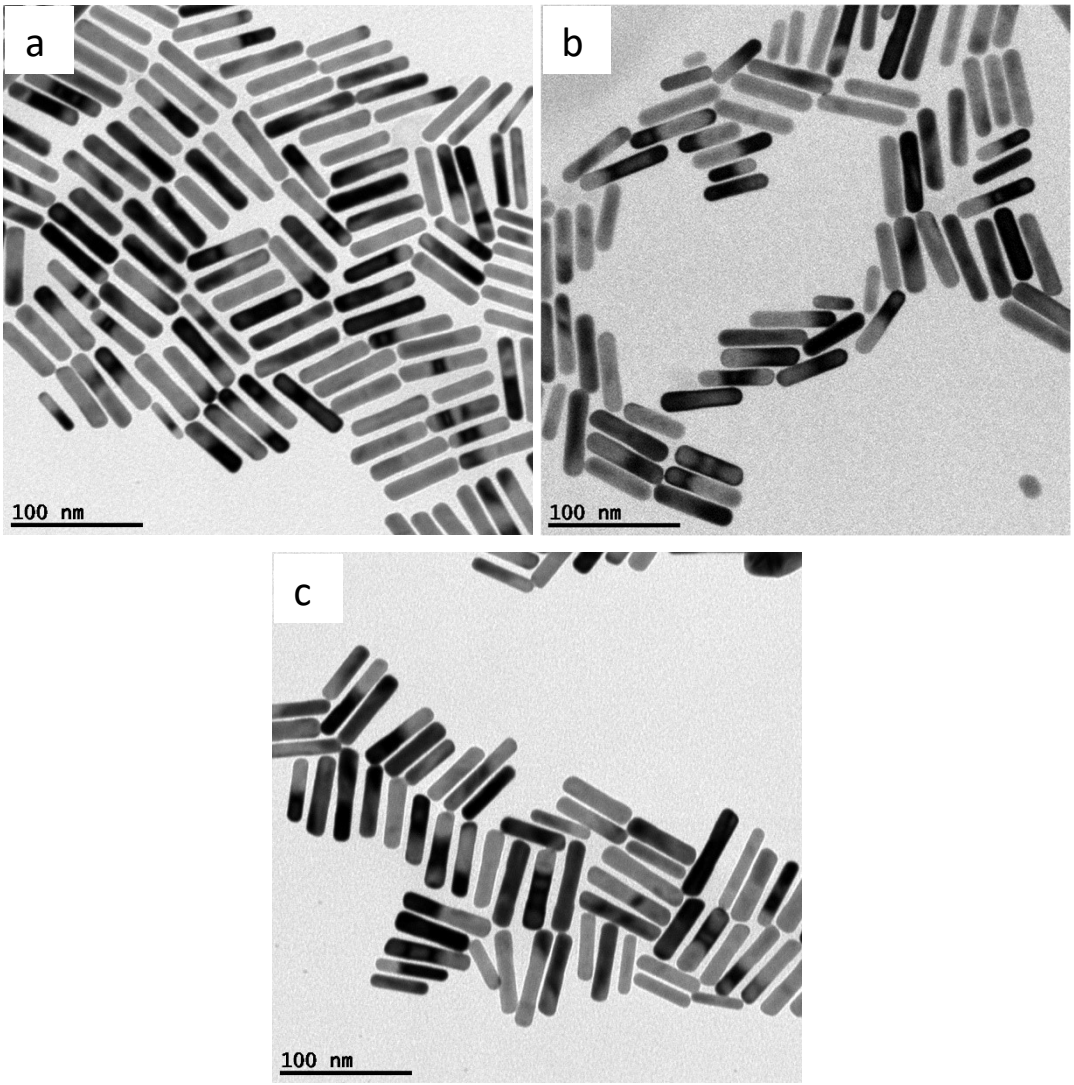


**Figure 3.2.1.2:** TEM micrographs of the 2nd (in **a**), the 6th (in **b**) and the 10th aliquot (in **c**) of Au NRs grown at 10 mL/min from seeds synthesized by hand, with scale bar of 100 nm.

| | **Length [nm]** | **Width [nm]** | **Aspect Ratio [adim]** | **NRs fraction [adim]** |
|---|---|---|---|---|
| **Aliquot 2** | 59 ± 8 (14%) | 14 ± 3 (21%) | 4,2 ± 0,7 (17%) | 99,0% |
| **Aliquot 6** | 57 ± 11 (19%) | 15 ± 2 (13%) | 3,8 ± 0,6 (16%) | 98,7% |
| **Aliquot 10** | 59 ± 8 (14%) | 14 ± 3 (21%) | 4,2 ± 0,7 (17%) | 99,4% |

**Table 3.2.1.2:** data from statistics on TEM images of the 2nd, the 6th and the 10th aliquot of Au NRs grown at 10 mL/min from seeds synthesized by hand.

As reported in Figure & Table 3.2.1.2, TEM micrographs of the second, the sixth and the tenth aliquot were taken, judged as significant samples since the second and the tenth enclose the interval of aliquots considered valid, while the sixth occupies the middle position, presenting also the lowest QR and longitudinal LSPR. The analysis reveals that the NRs of second and tenth aliquot present the same length and width of respectively 59 and 14 nm, with equal values of standard deviation, while

the NRs of the sixth aliquot are slightly shorter and thicker, in agreement with the positions previously found for the longitudinal LSPR peaks. As concerns the shape purity, no less than the 99% of the NPs photographed are the desired ones in the second and tenth aliquot, just the 98,7% in the sixth.

Besides the little differences just illustrated, statistical analysis of TEM micrographs confirms what already found with the measure of absorbance spectra. From the second to the tenth aliquot, the system works very efficiently, realizing the flow synthesis of several mL of monodisperse NRs solution (in contrast with the 10 mL generally obtained by batch synthesis), with a shape yield around 99% (higher than the 95% in batch). The characteristic dimensions of the NRs belonging to distinct aliquots may differ of few nm, since variations of such order are also evidenced by the position of longitudinal LSPR peaks: the performance of the reactor is to be considered stable with time.

Discordant data – for blue-shifted and more polydisperse in shape NRs, are found in the case of the first aliquot, constituted of the 10 mL of solution collected in a minute just after turning on the reactor: the solutions need time to mix properly along the channels of the system, otherwise the products quality is badly affected. In the successive experiences we assumed $3\tau$ as mixing time, i.e., the triple of the time required to the solution for running across the trait from the first mixing point to the second one; given the sum of the partial flow rates set in pump 1 and pump 2, $\tau$ corresponds to the ratio expressed by the volume of the channel between the two mixing points over the sum said.

After the mixing time, the system starts working properly and time does not affect the outcomes of the reactor; this behavior is verified also for the sample collected in the 10 minutes successive to the last aliquot: LSPR peak at 920 nm, with a 4,9 QR and a FWHM of 188 nm, the same features already described; moreover, it is to be remarked that this latest sample is a 100 mL solution, ten times the volume of the previous aliquots, without any loss of quality. Such proportion suggests that very large volumes of monodisperse Au NRs solution are collectable making the reactor work continuously for long time intervals, as we are going to deal with also in the next section.

### 3.2.2 Effect of the flow rates

The scale up hypothesis is undoubtedly the most interesting possibility offered by the reactor, and this objective was investigated with an apt experience, conceived to assess whether the use of distinct flow rates affects the outcomes of NRs synthesis collecting every time the same amount of final solution. Low and high flow rates regimes were tested, being aware that 0,5 – 40 mL/min is the interval of values counseled for each pump and knowing already that good results are provided at 10 mL/min, thereby used as reference to find any upper or lower limits for the performance of the reactor.

In two different days, 100 mL of final solution were collected at flow rates that varied in 1 – 10 mL/min and 10 – 80 mL/min. It is to denote that the lowest of the flow rates was given by setting 0,5 mL/min in pump1 and 0,25 mL/min in pump2 and in pump3, the latest below the minimum value at which the system performs well according to the producers; moreover, the time required to collect 100 mL at that flow rate is 100 min, approximately the time necessary to the complete growth of Au NRs in batch conditions, meaning that if synthesis works then the last droplets join the final solution when the latter has already assumed the typical color of Au NRs colloids.

Indeed, the situation just depicted was observed while we were operating: the flow synthesis of Au NRs was performed even at 1 mL/min and the 100 mL of final solution were completely collected with the brownish shade yet displayed. In the other day, testing the high flow rates regime, pumps were instead set to work within the range permitted (obtaining the maximum with 40 mL/min in pump1, 20 mL/min in pump2 and in pump3), the 100 mL volumes were totally collected in lesser time and were then characterized with the measurement of the absorbance spectra, as all the samples.

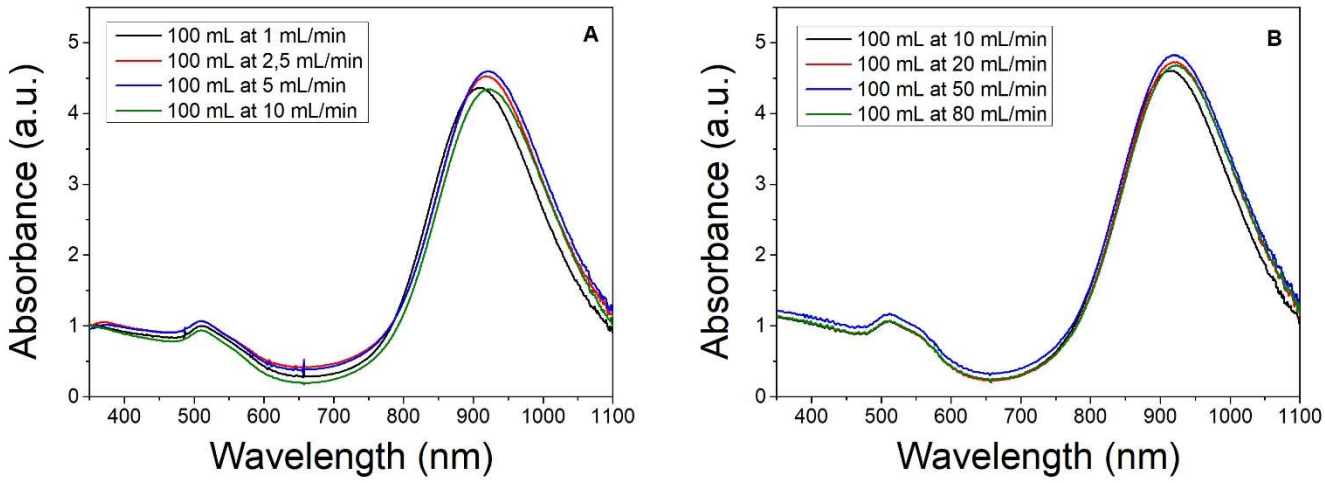


**Figure 3.2.2.1:** UV-vis-NIR absorbance spectra of the 100 mL samples of Au NRs grown in the low (in **A**) and in the high flow rates regime (in **B**) from seeds synthesized by hand.

| | Longitudinal LSPR position [nm] | Quality Ratio [adim] | FWHM [nm] |
|---|---|---|---|
| **1 mL/min** | 910 | 4.4 | 195 |
| **2.5 mL/min** | 918 | 4.2 | 200 |
| **5 mL/min** | 923 | 4.3 | 205 |
| **10 mL/min** | 920 | 4.6 | 199 |

**Table 3.2.2.1A:** data from the absorbance spectra of the 100 mL samples of Au NRs grown in the low flow rates regime from seeds synthesized by hand.

| | Longitudinal LSPR position [nm] | Quality Ratio [adim] | FWHM [nm] |
|---|---|---|---|
| **10 mL/min** | 918 | 4.3 | 205 |
| **20 mL/min** | 924 | 4.4 | 208 |
| **50 mL/min** | 923 | 4.1 | 213 |
| **80 mL/min** | 923 | 4.4 | 210 |

**Table 3.2.2.1B:** data from the absorbance spectra of the 100 mL samples of Au NRs grown in the high flow rates regime from seeds synthesized by hand.

As reported in Figure & Table 3.2.2.1, the 100 mL samples of Au NRs solution collected under the distinct regimes of low and high flow rates show to have very similar features. In both regimes the longitudinal LSPR peak is found to vary in a narrow range, from 910 to 924 nm, dominating in magnitude at least 4 times the transversal LSPR, and size dispersion appears to be the same, presenting in each case FWHM values of the same order.

These data evidently suggest us that a scale up in NRs synthesis is performable by the reactor: no loss of quality is detected in the 100 mL of solution collected varying the flow rate from 1 to 80 mL/min; such ratio may be extended to volumes, leading us to think that 8 L, i.e., 80 times 100 mL, of Au NRs solution are collectable using the reactor, characterized by the usual low dispersion in shape and size. Notwithstanding these speculations, that need to be proved experimentally, the samples had to be studied with TEM, to have a whole characterization on their dimensions too.

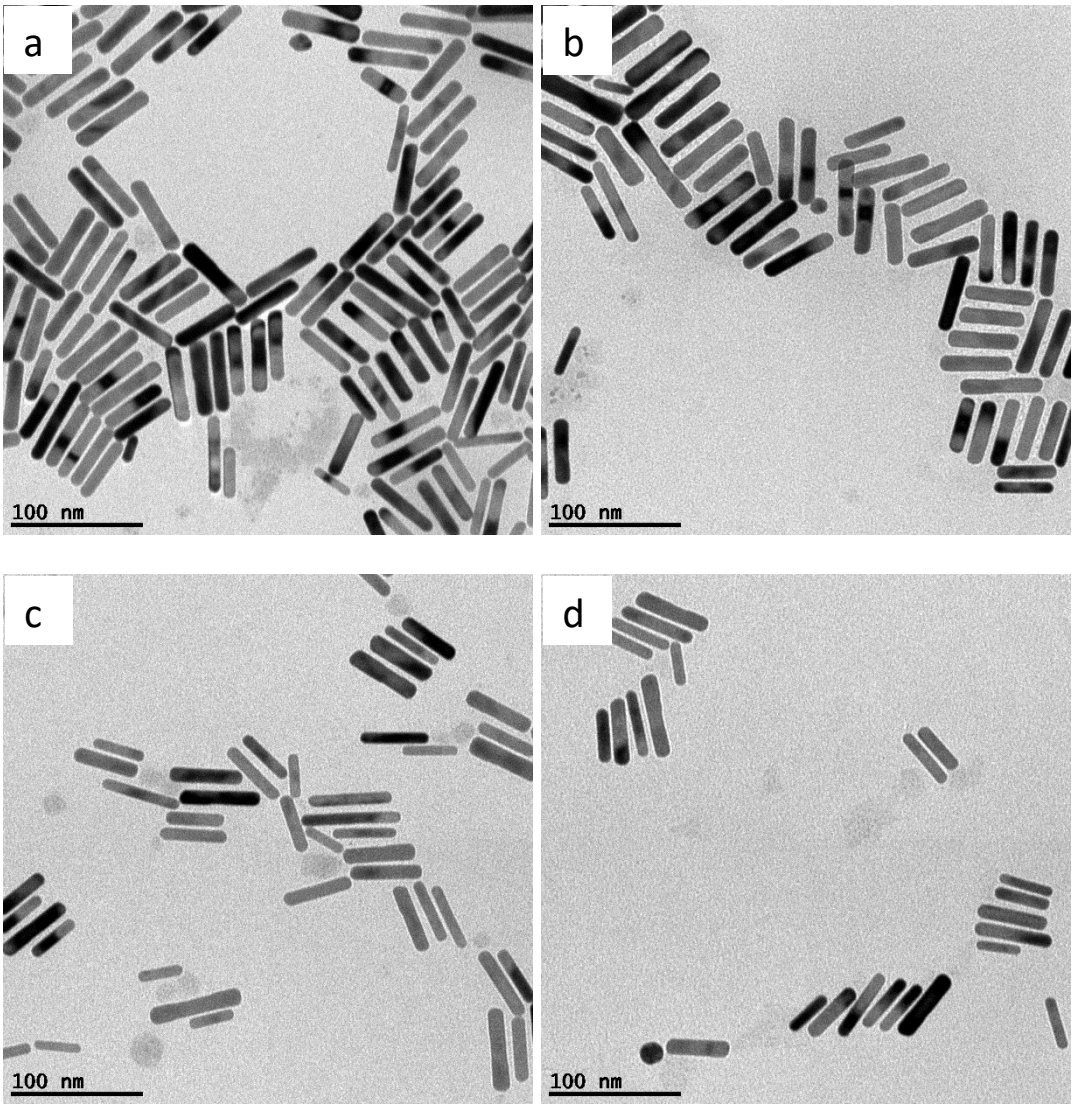


**Figure 3.2.2.2A:** TEM micrographs of the Au NRs grown at 1 mL/min (in **a**), at 2,5 mL/min (in **b**), at 5 mL/min (in **c**) and at 10 mL/min (in **d**) from seeds synthesized by hand, with scale bar of 100 nm.

| | **Length [nm]** | **Width [nm]** | **Aspect Ratio [adim]** | **NRs fraction [adim]** |
|---|---|---|---|---|
| **1 mL/min** | 52 ± 10 (19%) | 13 ± 3 (23%) | 4,2 ± 0,7 (17%) | 98,7% |
| **2.5 mL/min** | 52 ± 10 (19%) | 12 ± 3 (25%) | 4,3 ± 0,7 (16%) | 98,4% |
| **5 mL/min** | 49 ± 9 (18%) | 12 ± 3 (25%) | 4,2 ± 0,7 (17%) | 96,3% |
| **10 mL/min** | 49 ± 9 (18%) | 12 ± 2 (17%) | 4,3 ± 0,8 (19%) | 99,4% |

**Table 3.2.2.2A:** data from statistics on TEM images of the Au NRs grown in the low flow rates regime from seeds synthesized by hand.

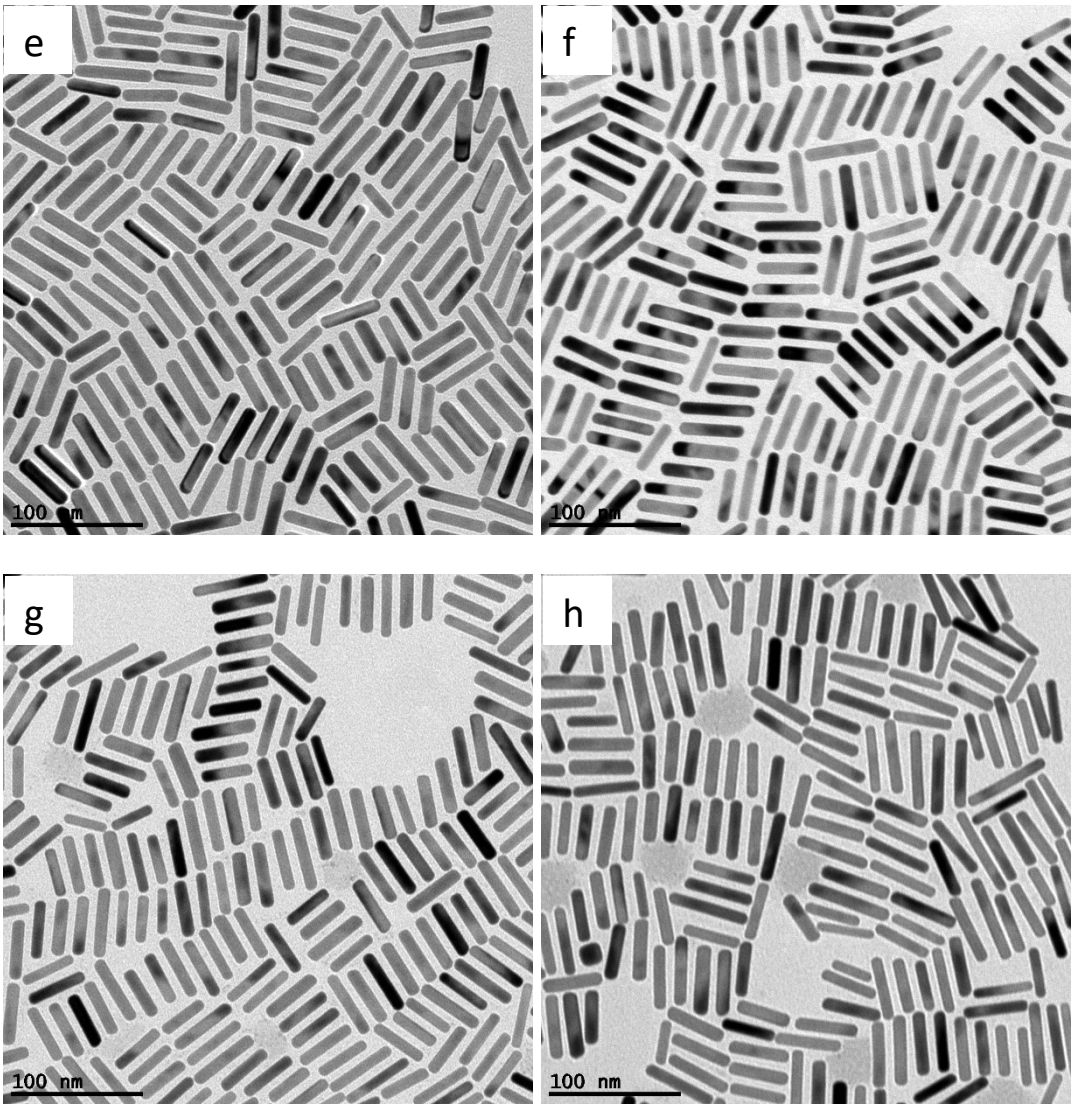


**Figure 3.2.2.2B:** TEM micrographs of the Au NRs grown at 10 mL/min (in **e**), at 20 mL/min (in **f**), at 50 mL/min (in **g**) and at 80 mL/min (in **h**) from seeds synthesized by hand, with scale bar of 100 nm.

| | **Length [nm]** | **Width [nm]** | **Aspect Ratio [adim]** | **NRs fraction [adim]** |
|---|---|---|---|---|
| **10 mL/min** | 46 ± 6 (13%) | 12 ± 2 (17%) | 4,1 ± 0,7 (17%) | 99,8% |
| **20 mL/min** | 47 ± 5 (11%) | 11 ± 2 (18%) | 4,3 ± 0,7 (16%) | 100% |
| **50 mL/min** | 45 ± 7 (16%) | 10 ± 1 (10%) | 4,4 ± 0,7 (16%) | 99,9% |
| **80 mL/min** | 47 ± 6 (13%) | 10 ± 1 (10%) | 4,5 ± 0,8 (18%) | 99,9% |

**Table 3.2.2.2B:** data from statistics on TEM images of the Au NRs grown in the high flow rates regime from seeds synthesized by hand.

As evidenced in Figure & Table 3.2.2.2A&B, the NRs synthesized in the low flow rates regime show to have lengths of 49 – 52 nm and widths of 12 – 13 nm, resulting in ARs of 4,2 – 4,3 while the NRs in the high regime appear to be a few nm shorter (length of 45 – 47 nm) and thinner

(width of 10 – 12 nm), presenting ARs of 4,1 – 4,5. Such difference results more explicit for the NRs synthesized at 50 and 80 mL/min, for which the lowest dimensions and highest ARs values are found.

The finding may be explainable thinking to the experiment itself. Seeds come in contact across the last channel with the solution containing $AgNO_3$, before being collected; as said, the control over anisotropic growth is given by $AgNO_3$, that in the latter cases is injected on the seeds with far higher speeds than in the previous ones: the maintenance of forced contact in the channel for shorter intervals of time may determine the shortness of dimensions. In order to demonstrate it, another experience would be necessary, with the flow synthesis of 100 mL at 5 and 50 mL/min (or at 8 and 80 mL/min) from the same growth solutions, for verifying whether the NRs differ in length and width as thought.

As concerns the shape purity, it is to be said that the values of NRs fraction reported are not trustingly representative, for an experimental reason which we report here. After being collected and characterized in the absorbance, all the samples were centrifuged at 8000 rpm for 40 min at least three times, to eliminate the surfactant in excess and to reduce the solution volume until 1,5 mL – the volume of the final vial in which the sample had to be stored before the deposition on TEM grid.

Such procedure worked generally for all the samples, except only the 100 mL ones. After the centrifugation stages, the solutions collected in 100 mL volumes resulted indeed more concentrated in the presence of nanospheres than before; it was necessary then another centrifugation at 3000 rpm for 1 h to remove the undesired NPs, that deposit at the bottom of the centrifuge vial. By doing this, the shape dispersion of the 100 mL samples was unavoidably altered, therefore the values of 99,9 – 100% for NRs fraction cannot be considered authentic outcomes of the flow synthesis.

Despite of the experimental artifact here illustrated, it must be remarked that the Au NRs solutions obtained with the reactor were monodisperse in shape, as emerges from the notable QR values and from the profile itself of absorbance spectra, taken before any centrifugation. Since the further elimination of nanospheres was executed only for the 100 mL samples, the values of NRs fraction found elsewhere are to be considered valid and characteristic indeed of the flow synthesis.

Finally, the conclusions to be drawn from the experience described are that the system performs the flow synthesis of 100 mL of Au NRs solution in the 1 – 80 mL/min range, without significant changes in the shape and size dispersion due to variations of the flow rate. Size may be affected, with the shortest length and width for the highest flow rates, but not the size dispersion, the real objective to reach by using automated reactors. The proportion between the flow rates and the volume collected lead us to believe that 8 L of monodisperse Au NRs solution are collectable, but

special attention must be paid then after the synthesis, during the centrifugation stage, since when dealing with big volumes it is easy to make mistakes such as concentrating spheres instead of NRs.

## 3.3 Flow synthesis of both seeds and NRs

After proving that seeds synthesized by hand can be successfully grown into NRs using the reactor, the next move was to perform even the synthesis of seeds into flow conditions. As known, when operating in batch, an aliquot of $NaBH_4$ solution is rapidly injected into an Au(III) solution under vigorous stirring; in our case, two of the three available pumps in the system were used, as depicted in Figure 3.3, with pump1 fluxing the CTAB solution containing Au(III), that mixes in the w-chamber with the $NaBH_4$ solution set in motion by pump2, while the final colloid of already formed seeds is collected in a beaker at the end of the channels system.

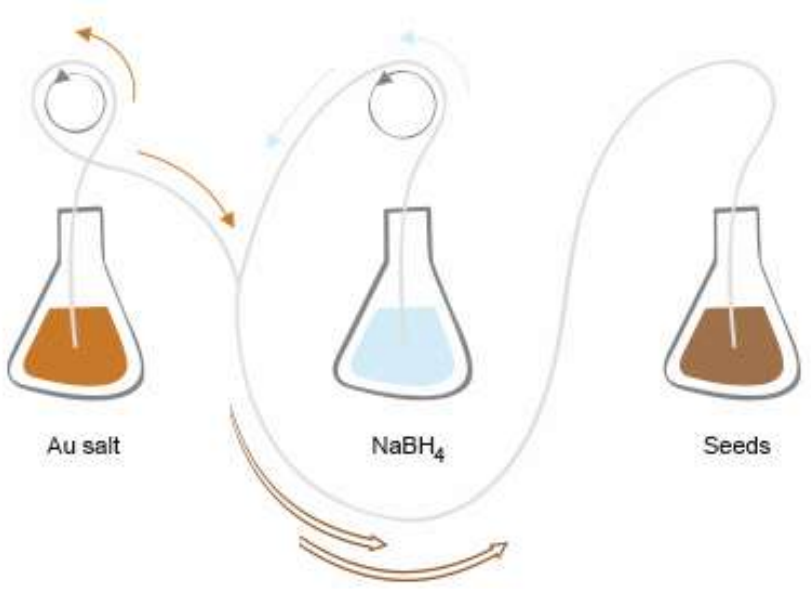


**Figure 3.3:** schematics of the millifluidic reactor as used for the seeds synthesis.

| Solution 1 | Solution 2 |
|---|---|
| 0.1 M in CTAB | 0.02 M in $NaBH_4$ |
| 0.001 M in $HAuCl_4$ | |

**Table 3.3:** composition of the Solutions in the beakers connected to the reactor.

The producers recommended 10:1 as the maximum ratio between the flow rates of two pumps to have proper mixing of the two solutions, and the rule was respected. Seeds were synthesized with the flow rates that we will see, and then always grown at 5 mL/min, a value chosen from those proved to be equally valid in the previous section. The main point here is to demonstrate whether the system provides us large amounts of monodisperse seeds, a clear advantage over the batch synthesis of 5 mL; we are also going to discuss the entity of the mixing time and to examine the consequences of aging the seeds, as well as the effects of changing the $AgNO_3$ and seeds concentrations during the growth.

### 3.3.1 Seeds reproducibility

As just introduced, if seeds are synthesizable by automated systems, consequently large amounts of seeds presenting almost identical features are collectable and can be grown into NRs with common characteristics. The reproducibility of seeds was thereby investigated: six consecutive 5 mL aliquots of seeds were collected at 11,2 mL/min (after waiting the proper mixing time for seeds, quantified in the next section), the system underwent cleaning with water and all the three pumps were then switched on; while pump1 and pump2 continued to flux the same growth solutions 1&2, pump3 worked pumping at turn from distinct beakers, containing some of the seeds aliquots (the 2$^{nd}$, the 4$^{th}$ and the 6$^{th}$), and three consecutive 10 mL samples of final solution were taken from each of it.

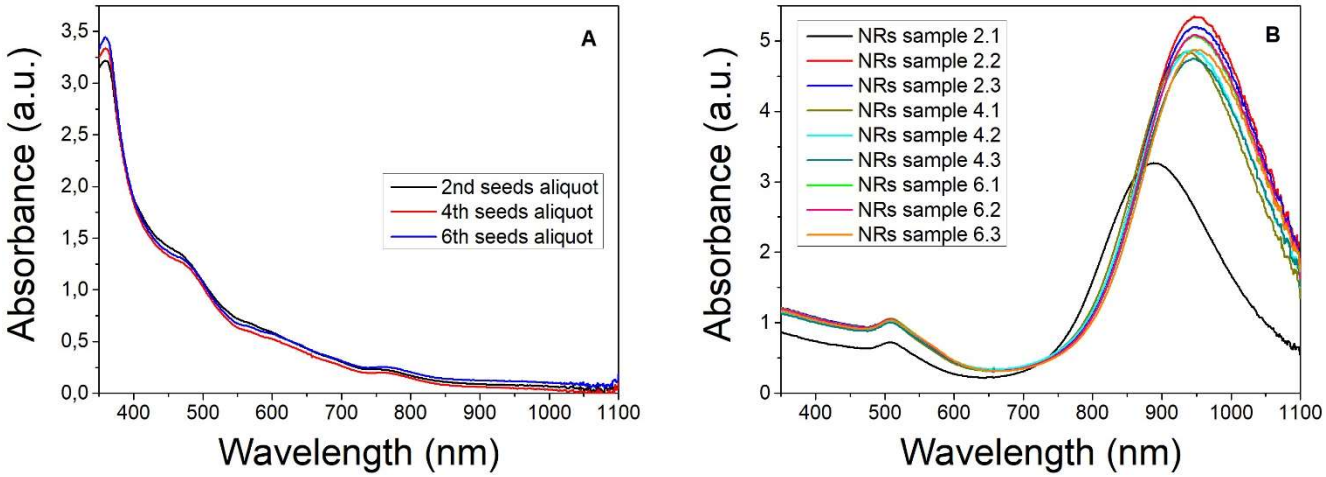


**Figure 3.3.1.1:** UV-vis-NIR absorbance spectra of three 5 mL aliquots of seeds synthesized at 11,2 mL/min (in **A**) and of the 10 mL samples of Au NRs grown at 5 mL/min from them (in **B**).

| | Longitudinal LSPR position [nm] | Quality Ratio [adim] | FWHM [nm] |
|---|---|---|---|
| **Sample 2.1** | 890 | 4,5 | 261 |
| **Sample 2.2** | 947 | 5,1 | 221 |
| **Sample 3.3** | 950 | 5,0 | 221 |
| **Sample 4.1** | 934 | 4,8 | 217 |
| **Sample 4.2** | 945 | 4,8 | 219 |
| **Sample 4.3** | 945 | 4,7 | 221 |
| **Sample 6.1** | 947 | 4,8 | 220 |
| **Sample 6.2** | 948 | 4,8 | 219 |
| **Sample 6.3** | 947 | 4,7 | 220 |

**Table 3.3.1.1:** data from the absorbance spectra of the 10 mL samples of Au NRs grown at 5 mL/min from distinct aliquots of seeds synthesized at 11,2 mL/min.

As evident in Figure 3.3.1.1A, the seeds of the three aliquots exhibit absorbance profiles that overlay for many intervals of wavelength, a proof of strong resemblance among them, while the exponentially decaying profile itself – typical of nanoclusters too small to support any plasmonic resonance, proves that the reactor is able to perform the synthesis of particle of less than 2 nm in size.

As reported in Figure & Table 3.3.1.1, except the NRs sample 2.1 (unfortunately collected before waiting the proper mixing time for the growth), all the samples present very similar characteristics, with the longitudinal LSPR peak in the range of 934 – 950 nm, together with QR and FWHM varying in narrow ranges too, i.e., respectively of 4,7 – 5 and 217 – 221 nm. Seeds from distinct aliquots were evidently grown into NRs appearing to have the same AR and dispersion in shape and size; some of the samples collected were then studied with TEM analysis.

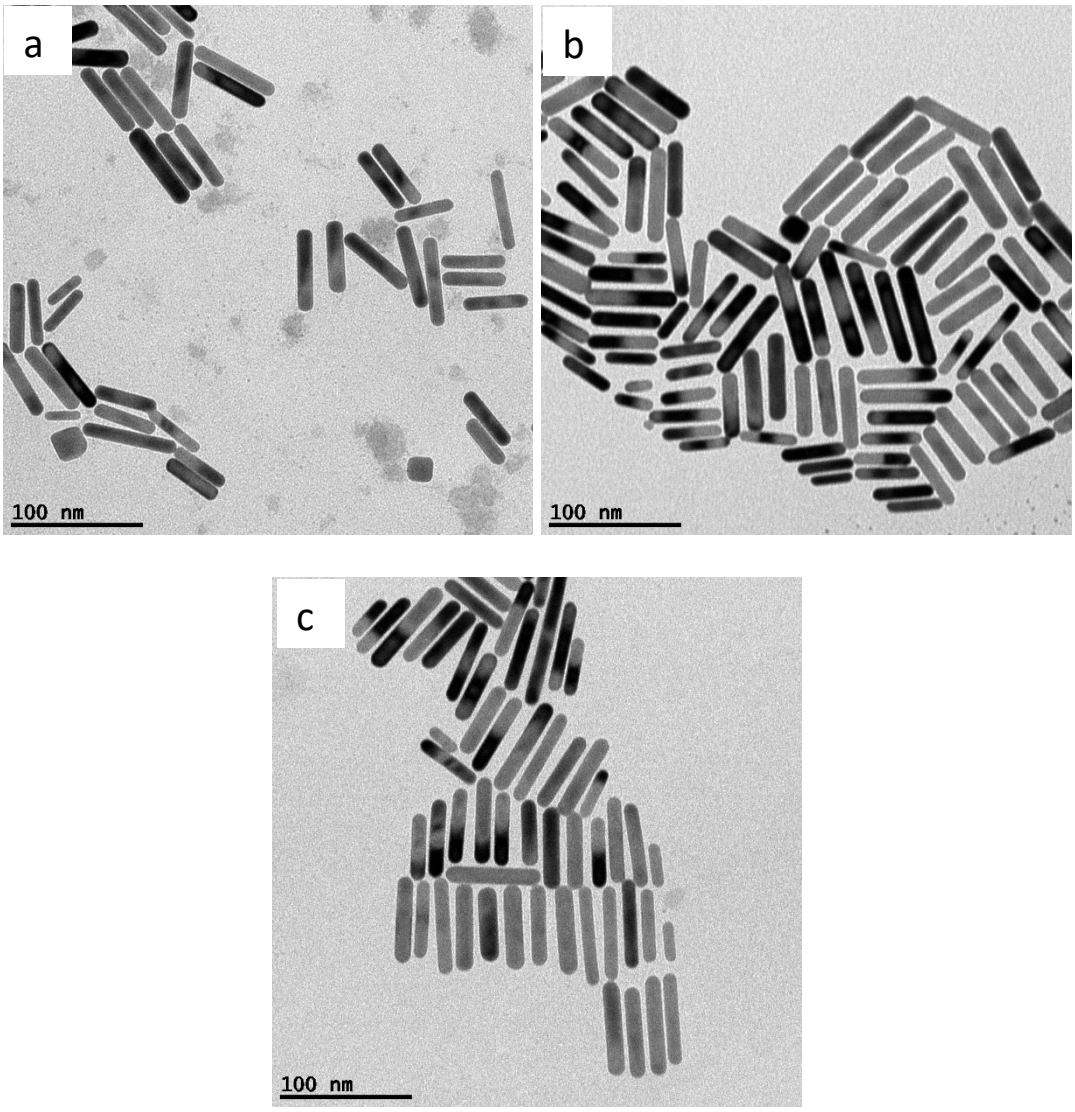


**Figure 3.3.1.2:** TEM micrographs of the samples 2.3 (in **a**), 4.3 (in **b**) and 6.3 (in **c**) of Au NRs grown at 5 mL/min from distinct aliquots of seeds synthesized at 11,2 mL/min.

| | **Length [nm]** | **Width [nm]** | **Aspect Ratio [adim]** | **NRs fraction [adim]** |
|---|---|---|---|---|
| **Sample 2.3** | 55 ± 11 (20%) | 12 ± 2 (17%) | 4,5 ± 0,8 (18%) | 97,7% |
| **Sample 4.3** | 53 ± 13 (25%) | 12 ± 2 (17%) | 4,2 ± 0,8 (19%) | 98,0% |
| **Sample 6.3** | 57 ± 12 (21%) | 13 ± 2 (15%) | 4,5 ± 0,8 (18%) | 99,0% |

**Table 3.3.1.2:** data from statistics on TEM images of Au NRs samples grown at 5 mL/min from distinct aliquots of seeds synthesized at 11,2 mL/min.

As reported in Figure & Table 3.3.1.2, the Au NRs in the samples grown from distinct seeds aliquots show to have almost the same characteristics in terms of size (length of 53 – 57 nm, width of 12 – 13 nm, and AR equal to 4,2 or 4,5) with comparable values of standard deviation; moreover, the shape dispersion is found to be low, with the fraction of undesired NPs below the 3% for each sample. Such outcomes furtherly confirm the reproducibility of seeds synthesized with the reactor.

### 3.3.2 Effect of flow rate on τ

Seeds and NRs solution cannot be collected from the system before waiting the mixing time, as written in the previous sections; in both cases, such amount of time corresponds to 3τ, defined as the ratio of the volume between the two mixing points and the sum of the partial flow rates set in pump1 and pump2 (even if during seeds synthesis no mixing takes place at the second w-chamber); for each flow rate, when flow synthesis of seeds is performed, a 3τ volume equals to 18 mL approximately.

The reproducibility of seeds has already been proved, after being collected at 11,2 mL/min in six consecutive 5 mL aliquots (for a total of 30 mL); what happens for larger volumes and longer times? We tested whether the use of different flow rates affects the outcomes and the mixing time to be waited: after turning on the reactor, six consecutive 3τ aliquots of seeds were collected, successively each of them was at turn diluted and put in the system to be grown from the same Growth Solutions 1&2; 20 mL samples of final solution were instead collected from each aliquot of seeds.

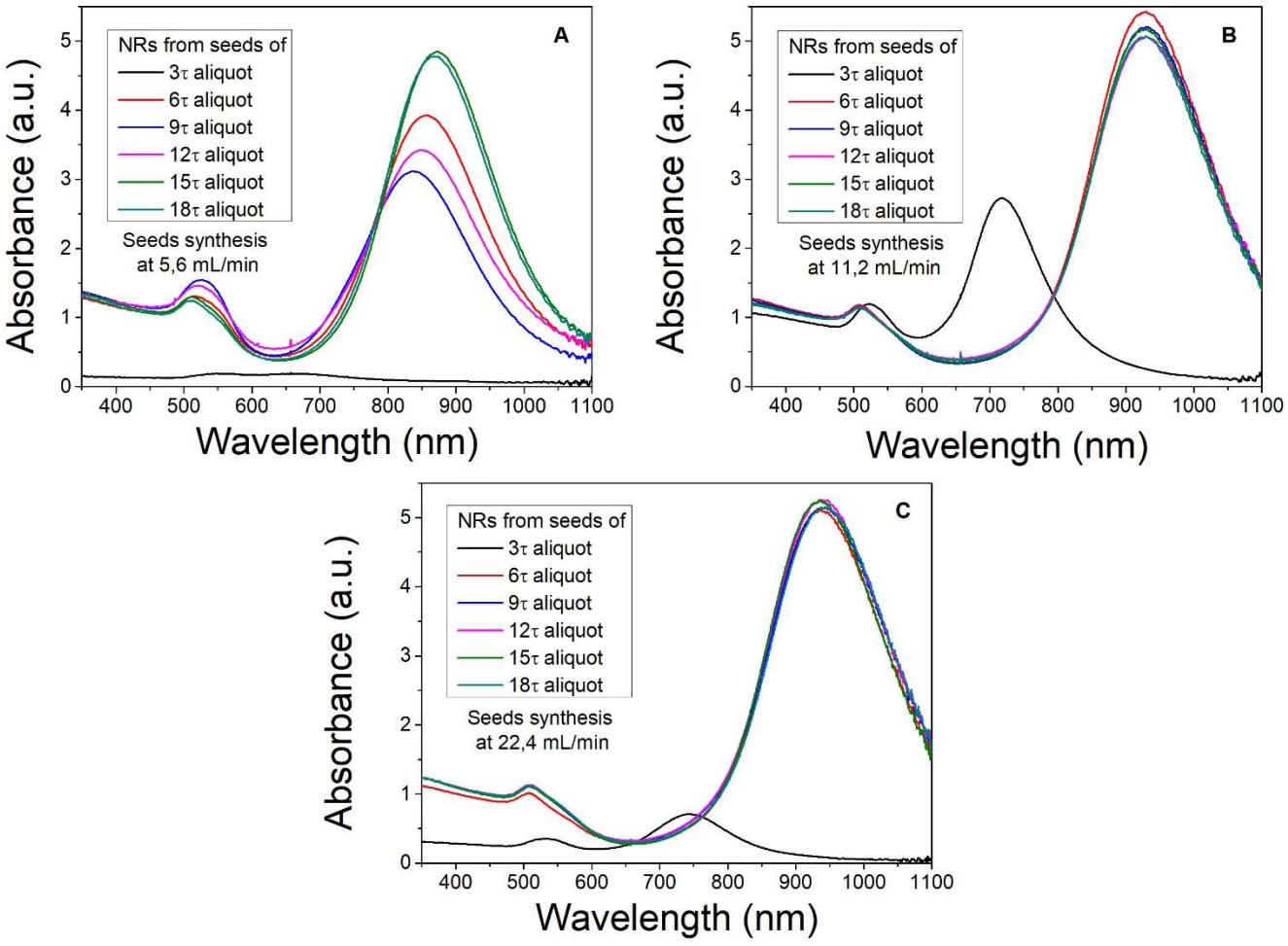


**Figure 3.3.2:** UV-vis-NIR absorbance spectra of the 20 mL samples of Au NRs grown at 5 mL/min from the 3-18τ aliquots of seeds synthesized at 5,6 mL/min (in **A**), at 11,2 mL/min (in **B**) and at 22,4 mL/min (in **C**).

| | 5.6 mL/min | 11.2 mL/min | 22.4 mL/min |
|---|---|---|---|
| **3τ aliquot** | X | 2.2 | 2.0 |
| **6τ aliquot** | 3.0 | 4.6 | 5.1 |
| **9τ aliquot** | 2.0 | 4.5 | 4.6 |
| **12τ aliquot** | 2.3 | 4.4 | 4.7 |
| **15τ aliquot** | 3.7 | 4.5 | 4.7 |
| **18τ aliquot** | 3.8 | 4.5 | 4.6 |

**Table 3.3.2:** QR data from the absorbance spectra of the 20 mL samples of Au NRs grown at 5 mL/min from the 3-18τ aliquots of seeds synthesized at 5,6 mL/min, at 11,2 mL/min and at 22,4 mL/min.

As evidenced in Figure & Table 3.3.2, the seeds were synthesized at three distinct flow rates; each 3τ aliquot of approximately 18 mL was taken respectively every 3 min 11 s at 5,6 mL/min, every 1 min 35 s at 11,2 mL/min and every 48 s at 22,4 mL/min – from such values it is easily understandable that the experiments took different intervals of time to be conducted, while it is known from batch synthesis of seeds that time has great influence over the quality of the final outcomes, given the hygroscopic nature of $NaBH_4$ that rapidly tends to evaporate in the atmosphere.

No NRs at 5,6 mL/min and the worst quality NRs at 11,2 and 22,4 mL/min were grown from the 3τ aliquot of seeds, confirming that it makes no sense collecting aliquots before the mixing time; the NRs most monodisperse in shape are found for the 18τ aliquot at 5,6 mL/min and for the 6τ at 11,2 and 22,4 mL/min. Anyway, in the next experiences 6τ was chosen as the optimal aliquot of seeds for every flow rate, since at 5,6 mL/min the 18τ aliquot is collectable only waiting 16 min and such interval of time is challenging for $NaBH_4$ evaporation in variable conditions of atmospheric humidity.

It is to remark here that such experience was aimed at observing the quality of NRs grown from seeds of aliquots taken every 3τ, in order to understand the optimal τ for each flow rate used in seeds synthesis; the experiences were conducted in three different days, the values of QRs obtained in each case are thereby not comparable in order to establish which is the flow rate for seeds synthesis giving the most monodisperse NRs, exactly the topic that we are going to deal with in the next section.

### 3.3.3 Effect of optimal τ

Once proven that 6τ is the optimal aliquot of seeds to grow into NRs, the best flow rate to use for seeds synthesis had yet to be identified; for addressing such question, seeds were synthesized from the same Au solution at the various flow rates (preparing each time a fresh $NaBH_4$ solution), the 6τ aliquot were collected and characterized using the spectrophotometer, diluted into three distinct beakers 0,1 M in CTAB and then put at turn into the system to grow as Growth Solution 3, maintaining instead the Growth Solutions 1&2 and collecting 20 mL of final solution in each case.

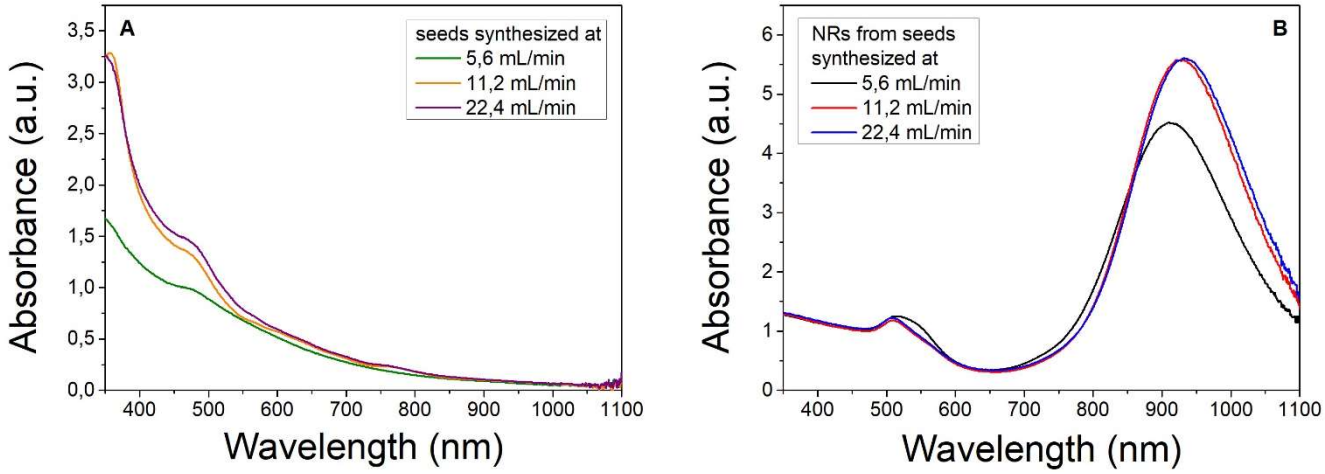


**Figure 3.3.3.1:** UV-vis-NIR absorbance spectra of the 6τ aliquots of seeds synthesized at various flow rates (in **A**) and of the 20 mL samples of Au NRs grown at 5 mL/min from them (in **B**).

| | **Longitudinal LSPR position [nm]** | **Quality Ratio [adim]** | **FWHM [nm]** |
|---|---|---|---|
| **5.6 mL/min** | 910 | 3,6 | 209 |
| **11.2 mL/min** | 921 | 4,7 | 202 |
| **22.4 mL/min** | 932 | 4,6 | 208 |

**Table 3.3.3.1:** data from the absorbance spectra of the 20 mL samples of Au NRs grown at 5 mL/min from the 6τ aliquots of seeds synthesized at various flow rates.

As evidenced in Figure & Table 3.3.3.1, the distinct flow rates gave us seeds with size below 2 nm, exhibiting the typical exponentially decaying absorbance profile, then grown into NRs, displaying the transversal and longitudinal plasmon bands; particularly, the seeds obtained at 5,6 mL/min show a flatter profile varying in a more delimited range of lower absorbance values, and the NRs grown from such seeds are blue-shifted and less monodisperse in shape, in comparison with the seeds synthesized at 11,2 and 22,4 mL/min and the NRs grown from these latter.

During the operations it was noticed that NRs proper color in the solution was assumed earlier when growing seeds synthesized at 5,6 mL/min, while the time to observe the change increased with those at superior flow rates; the phenomenon, due to the growth completion, may be related to differences in size of the seeds: those obtained at 11,2 and 22,4 mL/min could be smaller for the higher injection speed and therefore take longer time to grow into NRs. The samples had then to be studied with TEM, to reveal the characteristics of size and polydispersity.

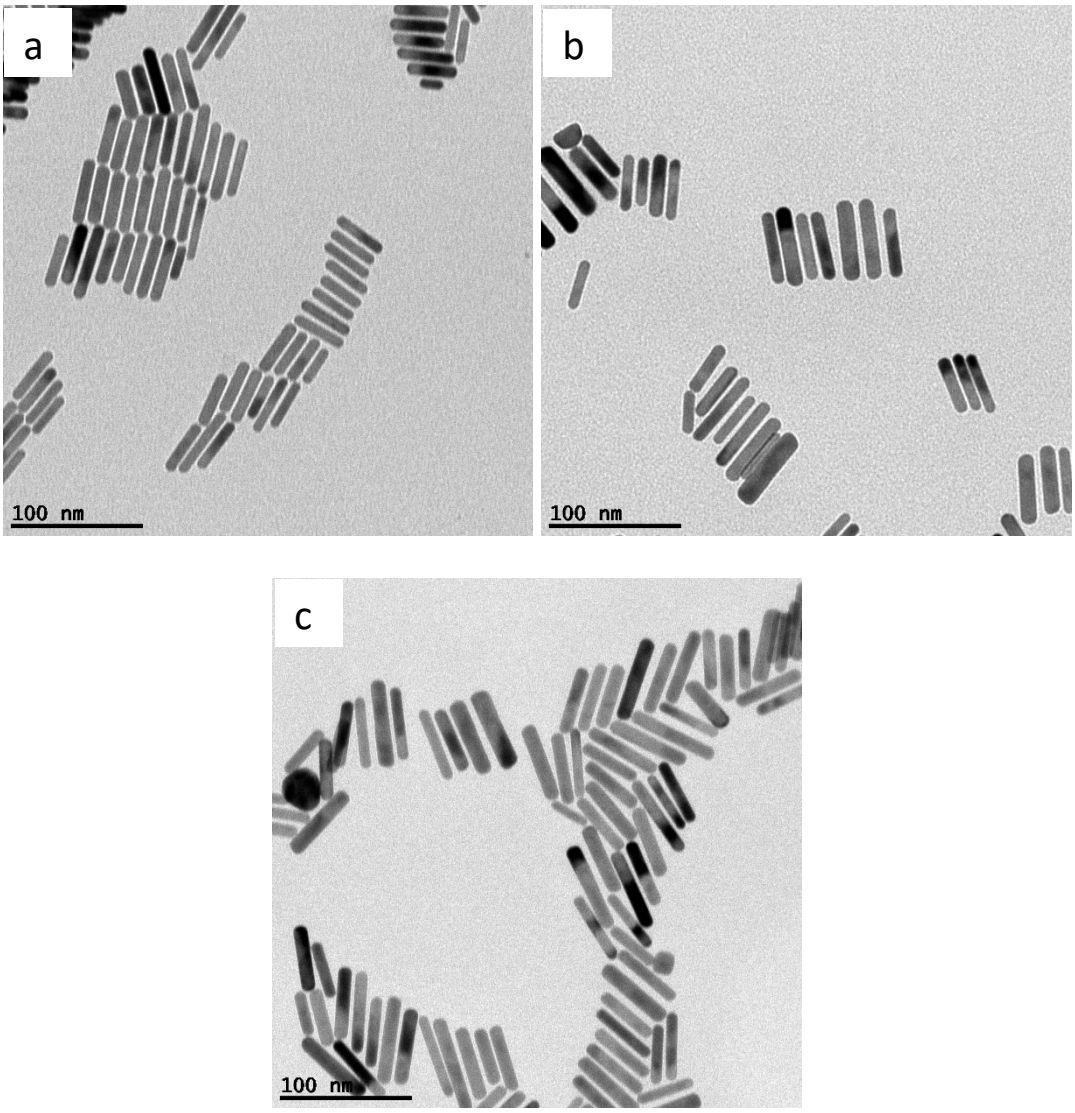


**Figure 3.3.3.2:** TEM micrographs of the Au NRs grown at 5 mL/min from seeds synthesized at 5,6 mL/min (in **a**), at 11,2 mL/min (in **b**) and at 22,4 mL/min (in **c**).

| | Length [nm] | Width [nm] | Aspect Ratio [adim] | NRs fraction [adim] |
|---|---|---|---|---|
| **5.6 mL/min** | 41 ± 8 (20%) | 10 ± 2 (20%) | 4,2 ± 0,8 (19%) | 97,6% |
| **11.2 mL/min** | 51 ± 9 (18%) | 11 ± 2 (18%) | 4,6 ± 0,8 (17%) | 98,6% |
| **22.4 mL/min** | 52 ± 9 (17%) | 11 ± 2 (18%) | 4,7 ± 0,8 (17%) | 98,0% |

**Table 3.3.3.2:** data from statistics on TEM images of the Au NRs grown at 5 mL/min from seeds synthesized at various flow rates.

As reported in Figure & Table 3.3.3.2, the NRs grown from seeds synthesized at 5,6 mL/min have length of 41 nm and width of 10 nm, resulting in AR of 4,2 – while the NRs from seeds at higher flow rates have 51 – 52 nm and 11 nm, for ARs of 4,6 – 4,7 and are also less monodisperse in size; from the point of view of the shape purity, the lowest fraction of undesired NRs is found for those grown from seeds synthesized at 11,2 mL/min, then at 22,5 mL/min and finally at 5,6 mL/min.

The experience and the outcomes just exposed led us to understand the conditions for having the best monodisperse NRs. Seeds must be synthesized at 11,2 mL/min, collecting the 6τ aliquot; NRs are then growable from such aliquot, at of 5 mL/min as we did, but also with the other flow rates that are available to the system. Other important considerations on the use of distinct flow rates, affecting the stability of the reactor with external factors, will be advanced in the conclusive section.

### 3.3.4 Effect of aging time on seeds

Several sources in literature report that aging time dramatically affects the growth of NRs, as in the case of seeds that in few hours become too old to be grown into anisotropic NPs and present instead plasmonic resonance themselves. We also investigated the effect of aging time on seeds, as in the batch synthesis, applying our protocol for NRs with the reactor; the same seeds synthesized in the previous experience at various flow rates were diluted and left into three distinct beakers for 24 h, then put at turn into the system to grow into NRs from the same Growth Solutions 1&2.

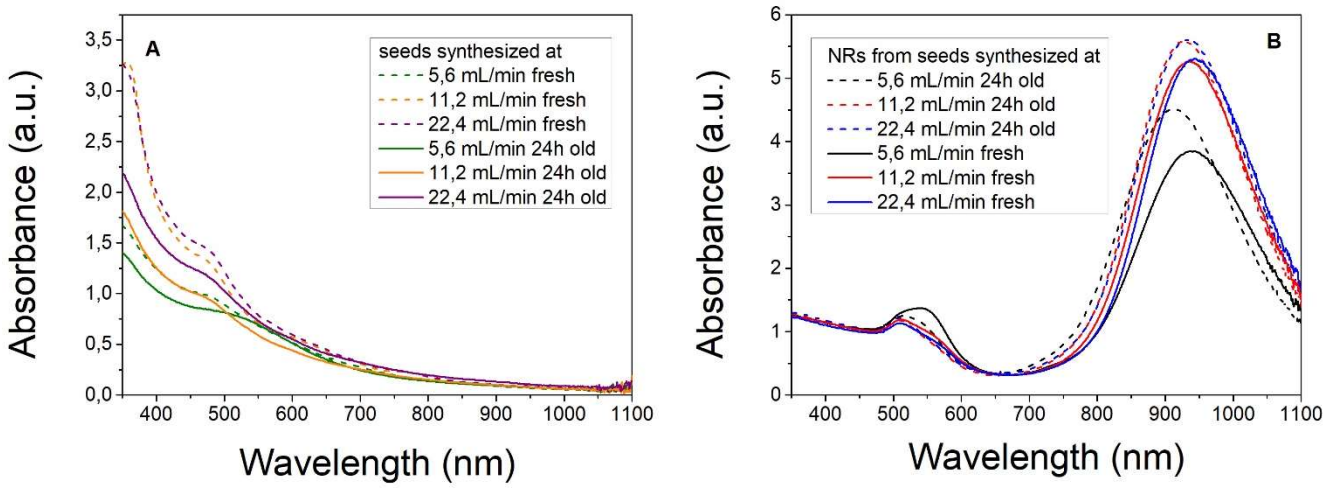


**Figure 3.3.4.1:** UV-vis-NIR absorbance spectra of the 6τ aliquots of seeds synthesized at various flow rates, fresh and 24 h old (in **A**) and of the 20 mL Au NRs samples grown at 5 mL/min from them (in **B**).

| | **Longitudinal LSPR position [nm]** | **Quality Ratio [adim]** | **FWHM [nm]** |
|---|---|---|---|
| **5.6 mL/min** | 944 | 2.8 | 215 |
| **11.2 mL/min** | 936 | 4.4 | 206 |
| **22.4 mL/min** | 942 | 4.7 | 206 |

**Table 3.3.4.1:** data from the absorbance spectra of the 20 mL samples of Au NRs grown at 5 mL/min from 24 h old seeds synthesized at various flow rates.

As evident in Figure & Table 3.3.4.1, the 24 h aging time does not determine the growth into plasmonic nanospheres of the seeds, that are instead still able to grow into NRs with the use of the reactor. 24 h after the synthesis, the various seeds continue to exhibit the exponentially decaying profiles of absorbance typical of nanoclusters below 2 nm in size, but flatter and delimited to shorter ranges of lower absorbance values, compared to the profiles measured just after seeds synthesis; it is also noticeable that the aging time results in red-shifted longitudinal in each case, while a sharp decrease in QR is observed only for the NRs grown from seeds synthesized at 5,6 mL/min.

The QR values here reported are not really comparable with those of NRs grown from fresh seeds, since distinct Growth Solutions 1&2 were used for the two experiences, conducted thereby in different conditions; anyway, it can be affirmed that the NRs grown from 24 h old seeds synthesized at 11,2 and 22,4 mL/min result to be monodisperse in shape, likely those from fresh seeds, unlikely those from seeds at 5,6 mL/min; the final account of the situation was then given by TEM analysis.

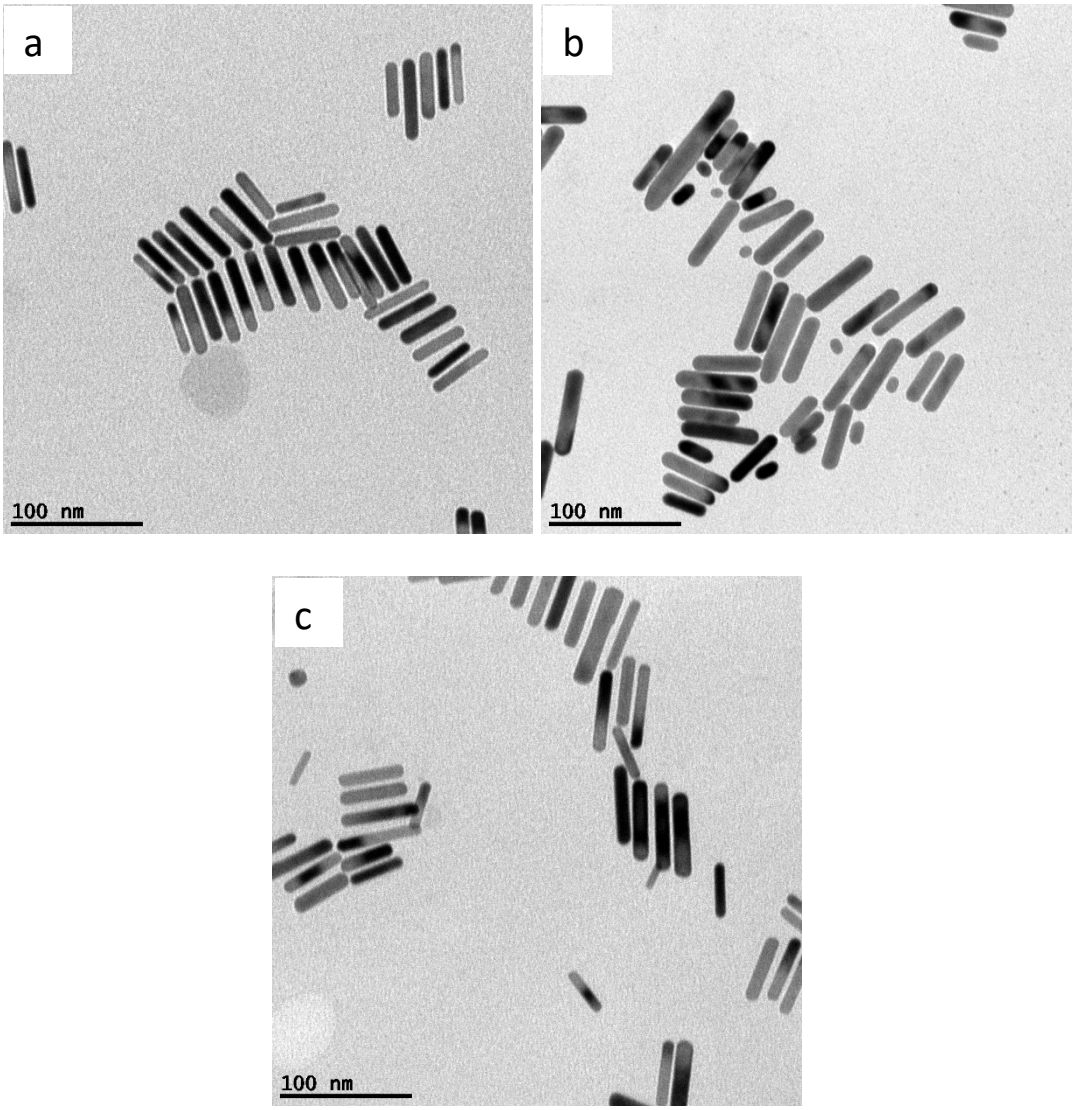


**Figure 3.3.4.2:** TEM micrographs of the Au NRs grown at 5 mL/min from 24 h old seeds synthesized at 5,6 mL/min (in **a**), at 11,2 mL/min (in **b**) and at 22,4 mL/min (in **c**).

| | **Length [nm]** | **Width [nm]** | **Aspect Ratio [adim]** | **NRs fraction [adim]** |
|---|---|---|---|---|
| **5.6 mL/min** | 50 ± 6 (12%) | 12 ± 2 (17%) | 4,3 ± 0,7 (16%) | 97,6% |
| **11.2 mL/min** | 54 ± 11 (20%) | 14 ± 2 (14%) | 3,8 ± 0,6 (16%) | 99,6% |
| **22.4 mL/min** | 54 ± 10 (19%) | 12 ± 2 (17%) | 4,4 ± 0,8 (18%) | 98,5% |

**Table 3.3.4.2:** data from statistics on TEM images of the Au NRs grown at 5 mL/min from 24 h old seeds synthesized at various flow rates.

As reported in Figure & Table 3.3.4.2, the aging time on seeds results in the growth of NRs with higher length and width, a probable consequence of the size increased in the seeds themselves; comparing the dimensional values here reported and in the previous section, it is soon verifiable the increase in length and width just announced in each case, while the ARs trend appears to differ: a decrease is found for NRs from seeds synthesized at 11,2 and 22,4 mL/min (from 4,6 to 3,8 and from 4,7 to 4,4) while an increase for NRs from seeds at 5,6 mL/min (from 4,2 to 4,3).

It is arduous to clarify the importance of the latest difference described, the seeds synthesized at the lowest flow rate are supposed to be the biggest ones and in 24 h may undergo to growth processes that lead finally to more anisotropic NRs; conversely, seeds obtained at higher flow rates are smaller and the aging time favors the formation of longer and wider but less anisotropic NRs.

As illustrated in the previous chapter, the anisotropic growth of single crystalline NRs from isotropic seeds involves stages of polycrystallinity, it is therefore hard to explain the mechanism responsible for the differences found in the ARs. Right conclusions from the experience could be drawn only by monitoring with TEM the evolution of seeds in time, but it is very difficult to take good images of it because seeds are likely be altered preparing the grid and during the analysis.

Beside the differences in anisotropic growth, it emerged that the lowest shape purity pertains NRs from 24 h old seeds synthesized at 5,6 mL/min, as deducible from absorbance spectra, while very high fractions of NRs are found for the remaining samples; as concerns the size dispersion, no significant differences are observed, with standard deviations always in the 12-20 percentage range.

Despite the obscure aspects unavoidably connected to the symmetry-breaking event and the anisotropic growth, the main point of the experience still shines: seeds aged of 24 h remain stable, below the critical size for supporting plasmon resonance, and continue to be growable into NRs resulting monodisperse in shape and size. The final quality varies for the flow rates used with the reactor, whereas instead the long-time stability of seeds derives from the protocol adopted in our case, as verified already in the chapter about the batch synthesis, different from that of other groups.

### 3.3.5 Effect of $AgNO_3$ concentration

Since the influence of $AgNO_3$ concentration on the anisotropic growth of Au NRs is well known, an experience was conducted to reproduce it with the reactor. Varying the $AgNO_3$ concentration as in the analogous batch experience, seven beakers of Growth Solution 1 were prepared and put at turn into the system, where Growth Solutions 2&3 were instead maintained all the time; at the end of the channels, 20 mL of final solution were collected for each concentration and successively analyzed.

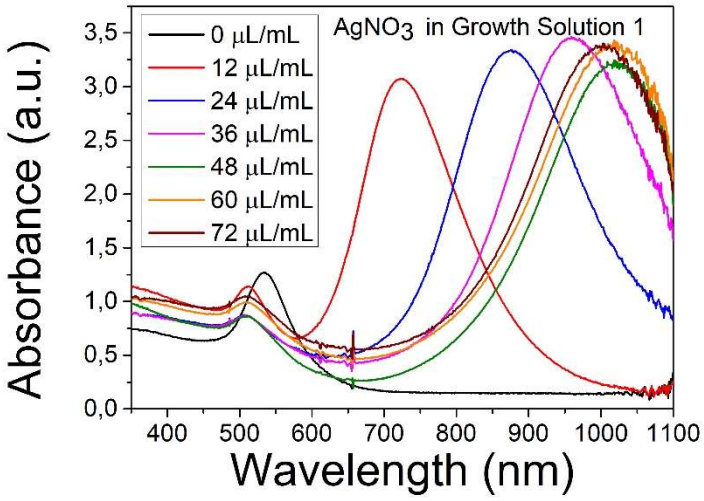


**Figure 3.3.5.1:** UV-vis-NIR absorbance spectra of the 20 mL samples of Au NRs grown at 5 mL/min from seeds synthesized at 11,2 mL/min, after adding 0-72 µL/mL of $AgNO_3$ 0,01 M in Growth Solution 1.

| | **Longitudinal LSPR position [nm]** | **Quality Ratio [adim]** | **FWHM [nm]** |
|---|---|---|---|
| **0 µL/mL** | 534 | 1 | 129 |
| **12 µL/mL** | 725 | 2.7 | 173 |
| **24 µL/mL** | 877 | 3.8 | 225 |
| **36 µL/mL** | 959 | 4.0 | 245 |
| **48 µL/mL** | 1018 | 3.8 | >205 |
| **60 µL/mL** | 1018 | 3.5 | >216 |
| **72 µL/mL** | 1003 | 3.2 | >226 |

**Table 3.3.5.1:** data from the absorbance spectra of the 20 mL samples of Au NRs grown at 5 mL/min from seeds synthesized at 11,2 mL/min, after adding 0-72 µL/mL of $AgNO_3$ 0,01 M in Growth Solution 1.

As evident in Figure & Table 3.3.5.1, the variation of [$AgNO_3$] expectedly led to solutions of NRs differently characterized: in absence of $AgNO_3$, the transversal and longitudinal plasmonic peaks coincide into one (as no NRs are presumably formed); then, increasing the content, a red-shift of the longitudinal LSPR is verified until 1018 nm, followed by a blue-shift for the latest addition. A quick

look at the values of QR and FWHM, respectively lower and higher than usual, may give us a clue that some mistake was made during the experience, maybe the wrong CTAB or water were used instead of the purest ones for Au NRs synthesis; not only the polydispersity, but also the characteristic dimensions and consequently the AR could be invalidated, as we are going to see in the TEM analysis.

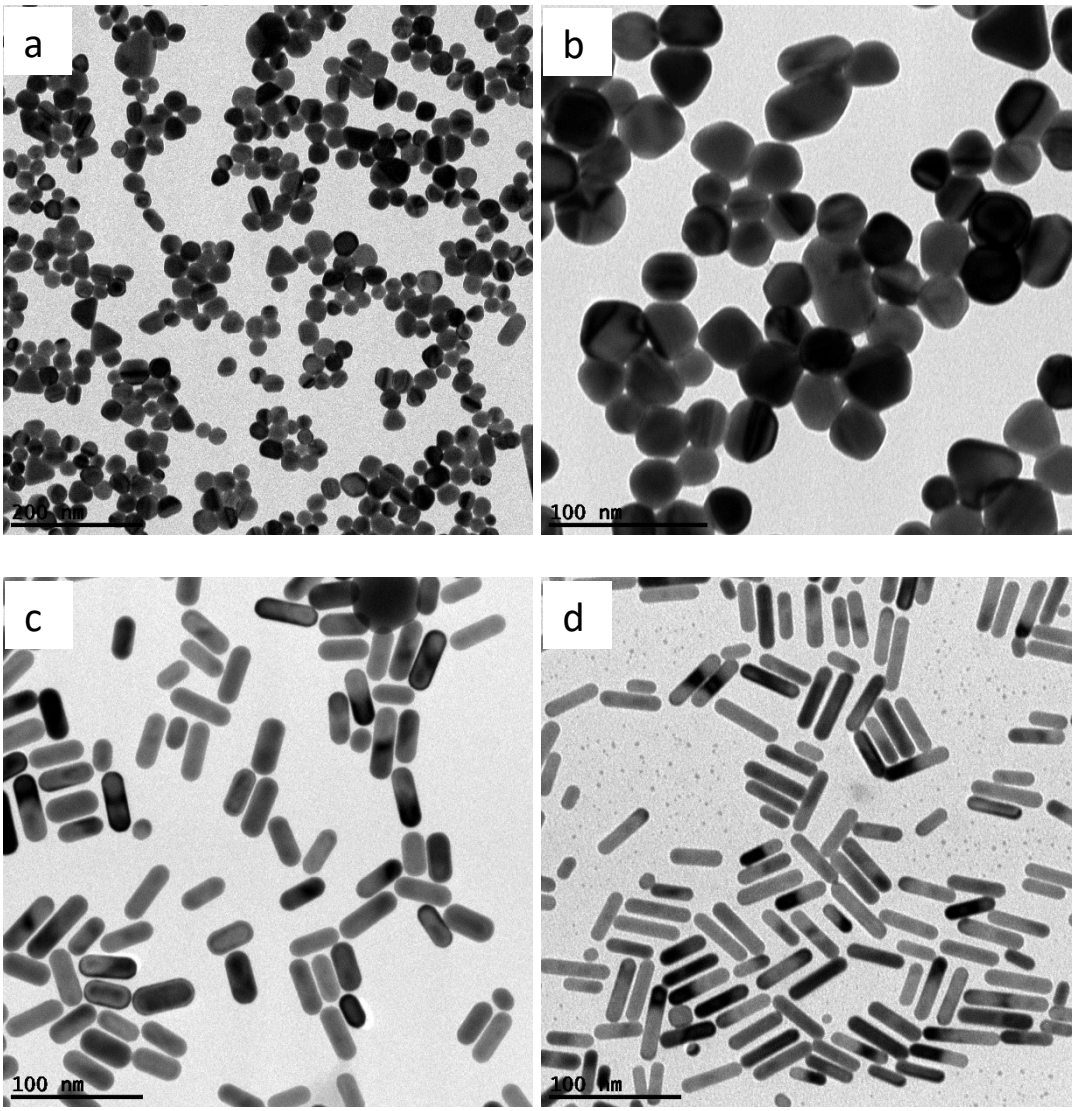


**Figure 3.3.5.2:** TEM micrographs of the Au NPs grown in absence of $AgNO_3$ (in **a** and in **b**) with scale bars of 200 and 100 nm, and of the NRs grown after adding 12 µL/mL (in **c**) and 24 µL/mL (in **d**) of $AgNO_3$, with scale bar of 100 nm.

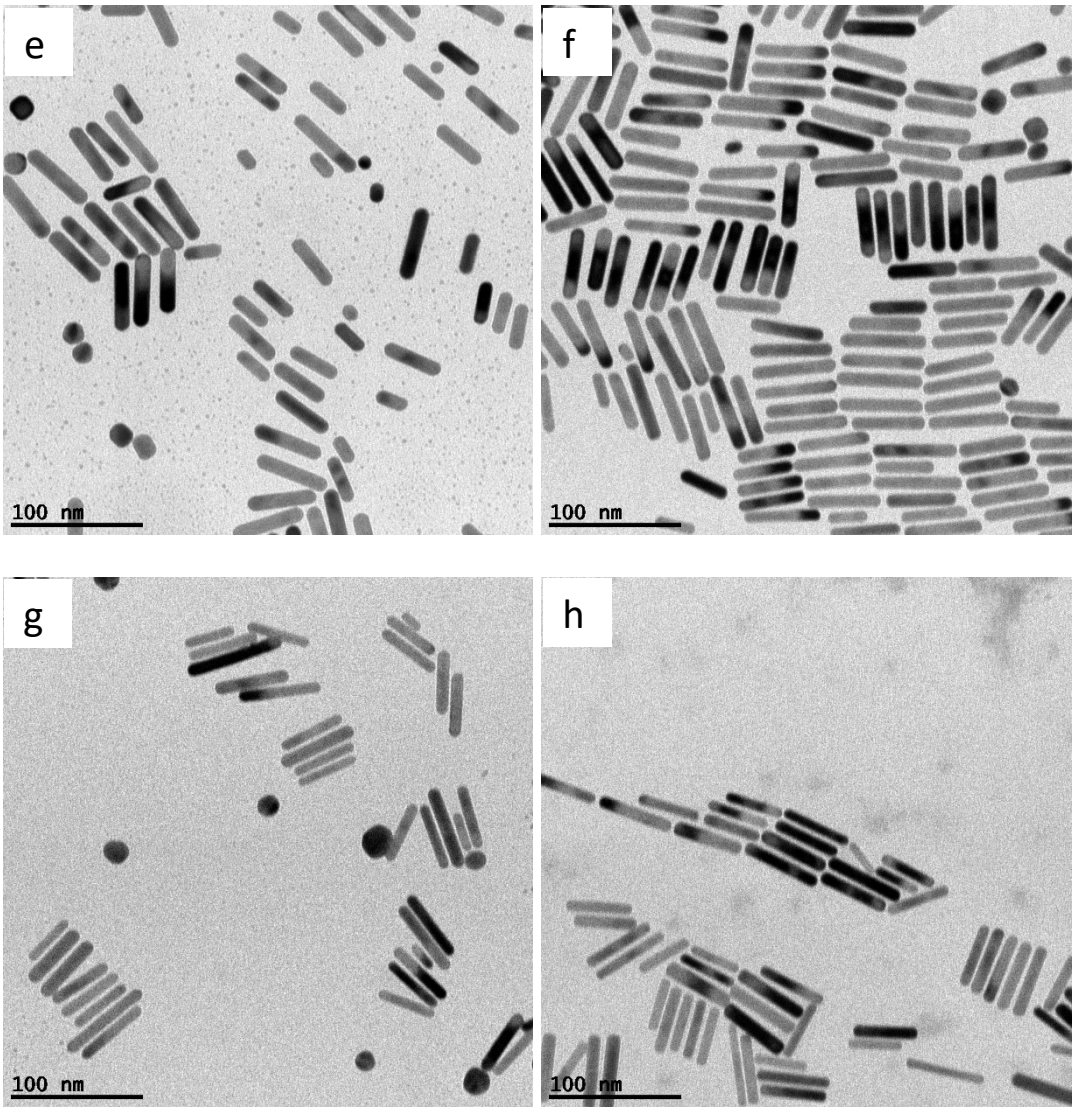


**Figure 3.3.5.2:** TEM micrographs of the Au NRs grown after adding 36 µL/mL (in **e**), 48 µL/mL (in **f**), 60 µL/mL (in **g**) and 72 µL/mL (in **h**) of $AgNO_3$, with scale bar of 100 nm.

| | **Length [nm]** | **Width [nm]** | **Aspect Ratio [adim]** | **NRs fraction [adim]** |
|---|---|---|---|---|
| **12 µL/mL** | 40 ± 8 (20%) | 18 ± 2 (11%) | 2,3 ± 0,4 (17%) | 94,1% |
| **24 µL/mL** | 43 ± 10 (23%) | 13 ± 1 (8%) | 3,3 ± 0,7 (21%) | 97,6% |
| **36 µL/mL** | 40 ± 13 (33%) | 12 ± 1 (8%) | 3,3 ± 1,0 (30%) | 94,0% |
| **48 µL/mL** | 53 ± 10 (19%) | 13 ± 2 (15%) | 4,3 ± 0,9 (21%) | 86,7% |
| **60 µL/mL** | 49 ± 12 (24%) | 11 ± 2 (18%) | 4,4 ± 1,0 (23%) | 88,5% |
| **72 µL/mL** | 53 ± 9 (17%) | 12 ± 2 (17%) | 4,4 ± 1,0 (23%) | 96,4% |

**Table 3.3.5.2:** data from statistics on TEM images of the Au NRs grown after adding 12-72 µL/mL of $AgNO_3$.

As reported in Figure & Table 3.3.5.2, the TEM analysis of the samples reveals the same trend exposed by absorbance spectra with further information. In absence of $AgNO_3$, the formation of

prevalently nanotriangles and nanospheres takes place, all NPs that look interestingly quite monodisperse; the increasing amount of $AgNO_3$ added leads to the growth of NRs presenting progressively higher ARs, which correspond to the most red-shifted longitudinal LSPR peaks found.

As already anticipated, something evidently went wrong during the synthesis. For instance, it can be noticed that the NRs obtained in the usual conditions, by adding 24 μL/mL of $AgNO_3$ to Growth Solution 1, present an AR of 3,3 – a value largely lower than in any experience; this fact, alongside with the smallest NRs fractions ever found using the reactor, hints us that some mistakes were made, and the experience must be repeated for providing reliable results.

Despite the adverse working conditions, probably due to the presence of undesired substances in the water or in the CTAB, the reactor performed the flow synthesis and in absence of $AgNO_3$ gave even monodisperse NPs different from NRs, resulting from the excellent mixing proper of the system.

### 3.3.6 Effect of seeds amount

The last experiment conducted with the reactor concerned the effect of varying the amount of seeds to grow into Au NRs, while maintaining the other conditions; seven beakers with increasing additions of seeds were set as Growth Solution 3 and put at turn into the system, where instead Growth Solutions 1&2 were kept the same all the time; in each case 20 mL of final solution were collected at the end of the channels and subsequently analyzed. Since the seeds amount is the only factor we are playing with, the expected outcome is a progressive decrease of both length and width in the NRs – corresponding to the increased number of seeds from which the anisotropic growth takes place.

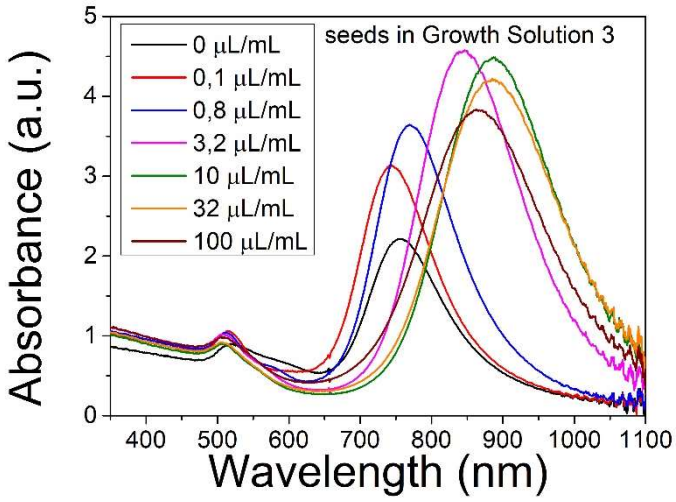


**Figure 3.3.6.1:** UV-vis-NIR absorbance spectra of the 20 mL samples of Au NRs grown at 5 mL/min, after adding 0-100 µL/mL of seeds synthesized at 11,2 mL/min in Growth Solution 3.

| | **Longitudinal LSPR position [nm]** | **Quality Ratio [adim]** | **FWHM [nm]** |
|---|---|---|---|
| **0 µL/mL** | 755 | 2.5 | 139 |
| **0.1 µL/mL** | 745 | 3.0 | 131 |
| **0.8 µL/mL** | 769 | 3.5 | 141 |
| **3.2 µL/mL** | 846 | 4.5 | 173 |
| **10 µL/mL** | 887 | 5.0 | 193 |
| **32 µL/mL** | 885 | 4.6 | 206 |
| **100 µL/mL** | 863 | 3.9 | 208 |

**Table 3.3.6.1:** data from absorbance spectra of the 20 mL samples of Au NRs grown at 5 mL/min, after adding 0-100 µL/mL of seeds synthesized at 11,2 mL/min in Growth Solution 3.

As evident in Figure & Table 3.3.6.1, formation of Au NRs was verified in each case; even in absence of seeds, auto-nucleation of seeds took place (and the experience was repeated several times

to confirm it), giving anyway the worst polydisperse NRs, with the longitudinal LSPR peak in the threshold between the visible and near-infrared regions of light, as those of the NRs obtained by adding 0.1 and 0.8 µL/mL of seeds. A red-shifting trend is found for further additions until 10 µL/mL, followed by a blue-shift for the latest two; generally good values of QR are recorded in time, accompanied by higher size polydispersity, a likely consequence of the dimensional reduction verified by the increase in the seeds amount. As usual, TEM characterization was finally executed.

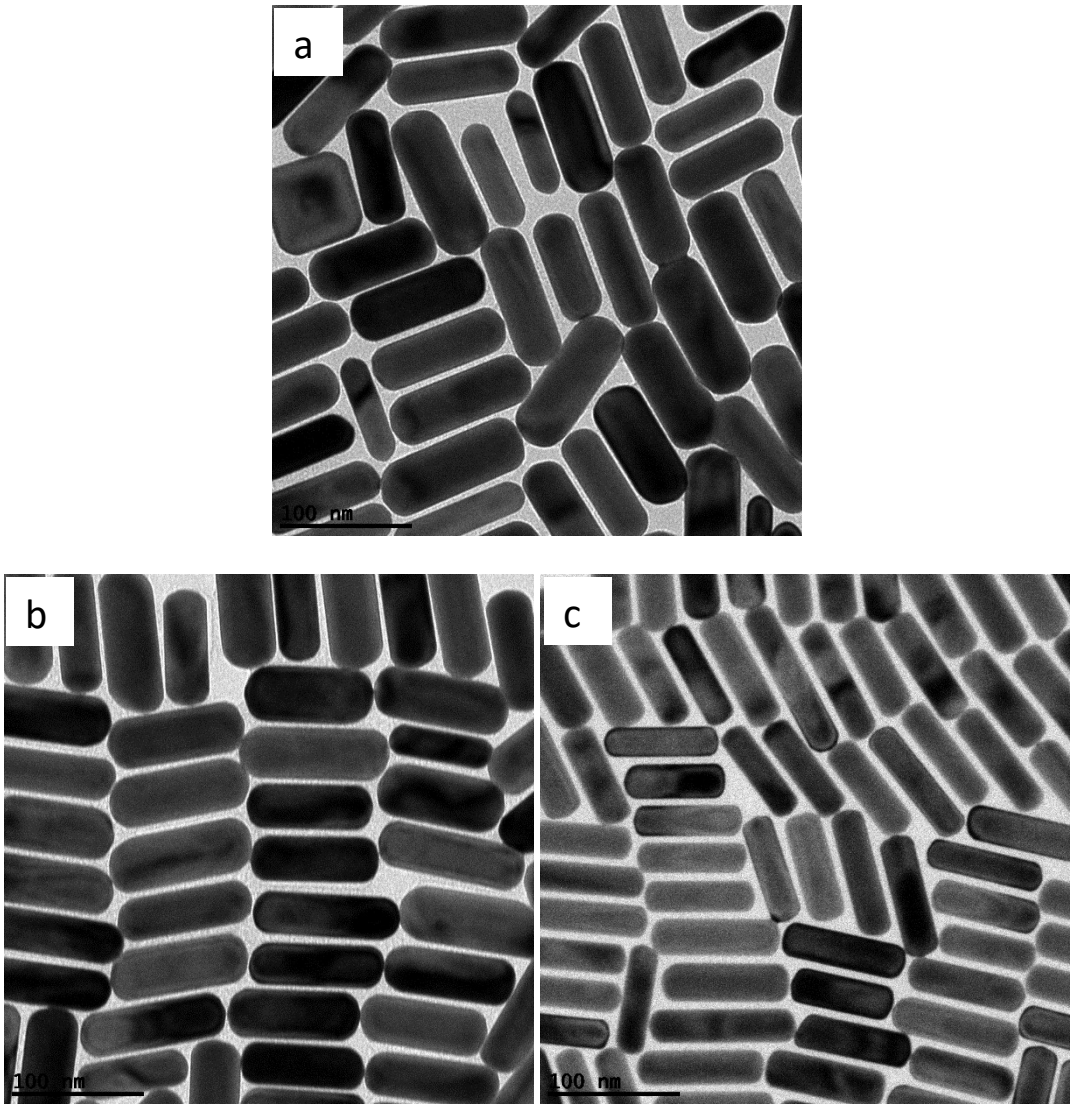


**Figure 3.3.6.2:** TEM micrographs of the Au NRs grown from no seeds (in **a**) and after adding 0,1 µL/mL (in **b**) and 0,8 µL/mL (in **c**) of seeds, with scale bar of 100 nm.

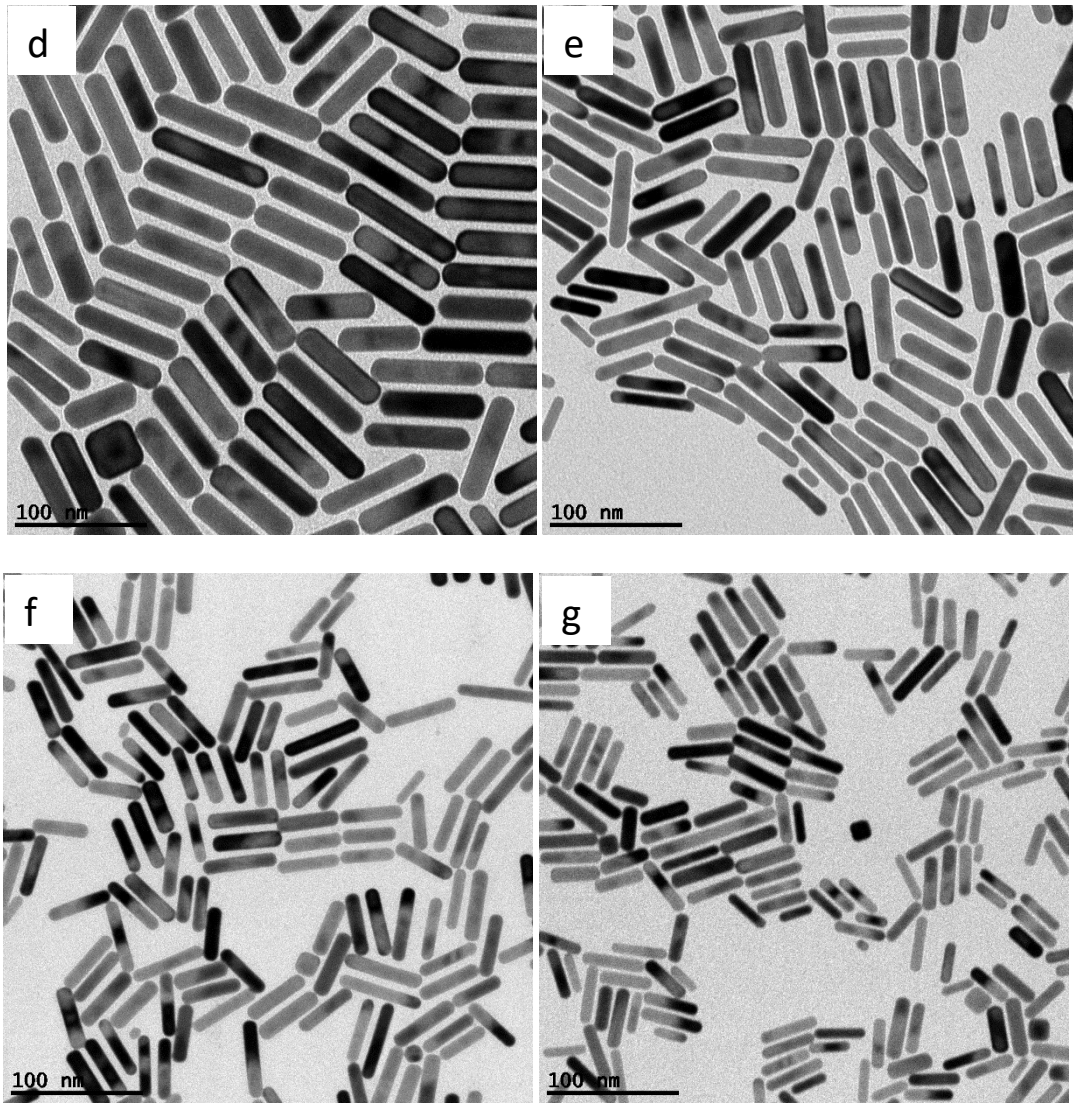


**Figure 3.3.6.2:** TEM micrographs of Au NRs grown after adding 3,2 µL/mL (in **d**), 10 µL/mL (in **e**), 32 µL/mL (in **f**) and 100 µL/mL (in **g**) of seeds, with scale bar of 100 nm.

| | **Length [nm]** | **Width [nm]** | **Aspect Ratio [adim]** | **NRs fraction [adim]** |
|---|---|---|---|---|
| **0 µL/mL** | 99 ± 11 (11%) | 36 ± 6 (17%) | 2,8 ± 0,5 (18%) | 98,6% |
| **0,1 µL/mL** | 98 ± 9 (9%) | 35 ± 6 (17%) | 2,8 ± 0,5 (18%) | 99,3% |
| **0,8 µL/mL** | 88 ± 8 (9%) | 29 ± 4 (14%) | 3,1 ± 0,5 (16%) | 97,3% |
| **3,2 µL/mL** | 76 ± 9 (12%) | 20 ± 2 (10%) | 3,8 ± 0,6 (16%) | 98,2% |
| **10 µL/mL** | 59 ± 12 (20%) | 15 ± 2 (13%) | 4,0 ± 0,7 (18%) | 97,8% |
| **32 µL/mL** | 49 ± 9 (18%) | 13 ± 3 (23%) | 3,9 ± 0,7 (18%) | 99,2% |
| **100 µL/mL** | 39 ± 9 (23%) | 12 ± 2 (17%) | 3,4 ± 0,7 (21%) | 97,5% |

**Table 3.3.6.2:** data from statistics on TEM images of the Au NRs grown after adding 0-100 µL/mL of seeds.

As reported in Figure & Table 3.3.6.2, it is proved that the availability of more seeds to grow results in the formation of shorter and thinner NRs; such trend is accompanied by an increase of the AR until the addition of 10 µL/mL of seeds, then by a decrease (testified also by the final blue-shift in the absorbance spectra), in presence of too many seeds to grow at the same time for the conditions given, a situation already predicted in the previous chapter on the batch synthesis of Au NRs.

As concerns the size dispersion, all the samples present near values of standard deviation for the AR, while the specific dimensions of length and width oscillate more for the furthest additions of 10 – 100 µL/mL of seeds, with the NRs presenting the smallest characteristic sizes. On the other hand, about the shape purity, the presence for instance of nanocubes or bipyramids is observable in some TEM micrographs included here too, but the lowest NRs fraction among all the samples amounts to 97,3% – a good result above the general outcomes of batch synthesis.

As conclusions of the section, it must be recognized that the reactor is clearly able to perform the flow synthesis from a wide range of seeds amount available in the system, growing NRs that are monodisperse in shape and size, and even promoting the auto-nucleation in absence of seeds. NRs of the required AR and dimensions are synthesizable by the reactor from the proper amount of seeds, as operating with batches, but with the advantages of having higher volumes and a superior shape yield.

## 3.4 Lessons from using the millifluidic reactor

The experiments conducted and presented here cover an extended area of issues and aspects, concerning both the Au NRs synthesis itself and the adoption of an automated reactor instead of batch systems. As stated in the introductory section, since the gram scale of NRs is still challenging in batch conditions while kilogram scale quantities are needed in the nanotechnology era, the flow and continuous synthesis performed for instance by a millifluidic device may solve the situation.

Our reactor proved to be able to grow monodisperse NRs from seeds synthesized by hand; after the mixing time, the system starts to work properly and provides continuously a colloid with the same characteristics, up to large volumes unobtainable with the batch synthesis; moreover, shape and size dispersions do not show significant variations when distinct flow rates of a wide range are applied, from 1 to 80 mL/min, suggesting us that at least 8 L of monodisperse NRs are collectable. The lowest value of NRs fraction found from the TEM analysis amounts to 98.7%, a clear sign of the superior performance given by the reactor, readable also in the profiles of the absorbance spectra.

The flow synthesis of both seeds and NRs was well executed too, guaranteeing high reproducibility for the results; from the various experiences, it emerged that the best choice is to use the flow rate of 11,2 mL/min for seeds synthesis and then to collect after the mixing time. External factors may interfere with the operations, for instance a sudden increase of temperature in the laboratory favoring the evaporation of hygroscopic substances such as $NaBH_4$ means that, while the system is still perfectly working – seeds are no longer synthesized after a certain amount of time.

Other highly undesirable effects were observed during the months spent using the reactor: detachments could occur at any connection point of the outline channels of the pumps, obviously causing leakages of the solutions prepared and then requiring lot of time to be fixed. The occurrence was attributed to the presence of obstructions in the channel, that once even caused the break of PEEK tubing at a low flow rate; such obstructions may be dirt unintentionally introduced into the system or more likely CTAB crystals formed consequently to unexpected decrease of surrounding temperature.

As a rule, the channels were cleaned pumping water after every use of the reactor, while the single components were dismantled and inspected in the cases of detachments; generally, before running an experiment, the flow rates were set, and water was fluxed for several minutes, to promote further cleaning but especially to assure of the system stability – snap changes from low to high flow rates were not recommended, since the detachments may also be favored by the sudden changes of pressure inside the channel. The latter point is also a good reason for choosing the flow rates that we adopted in successive experiences: 11,2 mL/min for seeds synthesis and 5 mL/min for NRs growth.

Besides the procedures of cleaning and testing the stability, valid measures are adoptable inserting new components in the reactor system. For instance, the presence of filters in the inlet channels would not allow to enter particles above a certain size, as well as the three beakers with the solutions could be put in a bath at strictly controlled temperature to prevent precipitation phenomena, in both cases avoiding possible obstructions in some points and the subsequent detachments. Naturally, such proposals were formulable only after using the reactor several times and knowing its weaknesses, as a useful experience with limits and problems in the field of millifluidics was attained.

Referring the issues encountered is the natural counterpart of exposing the results obtained with the reactor, to which we return to focus at this point; it was proved that, using our protocol, the seeds synthesized are long-time stable and are growable into NRs even after 24 h with good yields in terms of size and shape dispersion, a finding evidently in contrast with the studies reported elsewhere.

It must also be underlined that, when synthesizing both seeds and NRs with the reactor, the lowest NRs fraction found amounts to 97,6% considering all the flow rates used. Such results concern specifically NRs with AR around 4, obtainable from the growth conditions of our protocol; changes are anyway applicable, for having monodisperse NRs with characteristics differing from ours, as demonstrated with the experiments in which [$AgNO_3$] and seeds amount were varied.

For anybody interested to NRs with a certain AR or with the longitudinal LSPR peak positioned in a given range of wavelengths, as usual in many research laboratories, the millifluidic reactor constitutes therefore an irreplaceable resource, able to provide very large volumes of monodisperse colloids; to the challenge of the future, our device clearly appears as one of the answers.

# REFERENCES

[1] Lohse, S. E.; Eller, J. R.; Sivapalan, S. T.; Plews, M. R.; Murphy, C. J. A Simple Millifluidic Benchtop Reactor System for the High-Throughput Synthesis and Functionalization of Gold Nanoparticles with Different Sizes and Shapes. *ACS nano*, **2013**, *7* (5), 4135-4150.

[2] Orendorff, C. J.; Murphy, C. J. Quantitation of Metal Content in the Silver-Assisted Growth of Gold Nanorods. *Journal of Physical Chemistry B*, **2006**, *110*, 3990-3994.

[3] Jana, N. R. Gram-scale synthesis of soluble, near-monodisperse gold nanorods and other anisotropic nanoparticles. *Small*, **2005**, *1* (8-9), 875-882.

[4] Zhang, L.; Xia, Y. Scaling up the Production of Colloidal Nanocrystals: Should We Increase or Decrease the Reaction Volume? *Advanced Materials*, **2014**, *26* (16), 2600-2606.

[5] Li, Y.; Sanampudi, A.; Reddy, V. R.; Biswas, S.; Nandakumar, K.; Yemane, D.; Goettert, J.; Kumar, C. S. S. R. Size Evolution of Gold Nanoparticles in a Millifluidic Reactor. *ChemPhysChem*, **2012**, *13*, 177-182.

# Conclusions

Plasmonic nanostructures are nowadays object of study for the scientific community, since expected to play a prominent role in the future society, as part of devices applied to multiple and distinct fields, e.g., from green energy to biomedicine, with a strongly beneficial impact on our existences. Among such structures, anisotropic NPs constitute undoubtedly a promising choice, for the important properties deriving from the shape in terms of LSPR tunability and field enhancement; particularly, lot of interests goes to Au NRs, for the unparalleled chemical inertness and synthetic accessibility.

Colloidal chemistry allows the Au NRs synthesis, as found two decades ago, recurring to the seed-mediated growth method; despite the 95% shape yield, the synthesis is characterized by disadvantages too, such as the lack of reproducibility and the scale up issue. Difficulties are met when trying to reproduce results already obtained working in the same conditions, even more to reproduce those of other research groups, because of the many uncontrollable variables involved; on the other hand, the 15% yield appears as a limit unlikely to be overcome for the mass production of Au NRs.

The answer to the problems exposed may be given by a change from batch to flow conditions, with the use of an automated reactor for performing continuously the synthesis, consequently reducing the human error and producing large volumes of monodisperse NRs in time. The experience gained in our case is that a millifluidic reactor demonstrates to be a precious resource in research laboratories, where NPs properties and behavior are investigated daily – for instance, some of the NRs grown by the reactor were then introduced into cell cultures for running other experiments.

The project presented in this thesis required 6 months to be executed: batch synthesis of Au NRs had to be mastered in first place, then attention was focused on adapting and optimizing it to flow conditions, becoming fully aware of the weaknesses and maintenance aspects. For reasons of time, the experience was limited to Au NRs, but the reactor is expected to perform well the syntheses of other anisotropic NPs too, as the title of this thesis work reports. Next experiments – only planned, concerned Au nanostars, known for giving intense hot spots at the tips, and far more easily synthesizable in batches than NRs; as depicted in Figure, the reactor could grow Au nanostars too.

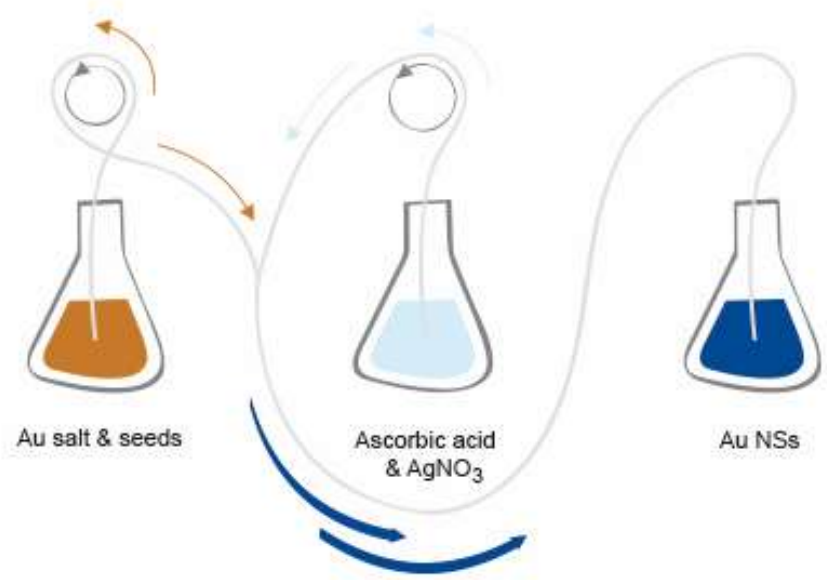


**Figure:** Schematics of the millifluidic reactor as usable for the growth of Au nanostars.

In batch conditions, seeds obtained by Turkevich method are added to an Au(III) solution, in which ascorbic acid and $AgNO_3$ are then injected simultaneously, observing a rapid turn of color into cobalt blue as the Au nanostars are synthesized. Our millifluidic system present only mixing points with two entries and one exit, the synthesis would thereby be performable with pump1 fluxing the solution of Au(III) and seeds, which meets the solution containing both ascorbic acid and $AgNO_3$ set in motion by pump2, and together form the final solution, running along the channel from the mixer until the collecting beaker while assuming the proper color. To us, it appears as feasible as with NRs.

Studying again the specific design, also the synthesis of Au nanotriangles may be performed in flow conditions – as it is demonstrated in the experimental section (with the growth of seeds in absence of $AgNO_3$), interesting for the scattering given and the modes associated to the edges. As announced, our millifluidic reactor is the new system expected to synthesize, continuously in time, several liters of monodisperse anisotropic Au NPs solution: nanorods, nanostars, nanotriangles.

At the current stage in the development of technologies based on plasmonic nanostructures, our reactor proves to be extremely useful to scientists and technologists that conduct researches for understanding how to deploy plasmonic properties into innovative devices and products. The application of such properties into everyday aspects of our lives is still far, as it is the kilogram scale production of NPs which would enable that; with our work, a little step in the right direction is made.